JACOBS UNIVERSITY

Efficient Advanced Indoor Localization: Analysis and Algorithms

BY

Omotayo Olabowale Oshiga

A Thesis submitted in partial fulfillment
of the requirements for the degree of

Doctor of Philosophy in Electrical Engineering

Approved Thesis Committee

Prof. Dr. Giuseppe Abreu, Jacobs University Bremen

Dr. Stefano Severi, Jacobs University Bremen

Dr. Mathias Bode, Jacobs University Bremen

Prof. Dr.-Ing. Oliver Michler, Technical University Dresden

Prof. Davide Dardari, University of Bologna

Date of Defense: January 26, 2015

Abstract

Wireless localization is a very mature area of research, with plenty of work done in recent years both in academia and industry. Despite the amount of effort put into this problem, wireless positioning systems are still far off their potential as a real-time locating technology (which requires automatic identification and tracking). It is commonly known that wireless localization systems are still inaccurate and unreliable in indoor environment, as a result indoor positioning systems are still quite frail and under-deployed.

One possible reason for this is that numerous constituents are available in the literature to solve parts of this problem, but still do not collectively combine to provide a complete solution. To qualify the above, two very important problems within the area of wireless localization have been treated as separate challenges. These problems are ranging (as defined by the process of estimating distances from physical quantities) and trilateration (as defined by the process of estimating the absolute location of sources given their distances to a set of references).

This is rationalized by the fact that the fundamental tools required to design accurate distance estimators and positioning algorithms are clearly distinct. From an error analysis point of view, these problems are intrinsically interdependent, by the reason of the fundamental limits on the root mean square error on the corresponding estimates (both distances and locations) being governed by the same likelihood function given as the product of the ranging error distributions. Therefore, an attempt at the unification of these problems, with the aim at improving the accuracy, precision, complexity and robustness of wireless localization for indoor positioning systems is reasonable.

During the course of this thesis, we provided estimation and reconstruction analyses on the statistics of the ranging error distributions, we then refrained from pursuing further positioning algorithms as both ranging and trilateration are governed by the same likelihood function, but rather presented efficient ranging and multipoint ranging techniques through the efficient collection of ranging information using Sparse and

Golomb rulers obtained utilizing evolutionary genetic techniques, with the adjustment of the ranging techniques to provide highly accurate solutions which aim at improving the quality of distance estimation. We then pursued effective trilateration techniques which allow results and information typically restricted to the ranging problem, to inform positioning algorithms, thereby conditioning results in light of knowledge extracted from ranging information in order to provide accurate wireless localization. Therefore, we bridged and inter-connected both ranging and trilateration methods, which resulted in efficient, robust, accurate, precise and low-complex ranging and trilateration techniques for advanced indoor localization.

Statutory Declaration

I, Omotayo Olabowale Oshiga hereby declare that I have written this PhD thesis independently, unless where clearly stated otherwise. I have used only the sources, the data and the support that I have clearly mentioned. This PhD thesis has not been submitted for conferral of degree elsewhere.

Bremen, February, 2015

Signature ______________________

Acknowledgments

Firstly, all adoration to God almighty for his grace and tender mercies throughout my masters program. Also, to him for giving me the capability to complete this research and the writing of my PhD thesis.

My undiluted appreciation goes to my able and awesome supervisor and professor; Prof. Dr. Giuseppe Abreu for his support, tutoring, encouragement and scolding during my research and also for guiding and putting me in the right part as a mentor and a father, while expanding and furthering my research skills and experience throughout my PhD program. I give my sincere gratitude and appreciation for without him, I would not have achieved this research results and goals, I am eternally grateful.

My enormous gratitude goes to my post-doctoral superior; Dr. Stefano Severi for his support and tutor during my research and also for guiding me throughout the writing of my thesis.

I would like to appreciate the work of the company ZIGPOS GmbH which gave me in-depth knowledge, training, data and positioning evaluation kits which were required for the analysis of algorithms proposed in this thesis.

I would like to appreciate my other Dissertation committee members – Dr. Mathias Bode, Jacobs University Bremen, Prof. Dr.-Ing. Oliver Michler, Technical University Dresden, Prof. Davide Dardari, University of Bologna – for their time, effort and dedication in reviewing this thesis and attending my defense, my appreciation towards them is enormous.

I would like to appreciate my parents and family, Mr. and Mrs. Gbolaga Oshiga, who raised me to be steadfast in achieving beyond my dreams and expectations, I also want to thank them for the education, training, financial support and prayer intercessions. I love you Daddy and Mummy and I am enormously thankful with a grateful heart. I wish to appreciate my siblings; Yemisi Aina, Taiwo Oshiga, Kehinde Oshiga and Folayemi Ogunfuye, for their immense support and encouragement throughout this years. Lastly, I also want to show my appreciation to my colleagues and friends, especially: Satya Vuppala, Simona Poilinca and Iyabode Esan for their help and support.

Dedication

To my Dear parents "Gbolaga and Omobolanle Oshiga", Siblings "Taiwo and Kehinde Oshiga, Folayemi Ogunfuye and Yemisi Aina" for their continual support and encouragement during the completion of my doctoral degree. Without their endless support and contributions, this thesis was would not have been possible.

Contents

List of Figures

List of Tables

Abbreviations

AoA Angle of Arrival

AWGN Additive White Gaussian Noise

BDNSS BeiDou Navigation Satellite System

CDF Cumulative Density Function

CLT Central Limit Theorem

CMRS Commercial Mobile Radio Service

CRLB Cramèr-Rao Lower Bound

CWRR Continuous Wave Radar Ranging

DoA Direction of Arrival

EDM Euclidean Distance Matrix

EE Edgeworth Expansion

FCC Federal Communications Commission

GLONASS Global Navigation Satellite System

GK Gaussian Kernel

GPS Global Positioning System

i.i.d. independent identically distributed

IoT Internet of Things

IRNSS Indian Regional Navigation Satellite System

ISM Industrial, Scientific and Medical

ITU International Telecommunication Union

JUB Jacobs University Bremen

KLD Kullback-Leibler Divergence

LOS Line-of-Sight

LTE Long Term Evolution

MUSIC Multiple Signal Classification

ND Nakagami Distribution

NFC Near Field Communication

NLOS Non-Line-of-Sight

OFDM Orthogonal Frequency Division Multiplexing

PDF Probability Density Function

PDoA Phase-Difference of Arrival

PEB Position Error Bound

PMU Phase Measurement Units

RFID Radio Frequency Identification

RMSE Root Mean Square Error

RMUSIC Root Multiple Signal Classification

RSS Received Signal Strength

RSSI Received Signal Strength Indicator

SDP Semi-Definite Programming

SMDS Super Multidimensional Scaling

SNR Signal-to-Noise Ratio

SRC Short-Range Communication

SQP Sequential Quadratic Programming

TDoA Time Difference of Arrival

ToA Time of Arrival

TWR Two-Way Ranging

UWB Ultra-WideBand

WiMAX Worldwide Interoperability for Microwave Access

WLAN Wireless Local Area Network

WPAN Wireless Personal Area Network

WSN Wireless Sensor Network

Chapter 1

Introduction and Review

1.1 Wireless Localization: Fundamental Mechanisms

Wireless localization is a very mature area of research in personal and wireless communications with its origin as far back as 1973 through the deployment of the Global Positioning System (GPS). The GPS technology with other satellite navigation systems such as Global Navigation Satellite System (GLONASS) and BeiDou Navigation Satellite System (BDNSS) first became fully operational in 1995, and recently Indian Regional Navigation Satellite System (IRNSS) in 2013. Altogether, the transformation in wireless localization started in 1996, when the U.S. Federal Communications Commission (FCC) released a notice through its "Notice of Proposed Rulemaking [1]" to Commercial Mobile Radio Service (CMRS) Providers. The FCC required providers and operators to implement an Enhanced 911 location-based emergency service, to enable the public to contact emergency services during a crisis while ensuring emergency services can locate the caller within some stringent accuracy requirements. By virtue of this policy, numerous location-based systems for emergency and commercial services have been developed in the U.S., Canada, Europe, Asia and other parts of the world.

Although, wireless localization was originally intended for cellular-based systems leading to operators and providers becoming decisive partners in the development and distribution location-based systems, currently, their roles were therefore challenged by various companies through the rise of smart devices – mobile phones, tablets, PCs, smart watches, and new technologies – ZigBee, Ultra-WideBand (UWB), Radio Frequency Identification (RFID), Near Field Communication (NFC), Wireless Local Area Networks (WLANs), Wireless Personal Area Networks (WPANs), Worldwide

Interoperability for Microwave Access (WiMAX), Mobile WiMAX, Long Term Evolution (LTE), LTE advanced etc. from the 3rd and 4th generation of wireless systems. Inherently the introduction and emergence of this new technologies, geographic location information are now a critical meta-data for location and context-awareness, which have been successfully exploited by vendor and middleware companies to provide services and applications for effective consumer market penetration.

From the 2014 ICT facts and figures features released by the International Telecommunication Union (ITU) [2], it showed that there are over 2.3 billions mobile-broadband subscriptions worldwide. Therein, the penetration levels for mobile-broadband is as follows with the largest in Europe (64%) and the North and South Americans (59%), the Middle-East States (25%), Asia-Pacific (23%) and Africa (19%) which depicts a large market available for mobile applications and services. Particularly, the market for Location-based services worldwide is currently \$8.12 billion which is estimated to grow at an annual rate of 25.5% to \$39.87 billion in 2019 [3]. Additionally, the market value for localization applications will further increase with the advent of technologies such as Smart-Connected Devices, Machine to Machine (M2M) commonly known as Internet of Things (IoT)), which estimates that 30 billion devices will be interconnected by 2020, forming an Internet of Everything which is supported by the advent of IPv6 [7].

Therefore, it is not surprising that wireless localization is one of the fundamental technologies in wireless networks in order to facilitate intelligent, secure, embodied and ubiquitous services for location and context-awareness as seen in various IoT projects such as BUTLER [4], IoT-A [5], OPENIoT [6] etc., thereby going beyond the attention of both scholars and the industry.

1.2 Open Challenges

It is therefore paradoxical that despite the formidable efforts and resources put into the wireless localization problem since 1996, wireless localization is still shy of its potential as a truly ubiquitous technology [8, 9, 11]. Ubiquity requires the technology to be available in every environment, and it is well-known that wireless localization systems are still inaccurate and unreliable in places such as urban canopies and indoor environments, which are characterized by high multipath and scarcity of LOS conditions.

Traditionally, the two major problems within the area of wireless localization have been, somewhat paradoxically, treated by authors as separate challenges. These problems are ranging (as defined by the process of estimating distances from physical quantities such as received signal strength, time of arrival or phase of arrival) and trilateration (as defined as the process of estimating the absolute or relative location of sources given their distances to a set of references).

This is justified by the fact that the fundamental mathematical tools utilized to design accurate distance estimators and positioning algorithms are somewhat distinct. For instance, most of literature on wireless localization is somewhat "biased" towards positioning algorithms where much of the theory available attempt to extract information from the geometry of the problem, leading to mechanisms – be it algebraic, optimization-theoretical, or statistical (Bayesian) in construction – that are often recursive and or fine-tuned for local optimality; whereas in distance estimation, old traditional techniques are still in use, which explains the gap between the breadth of the literature and the fact that the technology is struggling to penetrate effectively the indoor consumer market.

From an error-analytical point of view, however, these problems are inherently inter-connected, by which it is meant that the fundamental limits on the root mean square error on the corresponding estimates (distances and locations, respectively) are both governed by essentially the same function, namely, a likelihood function given be the product of the ranging error distributions which we would see later in the thesis.

Under the later observation, therefore, it is sensible to attempt a unification of the two problems, with the aim at improving the accuracy, precision, robustness, and complexity of indoor wireless localization systems, which is the goal of this Thesis.

During the course of the research to be conducted, we would provide estimation and reconstruction analyses on the statistics of ranging error distributions, and then refrain from pursuing positioning algorithms but rather present ranging and mutlitpoint ranging techniques through the efficient collection of ranging information using genetic techniques, with the adjustment of the techniques to provide high quality of distance estimation. We will then pursue effective trilateration methods that allow results and information typically restricted to the ranging problem, to inform positioning algorithms, thereby conditioning results in light of knowledge extracted from ranging information. Therefore in this thesis, we will bridge and inter-connect both ranging and trilateration techniques, which results in efficient, robust, accurate, precise and low-complex ranging and trilateration techniques for advanced indoor localization.

In the next sections, we take a close look at some popular traditional techniques for ranging as well as positioning algorithms. Therein, it is important to make a clear distinction between – ranging, positioning and localization. Localization is a process which entails both ranging (involves computing measured distances) and positioning (involves estimating the geographic coordinates of sources in a network from the mutual distances between devices).

1.3 Ranging Techniques for Wireless Localization

Typically, It is assumed that when a pair of devices mainly an anchor A and a target T are able to communicate with one another, they can measure their mutual distance, a process which is hereafter referred to as *ranging*.

In the years past, loads of research and promising work have been done in other to accurately and precisely measure the distance between a pair of devices using their wireless signals. Currently, three basic traditional ranging techniques exists which are Received Signal Strength (RSS), Time of Arrival (ToA) and Phase-Difference of Arrival (PDoA). In the following subsections, we describe these traditional techniques as well as the difficulties and challenges encountered using the aforementioned techniques for ranging.

1.3.1 Received Signal Strength-Based Ranging

A traditional technique for measuring the distance d between an anchor A and a target T is by calculating the attenuation of the transmitted signal strength, which is often referred to as received signal strength-based (RSS) or received signal strength Indicator-based (RSSI) ranging. This technique is widely used in wireless localization for range estimation as it requires no clock synchronization, while no expensive hardware is needed due to it very low computational complexity.

The principle of the RSS ranging is based mainly on the relationship between the transmitted power and received power of a signal which therefore transcribe into measured distance d [12], detailed below as

$$P_r \propto P_t - 10\,\gamma\,\log_{10}(d) + S, \tag{1.1}$$

where P_r is the received power of the signal measured at the target T, P_t is the transmitted power of the signal sent at anchor A, γ is the signal path loss factor which depends on the propagation environment and S is the large-scale fading which is typically assumed as a zero-mean Gaussian random variable.

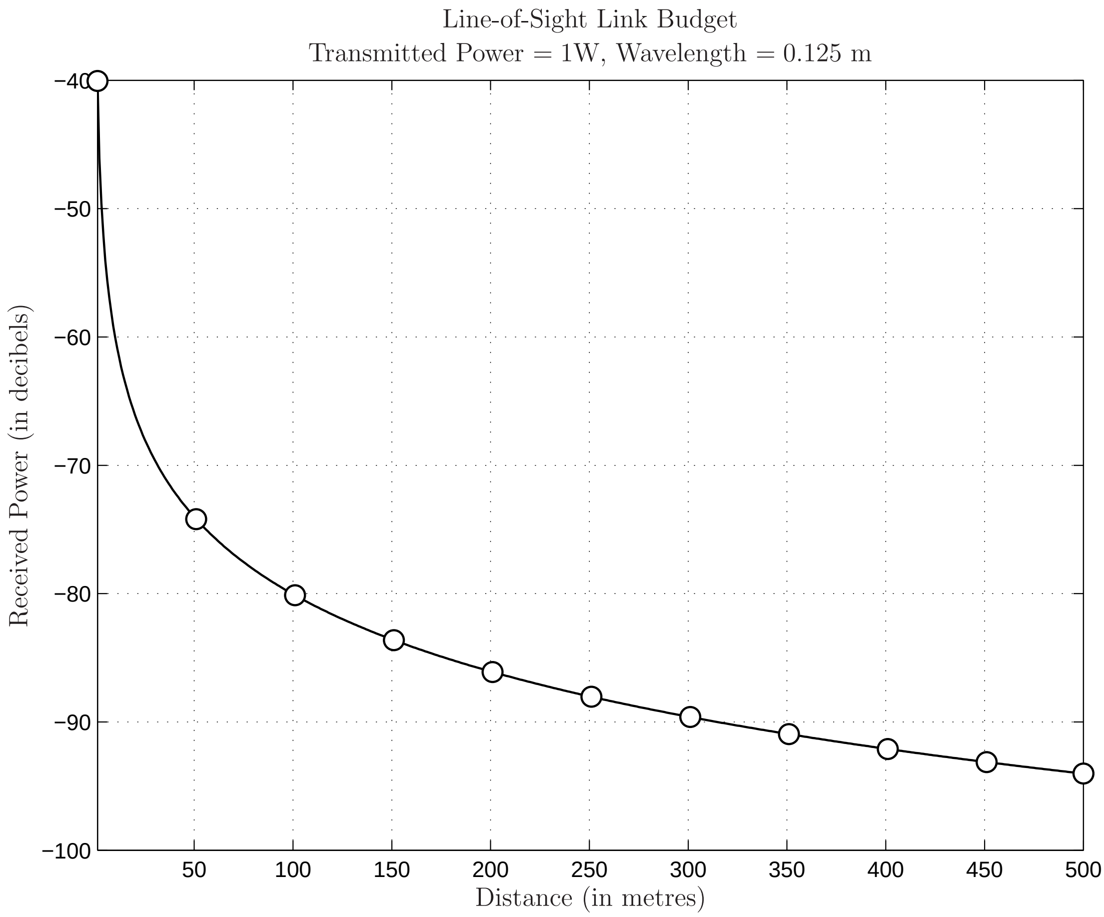

Figure 1.1: GSM Link budget using the free space propagation model.

Various empirical models have been proposed to model the propagation or attenuation of transmitted signals [12]. One of such models is the free-space path loss model which is applicable in scenarios where the distance to be measured is larger than both the antenna size and carrier wavelength λ, and there must exist a clear Line-of-Sight between the anchor and target. The corresponding Line-of-Sight link budget depicting the attenuation of a transmitted signal due to propagation in free space is given as

$$10\log_{10} P_r(dB) = 10\log_{10} P_t(dB) - 20\log_{10}(\frac{4\pi d}{\lambda}), \tag{1.2}$$

where antenna gains at both the transmitter and receiver as well as the path loss factor are taken to be one (1) while fading is assumed to be negligible. For illustration a calculated link budget is shown in Figure 1.1 for a range of distances $d = 1 - 100$m using a signal with a transmission power of 1W and wavelength of 0.125m.

Another popular model is the surface bidirectional reflectance model, this is quite accurate in modeling the path loss due to propagation when used in urban pico and micro-cellular environment [13]. A more widely used model is the Log-normal shadow model due to its suitability for both indoor and outdoor environments. This is a generalized propagation wireless channel model as it provides the option of different parameters which makes this model configurable for specific sites, thereby making it suitable for wireless environments [14].

Unfortunately, measured distances obtained using RSS-based methods are severely affected by multipath fading and shadowing in both LOS and NLOS conditions and most of the available path loss models do not always hold in indoor environments [14]. Also, from the experimental studies in [13, 14], it is said that RSS cannot be used as a reliable and accurate ranging technique for indoor wireless localization as these methods are highly inaccurate, very sensitive to the increase in distance d and easily affected by channel instability and inconsistency, as a result they require a precise channel propagation model which is almost impossible to achieve.

1.3.2 Time of Arrival-Based Ranging

Time of Arrival (ToA)-based ranging is another widely known traditional ranging technique which is the time it takes for a signal to travel from the anchor A to the target T, which is sometimes known as *Time of Flight*. It is a measure of the time for a signal to travel from one location to another given by

$$\Delta\tau \triangleq \frac{d}{c}, \tag{1.3}$$

where $c = 299792458$m/s and d is the distance between the anchor A and target T. With this ranging technique, various time difficulties and challenges such as clock offsets, drifts and jitters resulting from clock errors and the lack of synchronization between clocks at both the anchor and target and their effects on the measured time of arrival are illustrated in Figure 1.2.

There exist three commonly known ToA-based ranging techniques to have been proposed to solve the above clock challenges which are the One-Way ToA, Two-Way ToA and Differential ToA. The three different techniques ToA will be briefly explained here, while the Two-Way ToA will be described and utilized in Chapters 3 and 4 for illustration purposes.

The One-Way ToA is the simplest form of ToA as seen in Figure 1.3, where the time of arrival $\Delta\tau = \tau_2 - \tau_1$ is simply the time difference of the signal at A and T. In this technique, it is difficult to achieve accurate measured distance as the effects of a synchronization error could be quite devastating, where a clock offset of 1μs could lead to a distance error of about 299.79m. Also, this method of ToA ranging is as well largely affected by clock jitters and drifts leading to poor and highly inaccurate distance estimates.

For the Two-Way ToA Ranging shown in Figure 1.3, the round trip time $\tau_{\mathrm{RT}} = 2\Delta\tau + \tau_{\mathrm{T}}$ between the anchor and target which includes a time delay of τ_{T} is measured using a single packet exchange between A and T, where the time of arrival is computed as $\Delta\tau = \frac{((\tau_4 - \tau_1) - \tau_{\mathrm{T}})}{2}$. The effects of synchronization errors such as clock offset are mitigated using Two-Way Ranging but measured distances can still be affected by relative clock drift between A and T, clock jitters and inaccuracies, and arbitrary time delay τ_{T} at T. Some of these effects are mitigated using a variant of the Two-Way ToA Ranging known as the Differential Two-Way ToA Ranging.

For the Differential Two-Way ToA Ranging in Figure 1.3, the Two-Way ranging procedure is performed with a double packet exchange between A and T using a time delays of τ_{T} and $2\tau_{\mathrm{T}}$ at T and the time of arrival is thereby obtained as $\Delta\tau = \tau_4 - \tau_1 - (\tau_4' - \tau_1')/2$. Here, the effects of clock drift and arbitrary time delays are solved, which becomes negligible but unfortunately, this technique does not solve the effect of clock jitters.

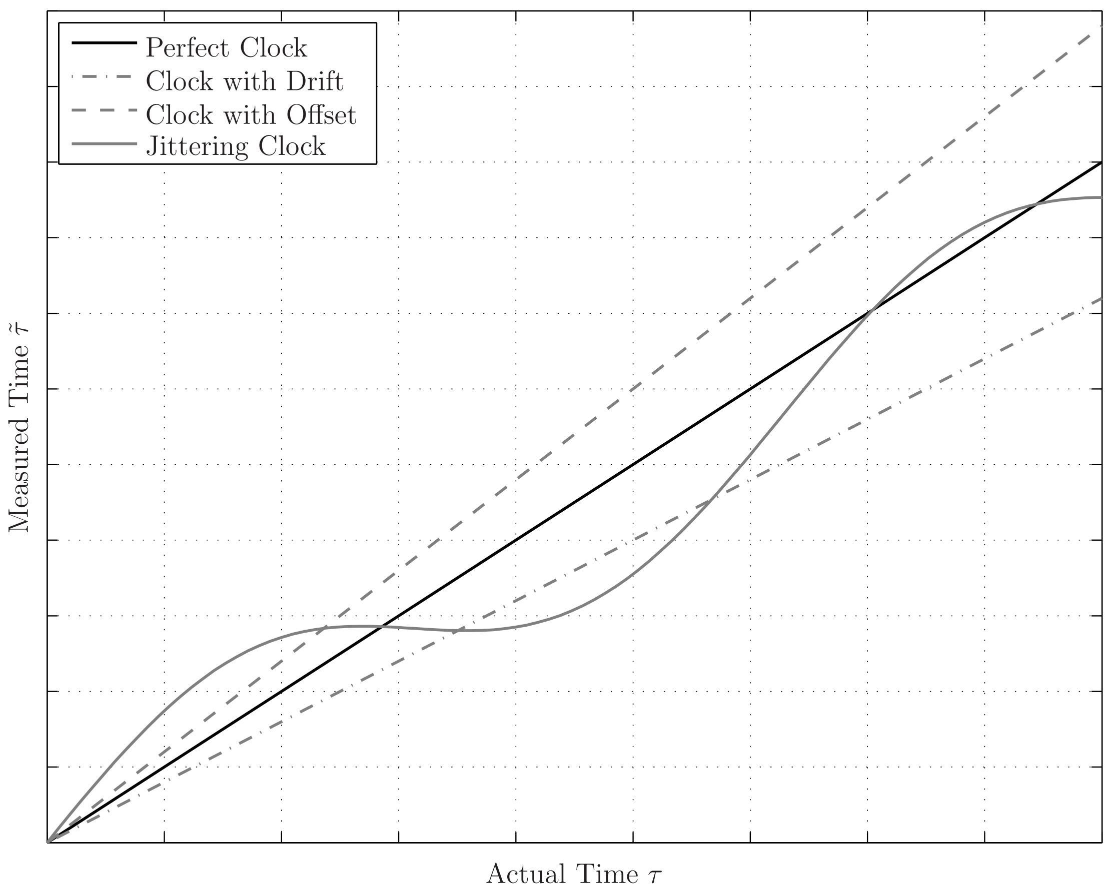

Figure 1.2: The effects of clock and synchronization errors on measured time [10].

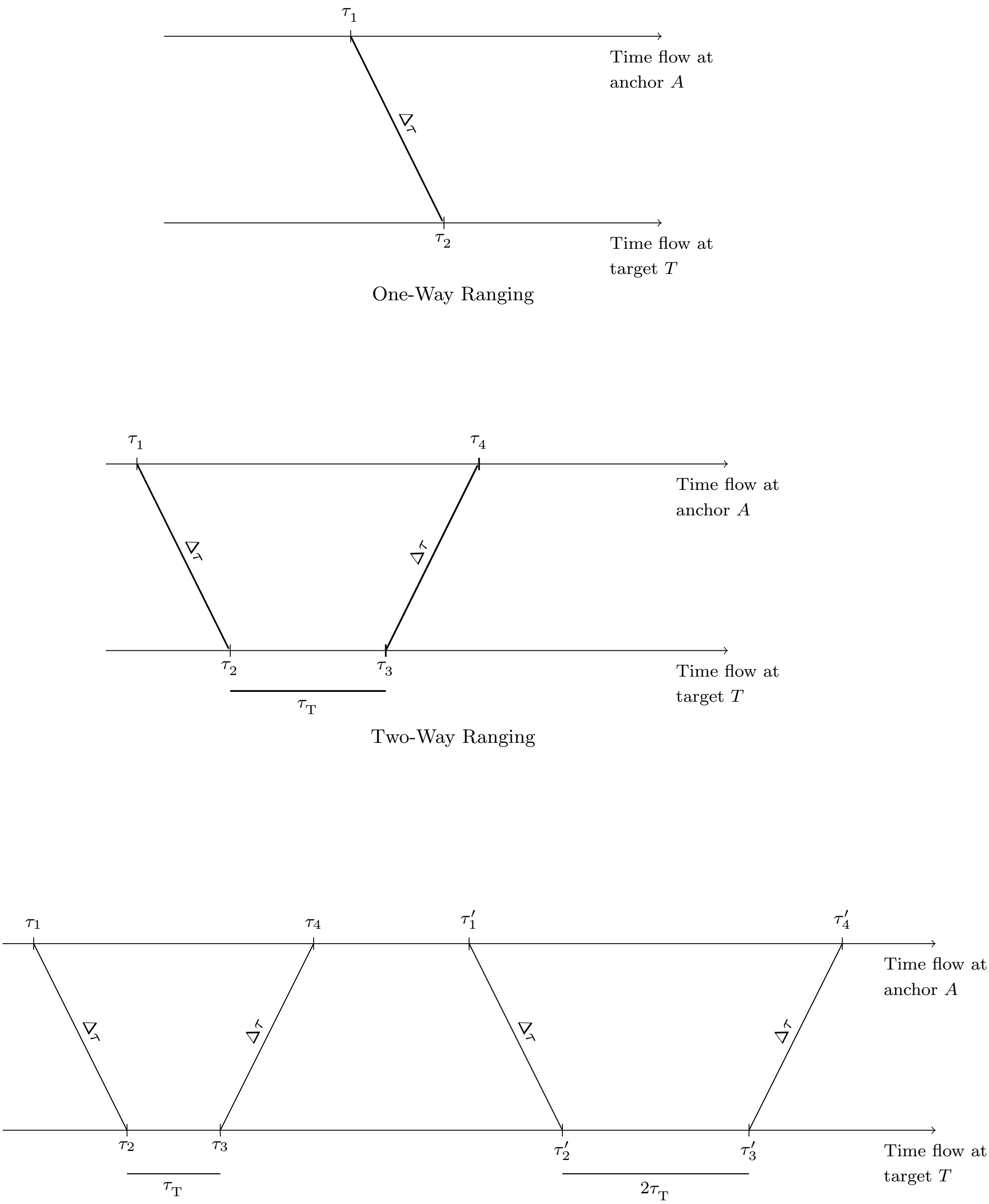

Figure 1.3: Different Types of Time of Arrival-Based Ranging Techniques.

In the literature [15,16], numerous state of art ToA-based ranging techniques have been proposed to mitigate against the various synchronization and clock effects encountered when using Time of Arrival Ranging. Irrespective of the results of presented techniques, ToA-based ranging stills suffers highly from multipath propagations and it is almost impossible to obtain clean ToA measurements in indoor environments, which results from the lack of LOS signals leading to inaccurate measured distances.

1.3.3 Phase-Difference of Arrival-Based Ranging

Phase-Difference of Arrival (PDoA)-based ranging is a traditional technique, which came into popularity in the early 2000s, through the introduction of RFIDs, which permitted consistent and intelligent signal processing for accurate distance estimation. PDoA-based ranging originates from the same idea in CW dual-frequency techniques utilized for distance estimation in radar systems [17–19].

In PDoA, a continuous wave signal is transmitted and received through an active reflector at a particular frequency. If operated at two frequencies f_1 and f_2, the observed phase difference $(\varphi_2 - \varphi_1)$ of the CW signal at these two frequencies is used to estimate the distance between the transmitter – anchor A and active reflector – target T as

$$d = \frac{c\Delta\varphi}{4\pi\Delta f} = \frac{c(\varphi_2 - \varphi_1)}{4\pi(f_2 - f_1)}. \tag{1.4}$$

For illustration, the PDoA-based ranging is explained in more details in Chapter 4.

The PDoA ranging technique is a much more improved ranging procedure compared to RSS-based and ToA-based ranging techniques and does not suffer severely in NLOS conditions due to multipath propagations. Also, this technique requires no clock synchronization or special hardware for measuring the phases. Regrettably, due to the dual-frequency scheme, the maximum possible distance that can be measured using PDoA for distance estimation is $d_{\text{max}} = \frac{c}{2\Delta f_{\text{min}}}$.

Irrespective of the traditional ranging technique used for distance estimation, measured distances obtained using the above schemes are still highly inaccurate and unreliable. In order to address this problem, later in the thesis, we propose various high resolution ranging techniques and algorithms for improving input measurements and obtaining accurate and reliable distance estimates over both ToA and PDoA measurements.

In the next section, we provide description of the different classes of positioning algorithms as well as the brief introduction of a few state-of-the-art algorithms in the aforementioned classes of algorithms.

1.4 Positioning Algorithms for Wireless Localization

In network localization, from the mutual distance obtained between devices, position information of a specific source (source localization) or all sources (network localization) in the network could be known. This position information (geographical or relative coordinates) of sources could be determined through an estimation algorithm, a process commonly known as *positioning*.

The devices in a positioning system are categorically divided into two forms which are *anchors* and *targets*. Anchors are devices which have a priori knowledge of their position, also called reference devices, while targets are devices which have no knowledge of their location which are to be estimated, also referred to as *sources*. In most systems, anchors are bigger devices which can be access points or wireless routers in a WLAN, base stations in mobile networks or devices with a GPS technology in them. On the other hand, targets are mostly small and portable devices such as mobile tags, mobile phones, smart watches etc.

As it is known, the focus of positioning algorithms is to estimate the position of unknown targets. As a result, on this subject, if the targets can only communicate with and obtain information from anchors only in the network, this kind of positioning is called *non-cooperative* positioning. Also, if targets can communicate with and obtain information from anchors as well as other targets, this scheme is called *cooperative* positioning.

Estimating the location of a target either by cooperative or non-cooperative positioning can be achieved by using distributed or centralized system of algorithms. Distributed algorithms, which are very much more popular in wireless sensor networks due to their scalability and low computational complexity, are highly inaccurate and much more susceptible to errors in the wireless channels, therefore sub-optimum [20]. As a contradiction, centralized algorithms are much more optimal, stable and accurate but far more computationally complex than distributed algorithms. Therefore, the choice between these systems of algorithms is usually related to the network scenarios therein a trade-off between accuracy and complexity [21] is needed in selecting the system of algorithms required in wireless networks.

Subsequently as part of the above problem and irrespective of the selected system of algorithms, accuracy is therefore a big challenge for positioning schemes in wireless localization mainly due to the inconsistency and sternness of the wireless propagation channel. For location coordinates to be estimated, positioning is required to be performed on physical quantities such as angles, distances, etc. Wherein, the angle between an anchor and a target can me measured using the Angle of Arrival (AoA) of the upcoming signal, and the distance can be measured using the traditional ranging techniques described in Section 1.3 – RSS, ToA and PDoA, which are all naturally affected by noise and bias.

Depending on the obtained types of information, different positioning algorithms can be constructed. Based on state-of-the-art algorithms, two main classes of positioning algorithms exists, which are range-based and range-free algorithms. In this thesis, we would only be considering range-based algorithms which are further divided into Angle of Arrival-based and Distance-based algorithms.

1.4.1 Angle of Arrival-Based Positioning Algorithms

Angle of Arrival-based positioning algorithms are triangulation algorithms which depend on the angle between the direction of propagation of an incident radio wave and some fixed (reference) direction against which the angles are to be measured, known as an *orientation* [22]. This localization algorithm has been widely investigated with success in the literature, thereby resulting in different closed-form and iterative solutions such as the Least Square (LS) [23], the probabilistic [22] and the iterative Constrained Total Least Square (CTLS) [24] for estimating the location of a single target.

For instance, the CTLS solution for a single target location $\boldsymbol{\theta}(\hat{\theta})$ is given as

$$\boldsymbol{\theta}(\hat{\theta}) = (\mathbf{P}^{\mathrm{T}}\mathbf{G}_{\boldsymbol{\theta}}^{-2}\mathbf{P})^{-1}\mathbf{P}^{\mathrm{T}}\mathbf{G}_{\boldsymbol{\theta}}^{-2}\mathbf{q}, \tag{1.5}$$

with

$$\mathbf{P} \triangleq \begin{bmatrix} \sin\theta_1 & -\cos\theta_1 \\ \vdots & \vdots \\ \sin\theta_{N_a} & -\cos\theta_{N_a} \end{bmatrix} \text{ and } \mathbf{q} \triangleq \begin{bmatrix} x_1\sin\theta_1 - y_1\cos\theta_1 \\ \vdots \\ x_{N_a}\sin\theta_{N_a} - y_{N_a}\cos\theta_{N_a} \end{bmatrix}, \tag{1.6}$$

where $\mathbf{G}_{\boldsymbol{\theta}} = x_r\mathbf{G}_1 + y_r\mathbf{G}_2 - \mathbf{G}_3$ with $\mathbf{G}_1 = \mathrm{diag}(\cos\theta_1, \cdots, \cos\theta_{N_a})$, $\mathbf{G}_2 = \mathrm{diag}(\sin\theta_1, \cdots, \sin\theta_{N_a})$ and $\mathbf{G}_3 = \mathrm{diag}(x_1\cos\theta_1 + y_1\sin\theta_1, \cdots, x_{N_a}\cos\theta_{N_a} + y_{N_a}\sin\theta_{N_a})$, $\theta_i = \arctan(\frac{y_r - y_i}{x_r - x_i})$ are the AoA between the direction of the incident radio wave from the anchors $i = \{1, 2, \cdots, N_a\}$ and the reference point $\boldsymbol{\theta}_r = [x_r, y_r]$ and N_a is the number of anchors.

For generalized network localization a solution was presented in [25] using multi-triangulation, which is a far more difficult approach as a large number of unknown variables are involved due to estimating the position of multiple targets simultaneously, thereby requiring a more complex optimization procedure. In this technique, the AoA-based localization problem is transformed into a distance-based localization problem by manipulating the angular properties of an encircled triangle.

1.4.2 Distance-Based Positioning Algorithms

This class of positioning algorithms are currently the algorithms with the widest interest in the literature mostly due to their ability to achieve high accuracy and as well their easy implementation and applicability. These refers to algorithms which require distances obtained from range measurements such as RSS, ToA and PDoA between targets and anchors to estimate the unknown positions of targets.

One of the commonly known and researched distance-based methods are the direct non-Bayesian positioning algorithms which are further divided into exact and approximate solutions. The exact solutions provide an accurate estimate of targets when there exist no error in the distance measurements, therefore suboptimal as they assume error-free measurements, while the approximate methods provide a coarse estimate of the target in the above mentioned condition.

The general focus of most direct non-Bayesian algorithms is to directly provide a solution to the source or network localization problems (a direct estimation of the target's coordinates). Therefore, for a given set of measured distances $\tilde{d}_{ij}$ from a target to anchors and other targets, these methods conform their parameters to the model been utilized in such a way that the error (distance) between the measured distances $\tilde{d}_{ij}$ and estimated distances $\hat{d}_{ij}$ are minimized. This minimization is achieved using by optimizing and exploiting the cost or objective function (convex or non-convex) used in presenting the problem. As a result, formulations for direct estimation are based on any of the methods below [26, 27]:

a) minimization of different variants of the weighted least square (WLS) cost function;

$$\hat{\mathbf{\Theta}}_{\mathrm{LS}} \triangleq \arg\min_{\mathbf{\Theta}} \sum_{i\in\mathbf{\Theta}} \sum_{j\in\mathbf{\Phi}} w_{ij}^2(\tilde{d}_{ij} - \hat{d}_{ij})^2 \tag{1.7}$$

b) maximization of the likelihood function;

$$\hat{\mathbf{\Theta}}_{\mathrm{ML}} \triangleq \arg\max_{\mathbf{\Theta}} \mathcal{L}(\tilde{\mathbf{d}}|\mathbf{\Theta}) \tag{1.8}$$

Though LS methods do not seem to assume any a priori knowledge of the statistics of the ranging error affecting the measured distances, these estimation methods are quite suboptimal compared to the maximum likelihood (ML) estimation. Nevertheless, both the ML and the LS techniques have been proven to be the same under the condition where the ranging error is an additive zero mean Gaussian noise. Also, it is quite necessary to note that the likelihood function and statistics of the measured distances are required to be known a priori in order to perform a ML estimation. Therefore, a large number of measure distances are required to approximate the above observations, which may not be achievable in practical scenarios, as a result the LS approaches are much more favored for target localization than ML approaches. Quickly, we provide brief description of a few positioning algorithms based on WLS minimization and also, a positive semidefinite kernel matrix, which would be used for performance evaluation in later parts of this thesis.

In [28], a new positioning algorithm referred to as the super multidimensional scaling (SMDS) was formulated, which is an continuation of the classic multidimensional scaling (MDS) [29, 30]. This formulation allows the utilization of both angle and distance ranging measurements which algebraically processed for the simultaneously localization of multiple targets, and also leads to the simplification of the positive semi-definite Gram Kernel matrix's structure, which is at the centre of the classic MDS. Results demonstrate a better performance of the super MDS algorithm when compared against the classic MDS.

In [31], different exact and approximate solutions of target localization problems using least square techniques were presented for the locating a target from range (R-LS) and range-difference (RD-LS) measurements collected from a set of anchors to the target. Also, LS solutions based on squared range (SR-LS) and squared range-difference (SRD-LS) were provided. Simulations show that the exact SR-LS and SRD-LS solutions outperform approximate solutions of R-LS, RD-LS, SR-LS and SRD-LS.

Finally in [33], a Geometry-Assisted Location Estimation algorithm was presented to estimate the location of targets, mostly under NLOS conditions. The algorithm is based on incorporating the geometric knowledge acquired from the anchor layout with the measured distances into the traditional two-step LS algorithm [34]. The target position is computed by bounding its approximation based on the signal variations and the geometrical arrangement between the targets and the anchors. Results indicate that this method outperforms the TS-LS method and it is reasonably robust in NLOS conditions.

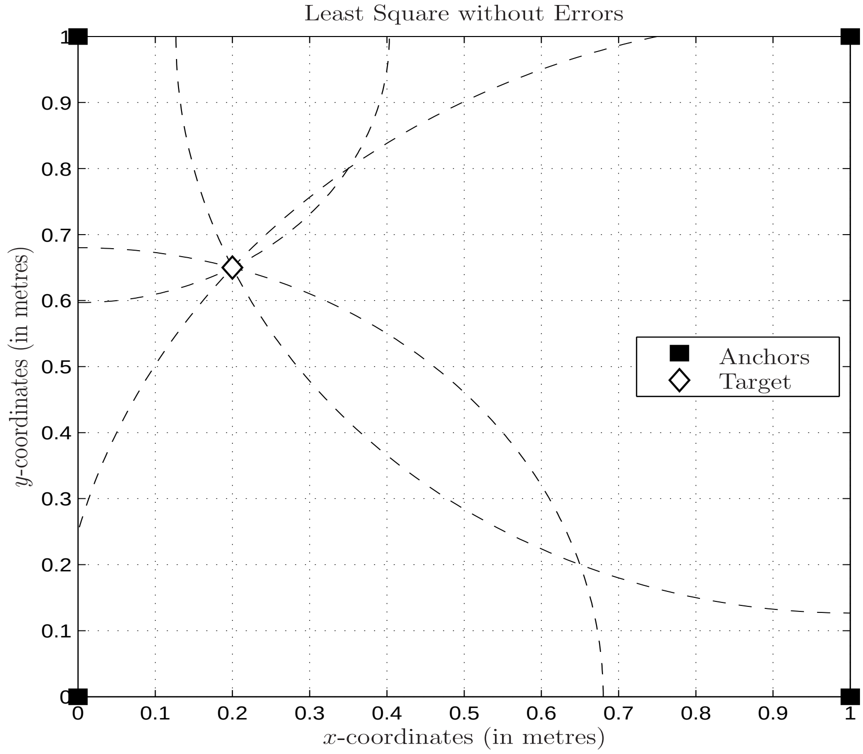

(a) Least Square without ranging error.

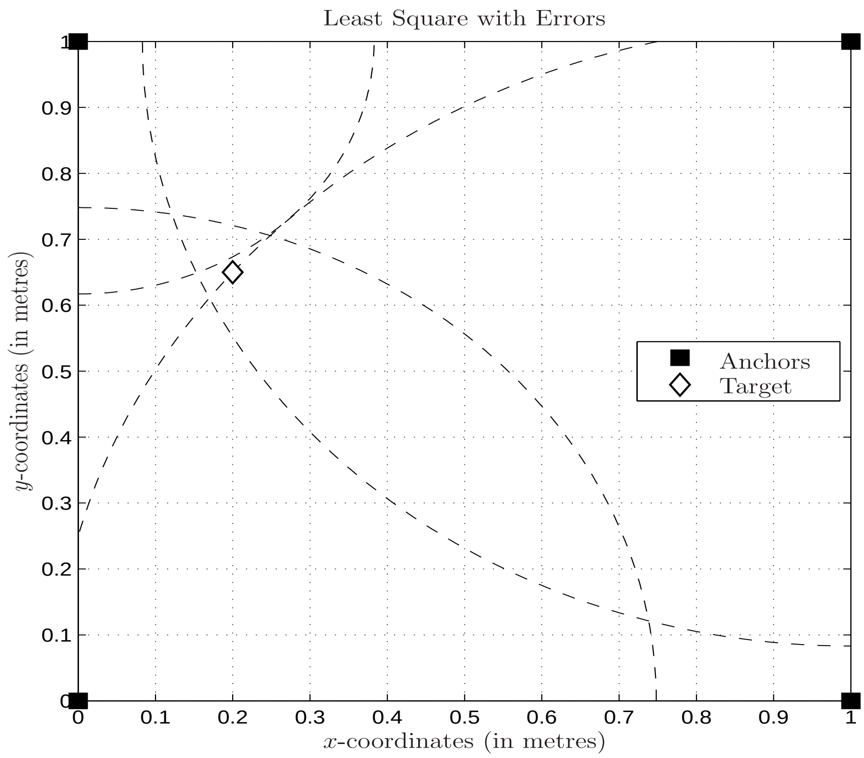

(b) Least Square with ranging error [32].

Figure 1.4: Intersection of measured distances with/without ranging errors.

1.5 Mitigation and Optimization Methods

Different error mitigation and optimization techniques have been presented for the minimization of the WLS cost function, so as to improve the accuracy of target estimates mostly due to ranging measurements been obtained in NLOS conditions. Therefore, we explore briefly some of the various effective error mitigation and optimization techniques currently in the literature.

1.5.1 Weighting Methods

Weighting Techniques are methods which allow adjustments to influence the optimization procedure (minimization) of the WLS objective function by highlighting differently the sizes of the terms $(\tilde{d}_{ij} - \hat{d}_{ij})$, where larger weights are assigned to the terms which desire the satisfaction of of stricter requirements thereby leading to improved and suitable solutions.

Various weighting techniques have been presented to influence differently the terms of the WLS objective function. In [30, 35], the weight is computed as the inverse of the noise variance $w_{ij}^2 = \frac{1}{\sigma_{ij}^2}$ which is related to the ML estimation assuming the ranging error is a zero-mean Gaussian random variable with variance σ_{ij}^2 but could also lead to inaccurate results, if the distribution of the ranging error is not Gaussian or the error variance is wrongly computed. Also, weights have been proposed as the inverse of the square of the measured distance $w_{ij}^2 = \frac{1}{\tilde{d}_{ij}^2}$, which is quite very reasonable as it is assumed ranging errors increase with measured distances and helps in mitigating against such errors. In [36], dispersive and penalty weighting strategies for network localization were proposed based on the reliability of ranging measurements and on the possibility of handling NLOS conditions as well.

1.5.2 Gradient Methods

Gradient methods are based on the derivative of the WLS objective function on the knowledge that the objective function is defined and differentiable. For example, gradient descent methods calculate the directional derivative (Gateaux derivative) of the objective function to be minimized to determine its route of convergence. Though, the rate of convergence of gradient descent methods is relatively slow, nevertheless, its accuracy could be improved by taking multiple iterations, if the curvature in various directions are different for the objective function [26]. These methods can are sometimes utilized with a line search in other to determine the optimal descent step size for each iteration, though regrettably with high computation cost. Newton methods with an inversion of the Hessian Matrix at each descent step which converge faster are also used as a better alternative but as well lead to an increase in computational cost [30, 35].

1.5.3 Majorizing Methods

Another alternative to the above optimization technique is the widely known Scaling by Majoring a Complicated Function (SMACOF) which is part of the various multi-dimensional scaling techniques [30]. In this technique, the algorithm attempts to find the minimum of the complex non-convex WLS objective function which it is referred to as a *stress* function with an iterative majorization scheme and as well tracking the global minimum of the majorizing function using a set of dissimilarity measures [30].

Iterative Majorization is a technique which generates monotone decreasing or equal series of stress function values by replacing iteratively the stress function by a majorizing (quadratic function) which must meet the following conditions: a) the majorizing function must be simpler to minimize than the stress function, b) the stress function must be smaller than or equal to the majorizing function, c) the majorizing function must touch the surface of the original function at a so-called supporting point where they are both equal to one another. Finally, the minimization of the majorizing function is achieved in closed-form using a Moore-Penrose inverse and Guttman transform [37].

A distance smoothing SMACOF algorithm was presented in [38], which generates monotone non-increasing sequences of stress function values without requiring a step-size procedure by replacing the absolute values $|\theta_i - \phi|$ in the estimated distances $\hat{d}_{ij}$ by an huber function $h_\epsilon(\theta_i - \phi)$, thereby creating a distance smoothing stress function with a smoothing parameter ϵ to replace the original stress function in SMACOF. Another recently proposed variant of the algorithm is the Circular-based Interval SMACOF (CIS or ISCAL), which is achieved by modifying the WLS stress function used in SMACOF [39, 40] while including a confidence region for the estimated target location.

In addition to the above described methods, other optimization and mitigation techniques that can be used for the minimization of the WLS objective function are the conjugate gradient and trust-region methods, simplex and interior-points methods, sequential quadratic programming, semi-definite programming etc.

1.6 Cramèr-Rao Lower Bound for Wireless Localization

Estimating the error limit on both ranging and localization associated with each target is a fundamental problem in wireless localization. In literature to this regards, the most widely and commonly used tool in statistical signal processing for estimating such fundamental limit is the Cramèr-Rao Lower Bound (CRLB) [41–43].

The CRLB is very popular in wireless localization as it is used in evaluating the accuracy of ranging and positioning algorithms, thereby ascertaining the minimum possible distance and location errors that can be achieved for a given network topology. Inadvertently, the CRLB relies on having a priori the knowledge of the true target location as well as the distribution and statistics of the ranging errors in the wireless network.

For example, considering a network of N nodes with $\eta = 2$ dimensional coordinate vectors denoted by $\boldsymbol{\theta}_i = [\theta_{i:x}, \theta_{i:y}]$, for $1 \leq i \leq N$. The location of a small fraction of N known as anchors (a-priori known location) with coordinates $[\boldsymbol{\theta}_1, \cdots, \boldsymbol{\theta}_{N_a}]$ and the remaining nodes known as the targets (unknown location) with coordinates $[\boldsymbol{\theta}_{N_a+1}, \cdots, \boldsymbol{\theta}_{N=N_a+N_t}]$. The Euclidean distance $d_{ij} \triangleq \|\boldsymbol{\theta}_i - \boldsymbol{\theta}_j\| = \sqrt{\langle \boldsymbol{\theta}_i - \boldsymbol{\theta}_j, \boldsymbol{\theta}_i - \boldsymbol{\theta}_j \rangle}$ is the true distance between the i-th and j-th nodes and the corresponding measured distance $\tilde{d}_{ij} = d_{ij} + n_{ij}$ is subject to ranging errors where n_{ij} is modeled as a Gaussian random variable $\mathcal{N}(0, \sigma_{ij}^2)$.

Let $\hat{\boldsymbol{\theta}}$ be an estimate of the vector parameter $\boldsymbol{\theta}$ and $\mathbb{E}[\hat{\boldsymbol{\theta}}]$ as the expected value of $\hat{\boldsymbol{\theta}}$. As a member of the family of the deterministic lower bounds in estimation theory, the CRLB, originating from the mean square error (MSE)

$$\mathrm{MSE}(\hat{\boldsymbol{\theta}}) = \mathbb{E}\left[(\hat{\boldsymbol{\theta}} - \boldsymbol{\theta})^{\mathrm{T}}(\hat{\boldsymbol{\theta}} - \boldsymbol{\theta})\right] = \mathrm{var}(\hat{\boldsymbol{\theta}}) + (\mathrm{Bias}(\hat{\boldsymbol{\theta}}, \boldsymbol{\theta}))^2, \tag{1.9}$$

indicates a lower bound on the variance or covariance of unbiased estimator $\mathrm{var}(\hat{\boldsymbol{\theta}})$ ($\mathrm{Bias}(\hat{\boldsymbol{\theta}}, \boldsymbol{\theta}) = 0$), thereby achieving full efficiency and the lowest possible MSE, this is sometimes referred to as the minimum variance unbiased estimator.

1.6.1 Cramèr-Rao Lower Bound for Ranging (Distances)

For a single distance measurement $\tilde{d}_{ij}$ from a target $\boldsymbol{\theta}_i$ to an anchor $\boldsymbol{\theta}_j$, which is distributed according to the probability density function $f(\boldsymbol{\theta}_i|d_{ij}) \sim \mathcal{N}(d_{ij}, \sigma_{ij}^2)$. The associated likelihood function $\mathcal{L}(\boldsymbol{\theta}_i|d_{ij})$ is given as

$$\mathcal{L}(\boldsymbol{\theta}_i|d_{ij}) \triangleq \frac{1}{\sqrt{2\pi\sigma_{ij}^2}}\exp\left(-\frac{(\tilde{d}_{ij}-d_{ij})^2}{2\sigma_{ij}^2}\right). \tag{1.10}$$

As a result, the Fisher Information J is computed as

$$J \triangleq -\mathbb{E}\left[\frac{\partial^2 \ln \mathcal{L}(\boldsymbol{\theta}_i|d_{ij})}{\partial \boldsymbol{\theta}_i^2}\right] = \frac{1}{\sigma_{ij}^2}. \tag{1.11}$$

Therefore, the CRLB $\bar{\varepsilon}$ is obtained as $\bar{\varepsilon} = J^{-1}$

1.6.2 Cramèr-Rao Lower Bound for Positioning (Location)

For a target θ_i specific approach which is to be estimated from a N_a distances $\mathbf{d}_i$ and distributed according to some probability density function $f(\boldsymbol{\theta}_i|\mathbf{d}_i)$, the associated likelihood function is given as

$$\mathcal{L}(\boldsymbol{\theta}_i|\mathbf{d}_i) \triangleq \prod_{j=1}^{Na} \frac{1}{\sqrt{2\pi\sigma_{ij}^2}}\exp\left(-\frac{(d_{ij}-\tilde{d}_{ij})^2}{2\sigma_{ij}^2}\right) \tag{1.12}$$

The CRLB relates the covariance matrix $\boldsymbol{\Omega}_{\boldsymbol{\theta}}$ to the Fisher Information Matrix $\mathbf{J}$ as

$$\boldsymbol{\Omega}_{\boldsymbol{\theta}} \succeq \mathbf{J}^{-1}. \tag{1.13}$$

Therein, the Fisher Information Matrix $\mathbf{J}$ is given as

$$\mathbf{J} \triangleq -\mathbb{E}\left[\frac{\partial^2 \ln \mathcal{L}(\boldsymbol{\theta}_i|\mathbf{d}_i)}{\partial \boldsymbol{\theta}_i^2}\right] = \begin{bmatrix} J_{\theta_{i:xx}} & J_{\theta_{i:xy}} \\ J_{\theta_{i:xy}} & J_{\theta_{i:yy}} \end{bmatrix}, \tag{1.14}$$

where

$$J_{\theta_{i:xx}} = \sum_{j=1}^{N_a}\left(\frac{(\theta_{ix}-\theta_{jx})^2}{\sigma_{ij}^2 d_{ij}^2}\right), \quad J_{\theta_{i:yy}} = \sum_{j=1}^{N_a}\left(\frac{(\theta_{iy}-\theta_{jy})^2}{\sigma_{ij}^2 d_{ij}^2}\right),$$
$$J_{\theta_{i:xy}} = \sum_{j=1}^{N_a}\left(\frac{(\theta_{ix}-\theta_{jx})(\theta_{iy}-\theta_{jy})}{\sigma_{ij}^2 d_{ij}^2}\right)$$

Therefore, the CRLB $\bar{\varepsilon}$ is obtained as $\bar{\varepsilon} = \mathrm{Tr}\{\mathbf{J}^{-1}\}$.

As mentioned earlier, the ranging and positioning problems are inter-connected as they are both governed by the same likelihood function given be the product of the ranging error distributions. Therefore, in this thesis, we seek to present ranging and trilateration techniques so as to enable accurate target localization while considering both fundamental localization problems as the same as depicted by their likelihood function rather than as separate entities as it is mostly done in the current literature.

1.7 Performance Evaluation of the SOTA Algorithms

In this section, we then to evaluate the performance of some described positioning and optimization techniques against the corresponding CRLB obtained from Subsection 1.6.2 with simulation analyses. In this regard, we consider the performance of these methods for both Line-of-Sight (LOS) and Non-Line-of-Sight (NLOS) conditions. To evaluate each technique, we calculate their corresponding average position error, which is the average Root Mean Square Error (RMSE) of the target position estimate

$$\bar{\varepsilon}_k \triangleq \frac{1}{M \cdot N_t} \sqrt{\sum_{m=1}^{M} \|\hat{\mathbf{\Theta}}_k^{(m)} - \mathbf{\Theta}\|_{\mathrm{F}}^2}, \tag{1.15}$$

where $\hat{\mathbf{\Theta}}_k^{(m)}$ corresponds to the targets position estimates computed for a specific k out of K algorithm in its m out of M measurements used for simulations. This will be evaluated as a function of the error standard deviation σ for LOS and maximum possible bias $b_{\max}$ for NLOS conditions.

For simulations, we consider a network of $N_a = 4$ anchors forming a square topology which are 14m away from one another and $N_t = 6$ targets which are randomly distributed inside the convex hull of the anchors[1]. Also, all anchors and targets communicate with one another to obtain distance measurements. In LOS conditions, the ranging errors are modeled as Gaussian random variables with zero-mean and variance σ^2.

For comparison, we evaluated the RMSE computed with the MDS in [30], the SR-LS algorithm in [31], the residual reweighting Linear LS algorithm in [29], the improve Two-Step Least Square (TS-LS) methods in [34, 44], the SMACOF algorithm in [38] is initialized with the solution of the MDS, the ISCAL algorithm in [39] and the SMDS algorithm in [28] are both initialized with the solution of a Centroid Min-Max algorithm, and all algorithms are compared against the CRLB.

[1] This scenario is common in indoor localization as well as in cellular and mobile networks.

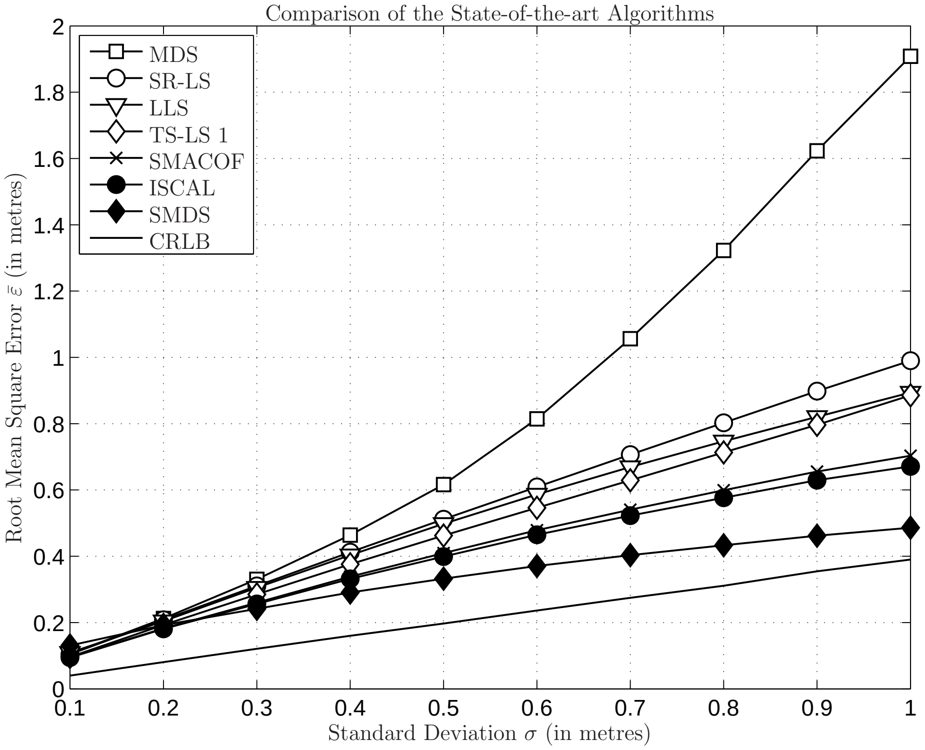

(a) LOS Conditions.

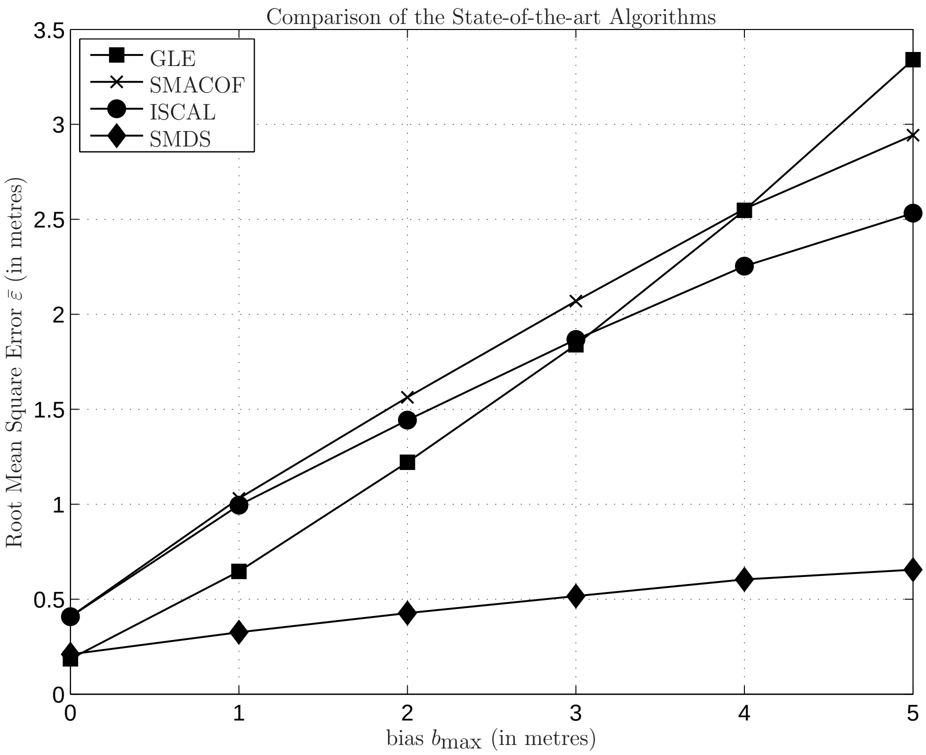

(b) NLOS Conditions.

Figure 1.5: Comparison of the SOTA algorithms in LOS and NLOS channel conditions.

The performance evaluation in Figure 1.5(a) shows that the MDS algorithm produces poor results, therefore depicting its inefficiency to act as an accurate algorithm for target localization even in LOS conditions, where it achieves decent result when the noise standard deviation $\sigma < 0.3$. The SR-LS, LLS and TS-LS1 have similar performances as well as the SMACOF and ISCAL, where they all produce decent RMSE across all standard deviation. From the RMSE of the compared algorithms, the RMSE of the SMDS is the closest to the CRLB and therefore the most accurate algorithm among those compared for target localization in LOS conditions. As seen in Figure 1.5(a), the SMDS is quite robust to high noise variance in LOS conditions which is not the same for other algorithms.

For NLOS conditions, the ranging error added to the distance was modeled as the sum of a Gaussian random variable with a zero-mean and variance $\sigma = 0.3$ and a positive maximum possible bias resulting from a uniform random variable between $[0, b_{\max}]$. In this simulation, the GLE algorithm in [33], SMACOF, ISCAL and SMDS algorithms were compared against each other. Results in Figure 1.5(b) show that the GLE, SMACOF and ISCAL all have similar RMSE and performance which depicts an average robustness, while the SMDS retains its accuracy even in NLOS conditions.

1.8 Outline and Thesis's Contributions

In this thesis, we attempt to solve the problem of a mutually conditional ranging and trilateration for indoor wireless location. We attempt a unification of the two problems – ranging and trilateration, with the aim at improving the accuracy, precision, complexity, and robustness of wireless localization systems, thereby presenting robust and accurate ranging and positioning techniques. The chapters of the thesis are organized as follows.

In this Chapter, we motivated the thesis by providing a background knowledge on wireless localization with its numerous available opportunities as well as describing the open challenges which we attempt to solve. This is followed by providing an overview on the state-of-art ranging and positioning techniques and a performance evaluation of these techniques with one another and the fundamental limit bound CRLB.

In Chapter 2, we focus on error analysis by estimating and reconstructing the statistics of the ranging error without a priori knowledge of the wireless channel. The common Gaussian kernel method would be used for the reconstruction from samples and its corresponding error bounds will be derived. We seek to propose an Edgeworth Expansion method, to reconstruct from samples by exploiting the power of moment convergence. The two methods will be compared against each other using two fundamental error bounds so as to determine the more efficient technique which required less number of samples to reach the same level of accuracy.

In Chapter 3, we propose a new accurate ranging algorithm, which combines superresolution algorithms popularly used in finding the direction of arrival of sources in antenna array systems such as MUSIC and Root MUSIC with the powerful mathematical notion of a sparse ruler, to perform efficient and accurate Time of Arrival-based ranging. The optimized solution will be compared against the naive unoptimized version in terms of samples to be collected, and above all, their performances will be compared against the fundamental limits depicted by the Cramèr-Rao Lower Bound.

In Chapter 4, we present an efficient and accurate solution to the multipoint ranging problem, based on an adaptation of superresolution techniques, with optimized sampling. Under a unified mathematical framework, we will construct a variation of the MUSIC and Root MUSIC algorithm to perform distance estimation over sparse sample sets determined by Golomb rulers. The design of the mutually orthogonal sets of Golomb rulers required for multipoint ranging method will be implemented via a proposed evolutionary genetic algorithm which would also be used to generate optimal Golomb rulers. A Cramèr-Rao Lower Bound analysis of the optimized multipoint ranging solution will be performed, to compare simulated results in other to quantify the gains achievable with this technique.

In Chapter 5, we present results for applications in wireless localization utilizing simulated and real time measurements. First, we present a ranging technique to obtain multiple measured distances by applying superresolution techniques to different set of measurements with an outliers detection technique and a new slope sampling algorithm utilizing a peak search on a computed spectrum of the residues. These distances will then be used in estimate the target position using the Super Multidimensional Scaling (SMDS) algorithm which requires an initial target estimate obtained using two proposed trilateration techniques (intersection of measured distances) in different localization scenarios. Lastly in Chapter 6, we present the final conclusions for this thesis and discuss future works to be done.

Chapter 2

Error Estimation Analysis

2.1 Introduction

Estimating the fundamental limit of localization error associated with each target node is a fundamental problem within the Wireless Sensor Network (WSN) context. In literature to this regards, the most widely used tools are the Cramèr-Rao Lower Bound (CRLB) [41–43], describing the average estimation error (i.e. the *distance* between the estimated and actual node location) and the Position Error Bound (PEB) [45], depicting the *region* where the node should be estimated within a certain confidence.

CRLB and PEB both rely on having the knowledge of the true target location, distribution and statistics of the ranging errors a priori; which depends on various environmental factors such that obtaining their formulation *a priori* is almost impossible.

The only practical solution is therefore to estimate this statistic directly on-site during the network deployment, collecting samples from each link and then obtaining the limit on localization error even before obtaining the target's location estimates.

To this end, the well known *maximum likelihood parametric approach* is not applicable, given the lack of a priori knowledge on the ranging error distribution and statistics. A truly non-parametric approach for estimating the ranging error distribution and statistics is therefore required; in particular the *kernel method* is very appreciated for its capability to reconstruct empirical distributions from samples, and in particular its Gaussian Kernel (GK) realization.

In this Chapter, a GK method to estimate on site the statistics of the ranging error is first proposed and then rewriting both the CRLB (similar to the proposed method in [46]) and the PEB. It is shown that this technique anyway requires a large amount of samples to reach a good level of accuracy, and consequently we introduce to the same end the Edgeworth Expansion (EE) method. Its greater efficiency, with respect to the GK method, is proved by the much lower number of samples needed to perform with the same level of accuracy.

The other parts of this chapter are coordinated as follows: in Section 2.2 the mathematical description of both the CRLB and PEB are provided and the description of the ranging model later employed. Section 2.3 introduces the GK methods and illustrates a revised mathematical formulation of the bounds on the localization error while the EE, our new proposed method used to derive the statistic of the ranging error from empirical samples, is described in turn in Section 2.4. Performance evaluation follows in Section 2.5, while conclusions are presented in Section 2.6.

2.2 Preliminaries on Error Bound

2.2.1 System Model

Consider a network of N nodes in an η-dimensional Euclidean space, out of which devices indexed $1, \cdots, N_t$ have no knowledge of their location (henceforth *targets*), while devices indexed $N_t + 1, \cdots, N_t + N_a$ are *anchors*, i.e. reference devices of *a priori* known location. For the sake of clarity, we shall hereafter scrutinize the case of when $\eta = 2$, with the remark that the analysis to follow can be straightforwardly extended to $\eta > 2$.

The localization problem consists of estimating the location of target nodes, given the knowledge on the location of anchors, and a set of measures of distances amongst these various devices, which are typically affected by errors [42].

To elaborate, let the position of the i-th device be denoted by (x_i, y_i), and let us append the ordinates of all targets into the vector $\boldsymbol{\theta_x}$, and the corresponding abscises into the vector $\boldsymbol{\theta_y}$, such that the target coordinate vector to be estimated can be described by

$$\boldsymbol{\Theta} \triangleq [\boldsymbol{\theta_x}, \boldsymbol{\theta_y}] = [x_1, \cdots, x_{N_t}, y_1, \cdots, y_{N_t}]. \tag{2.1}$$

Likewise, we describe the anchors' coordinate vector by

$$\boldsymbol{\Phi} \triangleq [\boldsymbol{\phi}_x, \boldsymbol{\phi}_y] = [x_{N_t+1}, \cdots, x_{N_t+N_a}, y_{N_t+1}, \cdots, y_{N_t+N_a}]. \tag{2.2}$$

It is assumed that when a pair of devices are able to communicate with one another, they are able to measure their mutual distances, a process which is hereafter referred to as *ranging*. Ranging measurements are, however, invariably affected by noise and often not conducted over a LOS link between the devices. In such NLOS conditions, an additional ranging error in the form of a positive deviation from the true distance appears, which is referred to as *bias*. Under these assumptions, the ranging model applicable to a pair of devices i-th and j-th is given by

$$\tilde{d}_{ij} = d_{ij} + n_{ij} + b_{ij} = \sqrt{(x_i - x_j)^2 + (y_i - y_j)^2} + v_{ij}, \tag{2.3}$$

where r_{ij} is the estimated distance, d_{ij} is the true distance, n_{ij} is an additive white Gaussian noise with a zero mean and variance σ_{ij}^2, b_{ij} is the bias, and the so-called *residual noise* v_{ij} models the ranging errors resulting from the noise and bias jointly.

Finally, it is assumed that not all pair-wise distances can be estimated, due to the devices being out of range or have limited link capacity [47]. In order to account for this frequent topological limitation, we define the *neighborhood function* as follows. First, let us define the *indicator operator* e_{ij}, which takes value 1 if devices i and j are connected, and 0 otherwise. Then, the neighborhood function associated with device i is defined as the set of indexes j such that $e_{ij} = 1$, that is

$$H(i) \triangleq \{j \mid e_{ij} = 1\}. \tag{2.4}$$

2.2.2 Standard Error Bound Formulations

In this subsection, we will clearly and briefly revise the formulation of the Fisher information matrix $\mathbf{J}$ [43], which is the fundamental matrix to get both the CRLB and the PEB, with the aim of clarifying the notation and steps to be employed in the following Sections 2.3 and 2.4, where the new error bounds, according to Gaussian Kernel (GK) [46] and Edgeworth Expansion (EE) (proposed) [48], will be discussed.

Let $\tilde{\mathbf{d}}$ be the range measurements vector denoted by

$$\tilde{\mathbf{d}} \triangleq \left\{ e_{ij} \cdot \tilde{d}_{ij} \right\}, \tag{2.5}$$

where $i, j = 1 \ldots N$ for $i \neq j$.

Let $\hat{\boldsymbol{\theta}}$ be an estimate of the vector parameter $\boldsymbol{\theta}$ and $\mathbb{E}[\hat{\boldsymbol{\theta}}]$ as the expected value of $\hat{\boldsymbol{\theta}}$.

The CRLB matrix relates to the Fisher information matrix $\mathbf{J}$ [43] as

$$\mathbb{E}\left[(\hat{\boldsymbol{\theta}}-\boldsymbol{\theta})(\hat{\boldsymbol{\theta}}-\boldsymbol{\theta})^T\right] \succeq \mathbf{J}^{-1}. \tag{2.6}$$

The Fisher information matrix $\mathbf{J}$ is accordingly given as

$$\mathbf{J} \triangleq \mathbb{E}\left[\frac{\partial \ln f(\tilde{\mathbf{d}}|\boldsymbol{\theta})}{\partial \boldsymbol{\theta}}\left(\frac{\partial \ln f(\tilde{\mathbf{d}}|\boldsymbol{\theta})}{\partial \boldsymbol{\theta}}\right)^T\right]. \tag{2.7}$$

The log of the joint conditional Probability Density Function (PDF) is

$$\ln f(\tilde{\mathbf{d}}|\boldsymbol{\theta}) = \sum_{i=1}^{N} \sum_{\substack{j\in H(i)\\ j<i}} l_{ij} \ , \tag{2.8}$$

where

$$l_{ij} = \ln f\left(\tilde{d}_{ij}|(x_i, y_i, x_j, y_j)\right). \tag{2.9}$$

Substituting equation (2.9) in (2.8) and as well in equation (2.7), the FIM is given as [47]

$$\mathbf{J} \triangleq \begin{bmatrix} \mathbf{J}_{xx} & \mathbf{J}_{xy} \\ \mathbf{J}_{xy} & \mathbf{J}_{yy} \end{bmatrix}, \tag{2.10}$$

where

$$\begin{aligned}
[\mathbf{J}_{xx}]_{kl} &= \begin{cases} \sum\limits_{j\in H(k)} \mathbb{E}\left[\left(\dfrac{\partial l_{kj}}{\partial x_k}\right)^2\right] & k=l \\ e_{kl}\,\mathbb{E}\left[\dfrac{\partial l_{kl}}{\partial x_k}\dfrac{\partial l_{kl}}{\partial x_l}\right] & k\neq l \end{cases} \\
[\mathbf{J}_{xy}]_{kl} &= \begin{cases} \sum\limits_{j\in H(k)} \mathbb{E}\left[\dfrac{\partial l_{kj}}{\partial x_k}\dfrac{\partial l_{kj}}{\partial y_k}\right] & k=l \\ e_{kl}\,\mathbb{E}\left[\dfrac{\partial l_{kl}}{\partial x_k}\dfrac{\partial l_{kl}}{\partial y_l}\right] & k\neq l \end{cases} \\
[\mathbf{J}_{yy}]_{kl} &= \begin{cases} \sum\limits_{j\in H(k)} \mathbb{E}\left[\left(\dfrac{\partial l_{kj}}{\partial y_k}\right)^2\right] & k=l \\ e_{kl}\,\mathbb{E}\left[\dfrac{\partial l_{kl}}{\partial y_k}\dfrac{\partial l_{kl}}{\partial y_l}\right] & k\neq l \ , \end{cases}
\end{aligned} \tag{2.11}$$

and $k, l = 1 \ldots n$ are the blindfolded devices. Note that $\mathbf{J}_{xx}, \mathbf{J}_{yy}, \mathbf{J}_{xy}$, and $\mathbf{J}$ are of sizes $n \times n$ and $2n \times 2n$, respectively.

2.2.3 Modeling Range Measurements

The statistics of range measurements - adopting a very general and widely recognised choice in literature [49] - has been modeled as a Nakagami Distribution (ND). The PDF of the residual noise v_{ij}, to be used in the following subsections to evaluate the performance of both the GK and EE methods, will therefore be

$$f_{v_{ij}}(v_{ij}) = \frac{2m_{ij}^{m_{ij}}}{\Gamma(m_{ij})\Omega_{ij}^{m_{ij}}} v_{ij}^{2m_{ij}-1} \exp\left(-\frac{m_{ij}}{\Omega_{ij}} v_{ij}^2\right), \tag{2.12}$$

where m_{ij} and Ω_{ij} are the shape and controlling spread parameters of the ND.

2.2.4 Bounds Derivation using Nakagami Distributions

Given the new PDF of the ranging model, it is now possible to get a revised formula of the Fisher information matrix. Taking the natural logarithm of equation (2.12) and substituting the result into $\frac{\partial l_{kl}}{\partial x_k}, \frac{\partial l_{kl}}{\partial y_k}, \frac{\partial l_{kl}}{\partial x_l}$ and $\frac{\partial l_{kl}}{\partial y_l}$ yields

$$\begin{aligned}
\frac{\partial l_{kl}}{\partial x_k} &= \frac{x_k - x_l}{d_{kl}} \left(\frac{2m_{kl}v_{kl}}{\Omega_{kl}} - \frac{2m_{kl}-1}{v_{kl}}\right), \\
\frac{\partial l_{kl}}{\partial y_k} &= \frac{y_k - y_l}{d_{kl}} \left(\frac{2m_{kl}v_{kl}}{\Omega_{kl}} - \frac{2m_{kl}-1}{v_{kl}}\right), \\
\frac{\partial l_{kl}}{\partial x_l} &= -\frac{x_k - x_l}{d_{kl}} \left(\frac{2m_{kl}v_{kl}}{\Omega_{kl}} - \frac{2m_{kl}-1}{v_{kl}}\right), \\
\frac{\partial l_{kl}}{\partial y_l} &= -\frac{y_k - y_l}{d_{kl}} \left(\frac{2m_{kl}v_{kl}}{\Omega_{kl}} - \frac{2m_{kl}-1}{v_{kl}}\right),
\end{aligned} \tag{2.13}$$

and therefore

$$[\mathbf{J}_{xx}]_{kl} = \begin{cases} \sum_{j \in H(k)} A_{kj} \frac{(x_k - x_j)^2}{d_{kj}^2} & k = l \\ e_{kl}\, A_{kl} \frac{(x_k - x_l)^2}{d_{kl}^2} & k \neq l \end{cases}$$

$$[\mathbf{J}_{xy}]_{kl} = \begin{cases} \sum_{j \in H(k)} A_{kj} \frac{(x_k - x_j)(y_k - y_j)}{d_{kj}^2} & k = l \\ e_{kl}\, A_{kl} \frac{(x_k - x_j)(y_k - y_j)}{d_{kl}^2} & k \neq l \end{cases}$$

$$[\mathbf{J}_{yy}]_{kl} = \begin{cases} \sum_{j \in H(k)} A_{kj} \dfrac{(y_k - y_j)^2}{d_{kj}^2} & k = l \\ e_{kl}\, A_{kl} \dfrac{(y_k - y_l)^2}{d_{kl}^2} & k \neq l \ , \end{cases} \tag{2.14}$$

where

$$\begin{aligned} A_{kl} &= \mathbb{E}\left[\left(\frac{2m_{kl} v_{kl}}{\Omega_{kl}} - \frac{2m_{kl} - 1}{v_{kl}} \right)^2 \right] \\ &= \int_{-\infty}^{\infty} \left(\frac{2m_{kl} v_{kl}}{\Omega_{kl}} - \frac{2m_{kl} - 1}{v_{kl}} \right)^2 f_{v_{kl}}(v_{kl}) \mathrm{d}v_{kl} \ . \end{aligned} \tag{2.15}$$

2.2.5 Generality of the Nakagami Model

The aim of this subsection is to further demonstrate the generality of the choice of ND, even for LOS scenarios. First, we will derive the Kullback-Leibler Divergence (KLD) of Gaussian distribution (typical of AWGN ranging error) and ND (better describing NLOS environments), showing that the latter is just a shifted version of the former, as the median of the distribution increases from zero. The second step is then to express the residual noise, modeled using ND $f_{v_{ij}}(v_{ij}; m_{ij}, \Omega_{ij})$, as a functions of both the bias and Gaussian error. Even in on-field measurements, it is not possible to evaluate their respective impacts to the total ranging error, it is convenient for theoretical purposes to treat them as separate parameters of the same distribution. The most immediate effect is to show that when the bias tends to zero, these error model - ND converges to a Gaussian distribution as seen in their KLD.

From the PDFs of Gaussian and NDs, we have

$$\begin{aligned} p(x) &= \frac{1}{\sqrt{2\pi}\sigma} e^{-\frac{(x-\mu)^2}{2\sigma^2}}, \\ q(x) &= \frac{2m^m}{\Gamma(m)\Omega^m} x^{2m-1} e^{-\frac{m}{\Omega}x^2}; \quad x > 0 \ , \end{aligned} \tag{2.16}$$

then their KLD is given as

$$\begin{aligned} \mathrm{KL}(q \parallel p) &= \int_{-\infty}^{\infty} q(x) \log q(x) \mathrm{d}x - \int_{-\infty}^{\infty} q(x) \log p(x) \mathrm{d}x \\ &= H\left(q(x)\right) - H\left(q(x), p(x)\right). \end{aligned} \tag{2.17}$$

The entropy of the ND [50] is given as

$$\begin{aligned} H\left(q(x)\right) &= \int_{-\infty}^{\infty} q(x) \log q(x) \mathrm{d}x \\ &= \log\left(\frac{\Gamma(m)\sqrt{\Omega}}{2\sqrt{m}}\right) - \left(\frac{2m-1}{2}\right)\psi(m) + m, \end{aligned} \tag{2.18}$$

where $\psi(m)$ is the Digamma function.

The cross entropy between the Gaussian and NDs [51, 52] is given as

$$\begin{aligned} H\left(q(x), p(x)\right) &= \int_{-\infty}^{\infty} q(x) \log p(x) \mathrm{d}x \\ &= \frac{1}{2}\log(2\pi\sigma^2) + \frac{\mu^2}{2\sigma^2} + \frac{m^m}{\sigma^2\Gamma(m)\Omega^m}\left(\frac{\Gamma(m+1)}{2\left(\frac{m}{\Omega}\right)^{m+1}} - \frac{\mu\Gamma(m+1/2)}{\left(\frac{m}{\Omega}\right)^{m+1/2}}\right). \end{aligned} \tag{2.19}$$

This divergency is highlighted by Figure 2.1, where the KLD of Gaussian distribution and ND, which is relatively the same for any standard deviation σ, decreases rapidly as the median of the distribution μ/σ increases from zero.

Then, let us define a function Naka$(d_{ij} + b_{ij}, \sigma)$ for obtaining the parameters (m_{ij}, Ω_{ij}) of the residual noise v_{ij}, where σ^2 is the variance of the residual noise which is constant across the network space. The controlling spread parameter of the ND is defined as

$$\Omega_{ij} = (d_{ij} + b_{ij})^2 \tag{2.20}$$

where the median of the distribution is $\sqrt{\Omega_{ij}}$.

The shape parameter can be obtained from its variance using [53]

$$\begin{aligned} \Omega_{ij}\left(1 - \frac{1}{m_{ij}}\left(\frac{\Gamma(m_{ij}+1/2)}{\Gamma(m_{ij})}\right)^2\right) &= \sigma^2 \\ \frac{1}{m_{ij}}\left(\frac{\Gamma(m_{ij}+1/2)}{\Gamma(m_{ij})}\right)^2 &= 1 - \frac{\sigma^2}{\Omega_{ij}}. \end{aligned} \tag{2.21}$$

From [54], an asymptotic series used in probability theory is given as

$$\frac{\Gamma(m_{ij}+1/2)}{\Gamma(m_{ij})} = \sqrt{m_{ij}}\left[1 - \frac{1}{8m_{ij}} + \frac{1}{128m_{ij}^2} + \dots\right]. \tag{2.22}$$

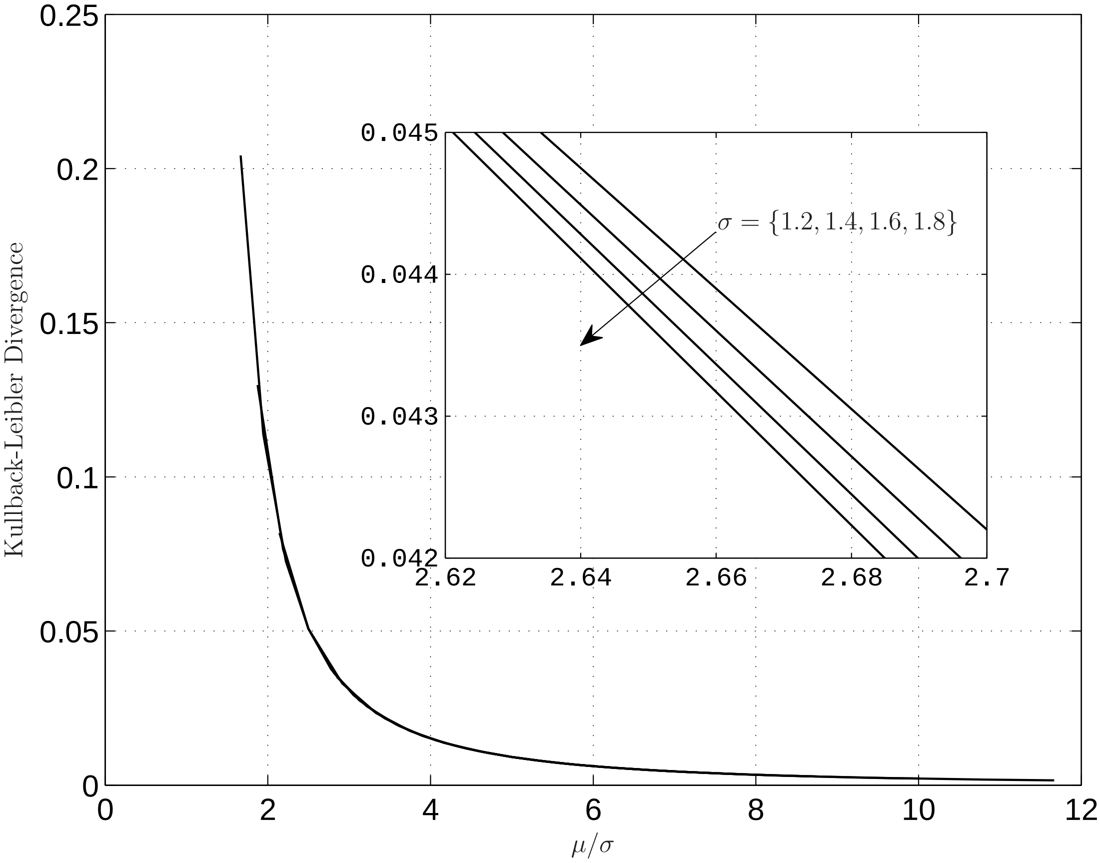

Figure 2.1: KL Divergence of the Gaussian and Nakagami Distribution.

Substituting equation (2.22) in (2.21), we have

$$1 - \frac{1}{8m_{ij}} + \frac{1}{128m_{ij}^2} \approx c, \tag{2.23}$$

where

$$c \approx \sqrt{1 - \frac{\sigma^2}{\Omega_{ij}}}. \tag{2.24}$$

Therefore, the shape parameter of the ND is

$$m_{ij} \approx \frac{1 + \sqrt{2c-1}}{16(1-c)}. \tag{2.25}$$

2.3 Error Estimation via Gaussian Kernel

In [46], an error bound formulation was derived using a Gaussian Kernel (GK) method to model the PDF of the bias b_{ij}. This was done to allow the ranging errors due to Gaussian noise n_{ij} and bias b_{ij} to be modeled separately and independently. In this Chapter, we modify the work in [46] to enable the noise and bias to be modeled jointly as the residual noise v_{ij}, due to the inseperability of LOS noise from NLOS bias in a wireless environment.

2.3.1 Error Distribution Reconstruction

The PDF of the residual noise v_{ij} is firstly created from samples. This is, of course, an approximation of the true distribution by building a sum of kernels (exponentially decaying function) of each collected samples, whose accuracy depends on the number P of samples collected. Having defined Sv_{ijq} as the q-th sample over the link between the i-th and j-th nodes, the non-parametric GK method can estimate the PDF of the residual noise using

$$f_{v_{ij}}(v_{ij}) = \frac{1}{\sqrt{2\pi}Ph_{ij}} \sum_{q=1}^{P} \exp\left(-\frac{(v_{ij} - Sv_{ijq})^2}{2h_{ij}^2}\right), \tag{2.26}$$

where $\exp(-)$ is the Gaussian kernel exponential function and the smoothing constant h_{ij} is the width of this Gaussian kernel function given as $1.06\sigma_s P^{-1/5}$ (σ_s is the sample standard deviation of the residual noise).

2.3.2 Bounds Derivation using Gaussian Kernel

Following the same approach as in Subsection 2.2.4, the natural logarithm of equation (2.26) can be substituted into $\frac{\partial l_{kl}}{\partial x_k}, \frac{\partial l_{kl}}{\partial y_k}, \frac{\partial l_{kl}}{\partial x_l}$ and $\frac{\partial l_{kl}}{\partial y_l}$ obtaining

$$\begin{aligned}
\frac{\partial l_{kl}}{\partial x_k} &= \frac{x_k - x_l}{d_{kl}} \frac{g_{kl}(v_{kl})}{f_{v_{kl}}(v_{kl})}, \\
\frac{\partial l_{kl}}{\partial y_k} &= \frac{y_k - y_l}{d_{kl}} \frac{g_{kl}(v_{ij})}{f_{v_{kl}}(v_{kl})}, \\
\frac{\partial l_{kl}}{\partial x_l} &= -\frac{x_k - x_l}{d_{kl}} \frac{g_{kl}(v_{ij})}{f_{v_{kl}}(v_{kl})}, \\
\frac{\partial l_{kl}}{\partial y_l} &= -\frac{y_k - y_l}{d_{kl}} \frac{g_{kl}(v_{kl})}{f_{v_{kl}}(v_{kl})},
\end{aligned} \tag{2.27}$$

where

$$g_{kl}(v_{kl}) = \frac{1}{\sqrt{2\pi} P h_{ij}} \sum_{t=1}^{P} \exp\left(-\frac{(v_{kl} - Sb_{klt})^2}{2h_{kl}^2}\right) \frac{v_{kl} - Sb_{klt}}{h_{kl}^2}. \tag{2.28}$$

and the element of the FIM are the same as in equation (2.14) with the only exception of:

$$A_{kl} = \mathbb{E}\left[\left(\frac{g_{kl}(v_{kl})}{f_{v_{ij}}(v_{kl})}\right)^2\right] = \int_{-\infty}^{\infty} \frac{g_{kl}(v_{kl})^2}{f_{v_{kl}}(v_{kl})} \mathrm{d}v_{kl}. \tag{2.29}$$

The FIM computed as above is still valid in LOS environment. In this case, A_{kl} is given as:

$$\mathbf{A}_{kl} = \begin{cases} \frac{1}{\sigma_{kl}^2} & kl \in \text{LOS} \\ \int_{-\infty}^{\infty} \frac{g_{kl}(v_{kl})^2}{f_{v_{kl}}(v_{kl})} \mathrm{d}v_{kl}. & kl \in \text{NLOS}. \end{cases} \tag{2.30}$$

where $kl \in$ LOS and $kl \in$ NLOS represent that propagation paths between devices k and l are LOS and NLOS paths, respectively.

2.4 Error Estimation via Edgeworth Expansion

The error estimation method presented in the previous section, although robust, is limited by the large amount of samples required to get a decent accuracy. In the following, we introduce a more efficient and general method, based on the EE, with two pratical advantages: a much lower number of required samples and the possibility to jointly model both the Gaussian noise and the bias. While the importance of reducing the dependence from the number of samples is self-evident, it is also fundamental to remark that, in practical wireless channels, bias and Gaussian errors cannot be separated from one another.

First we describe the process of reconstructing the error distribution from samples, then we prove the convergence of sample moments proving a clear improvement, in terms of efficiency with respect to the GK method, and finally we derive the new formulation of PEB and CRLB.

2.4.1 Error Distribution Reconstruction

The Edgeworth Expansion as an improvement on the Central Limit Theorem (CLT) is a true asymptotic series or expansion of the PDF of a normalized variable $\hat{x} = (x-\mu)/\sigma$ in the powers of the mean μ. As a true asymptotic expansion,it is a formal series of functions that has the attribute of been able to truncate a series after some specific finite number of terms, which is therefore sufficient enough to provide an accurate approximation or estimation to this given function, wherein the approximation error is controlled [48].

The EE as a non-parametric estimator can be used for approximating the PDF of given error measurements from their sample moments α_w [48]. The EE is given as

$$f(x) = \mathcal{N}(\mu, \sigma^2) \left[1 + \sum_{s=1}^{\infty} \sigma^s \sum_{\{k_w\}} He_{s+2r}(\hat{x}) \prod_{w=1}^{s} \frac{1}{k_w!} \left(\frac{S_{w+2}}{(w+2)!} \right)^{k_w} \right], \tag{2.31}$$

where, $\mathcal{N}(\mu, \sigma^2)$ is the PDF of a Gaussian distribution with mean μ and variance σ^2, $S_{w+2} = \frac{\kappa_{w+2}}{\kappa_2^{w+1}}$, κ_w are the cumulants obtained from the sample moments α_w as

$$\kappa_s = s! \sum_{\{k_w\}} (-1)^{(r-1)} (r-1)! \prod_{w=1}^{s} \frac{1}{k_w!} \left(\frac{\alpha_w}{w!} \right)^{k_w}. \tag{2.32}$$

The set $\{k_w\}$ consists of all non-negative integer solutions of the Diophantine set of equations $s = k_1 + 2k_2 + \cdots + sk_s$ and $r = k_1 + k_2 + \cdots + k_s$. The Chebyshev-Hermite polynomial $He_n(\hat{x})$ is given as

$$He_s(\hat{x}) = s! \sum_{k=0}^{s/2} \frac{(-1)^k \hat{x}^{s-2k}}{k!(s-2k)!2^k}. \tag{2.33}$$

The mean and variance of the given error measurements are $\mu = \alpha_1$ and $\sigma^2 = \kappa_2$, respectively.

The sample moments from the given error measurements are

$$\alpha_w = 1/n \sum_{i=1}^{n} {X_i}^w, \tag{2.34}$$

where X_i are the measurement errors and $w = 1, 2, \ldots$ are the orders of the moment.

To determine the number of orders of moment α_w required to approximate a given sample, the standard error s of the samples is calculated using $\sigma_s^2/\sqrt{P}$, where s must be ≤ 0.3, for each order w.

The EE is directly used to model the residual noise v_{ij}. Hence, the estimated PDF of the residual noise $f_{v_{ij}}(v_{ij})$ is given as

$$f_{v_{ij}}(v_{ij}) = \frac{1}{\sqrt{2\pi\sigma_{ij}^2}} \exp\left(-\frac{(v_{ij}-\mu)^2}{2\sigma_{ij}^2}\right)\left(1 + \sum_{s=1}^{\infty} \sigma^s \sum_{\{k_w\}} A_s He_{s+2r}(\hat{x})\right), \tag{2.35}$$

where $A_s = \prod_{w=1}^{s} \frac{1}{k_w!}\left(\frac{S_{w+2}}{(w+2)!}\right)^{k_w}$ and $v_{ij} = r_{ij} - d_{ij}$.

2.4.2 Convergence of Sample Moments and Efficiency over Gaussian Kernel Method

To prove the efficiency and effectiveness of the EE method, it is first necessary to show the convergence of sample moments as P increases (using the ND as in Section 2.2) [55], then to compare its efficiency over the GK method.

In Figure 2.2, the true moments γ_w of a ND ($m = 1, \Omega = 1$) is compared with sample moments α_w from Nakagami distributed random variables [55] using different number of samples, for moment orders $w = 1, \ldots, 4$. The error $\hat{e}_w$ contained in the sample moments is calculated using the absolute value of $(\alpha_w - \gamma_w)/\gamma_w$.

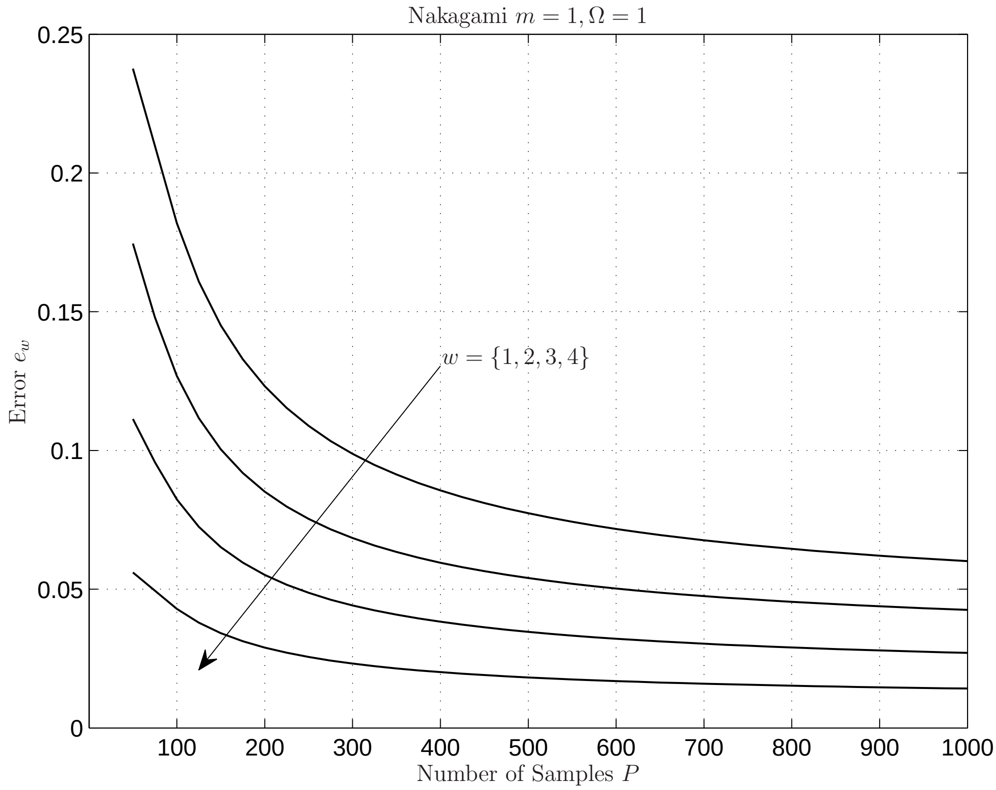

Figure 2.2: Convergence of Sample Moments α_w

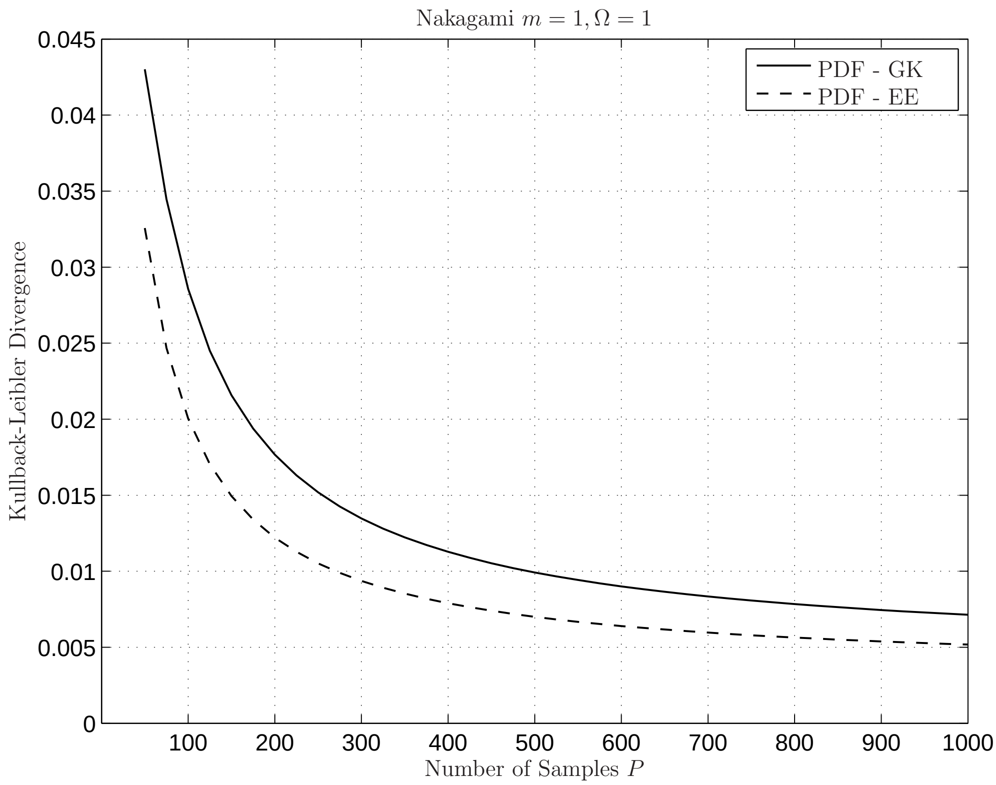

Figure 2.3: KL Divergence of the two non-parametric estimators

In Figure 2.3, we plotted the KLDs of the PDFs reconstructed with the two methods (GK and EE) with respect to the theoretical Nakagami PDF. For KLD=0.01, our EE method requires less than 300 samples, while the GK needs approximately 500 samples. This delta increases even more for lower level of divergency: to reach a KLD=0.0075, the GK method needs almost twice the number of samples (800 vs 400) than the EE method. As a result, the EE method is good selection for reconstructing error distribution from samples.

2.4.3 Bounds Derivation using Edgeworth Expansion

Given the formulation of the reconstructed PDF of the residual error in equation (2.35), the creation of the FIM is quite similar to the GK method: by taking its natural logarithm and substituting it into $\frac{\partial l_{kl}}{\partial x_k}, \frac{\partial l_{kl}}{\partial y_k}, \frac{\partial l_{kl}}{\partial x_l}$ and $\frac{\partial l_{kl}}{\partial y_l}$ yields

$$\begin{aligned}
\frac{\partial l_{kl}}{\partial x_k} &= \frac{x_k - x_l}{d_{kl}} \left(\frac{v_{kl} - \mu}{\sigma_{kl}^2} - \frac{g_{kl}(v_{kl})}{\sigma_{kl} f_{v_{kl}}(v_{kl})} \right), \\
\frac{\partial l_{kl}}{\partial y_k} &= \frac{y_k - y_l}{d_{kl}} \left(\frac{v_{kl} - \mu}{\sigma_{kl}^2} - \frac{g_{kl}(v_{kl})}{\sigma_{kl} f_{v_{kl}}(v_{kl})} \right), \\
\frac{\partial l_{kl}}{\partial x_l} &= -\frac{x_k - x_l}{d_{kl}} \left(\frac{v_{kl} - \mu}{\sigma_{kl}^2} - \frac{g_{kl}(v_{kl})}{\sigma_{kl} f_{v_{kl}}(v_{kl})} \right), \\
\frac{\partial l_{kl}}{\partial y_l} &= -\frac{y_k - y_l}{d_{kl}} \left(\frac{v_{kl} - \mu}{\sigma_{kl}^2} - \frac{g_{kl}(v_{kl})}{\sigma_{kl} f_{v_{kl}}(v_{kl})} \right),
\end{aligned} \tag{2.36}$$

where

$$g_{kl}(v_{kl}) = \frac{1}{\sqrt{2\pi\sigma_{ij}^2}} \exp\left(-\frac{(v_{ij} - \mu)^2}{2\sigma_{ij}^2} \right) \sum_{s=1}^{\infty} \sigma^s \sum_{\{k_m\}} (s + 2r) A_s He_{s+2r-1}(\hat{x}). \tag{2.37}$$

The element of the FIM are the same as in equation (2.14) with the only exception of:

$$\begin{aligned}
A_{kl} &= \mathbb{E}\left[\left(\frac{v_{kl} - \mu}{\sigma_{kl}^2} - \frac{g_{kl}(v_{kl})}{\sigma_{kl} f_{v_{kl}}(v_{kl})} \right)^2 \right] \\
&= \int_{-\infty}^{\infty} \left(\frac{v_{kl} - \mu}{\sigma_{kl}^2} - \frac{g_{kl}(v_{kl})}{\sigma_{kl} f_{v_{kl}}(v_{kl})} \right)^2 f_{v_{kl}}(v_{kl}) \mathrm{d}v_{kl}.
\end{aligned} \tag{2.38}$$

2.5 Performance Evaluation

Beyond the theoretical analysis of the previous sections, stating that the EE methods can reconstruct the statistics of the ranging error, using Nakagami Distribution, with less number of samples or with more accuracy with respect to the GK method, we now consider some network realization to better evaluate the performances of these two methods. To this end, we employ a region of $14m \times 14m$ where three ($a_n = 3$) anchors are placed at corners to form a triangle and three ($n = 3$) blindfolded devices (targets), not connected together, are randomly placed in this region.

From the FIM two types of error bounds are derived to evaluate the performance of the estimators: the CRLB and the PEB. The average CRLB, given this network realization, can be computed as

$$\bar{\varepsilon} = \frac{1}{n}\,\mathrm{Tr}\{\mathbf{J}^{-1}\}, \tag{2.39}$$

while the PEB is graphically represented by the 95% *Fisher Ellipse* (Confidence Interval $C_i = 0.95$), whose mathematical formulation is explained.

The Fisher Ellipse parameters of the i-th target $\boldsymbol{\theta}_i$ are obtained directly from its covariance matrix $\boldsymbol{\Omega}_{\boldsymbol{\theta}_i}$, which includes the error variance $\sigma^2_{i:\mathrm{x}}$ and $\sigma^2_{i:\mathrm{y}}$ on the "x" and "y" dimensions, respectively and the cross-term $\sigma_{i:\mathrm{xy}}$, is given as

$$\boldsymbol{\Omega}_{\boldsymbol{\theta}_i} \triangleq \begin{bmatrix} \sigma^2_{i:\mathrm{x}} & \sigma_{i:\mathrm{xy}} \\ \sigma_{i:\mathrm{xy}} & \sigma^2_{i:\mathrm{y}} \end{bmatrix}. \tag{2.40}$$

The directions of the scattering in the space for the vector $\boldsymbol{\theta}_i$ are known to be proportional, up to a factor κ_i, to the eigenvalues associated to $\boldsymbol{\Omega}_{\boldsymbol{\theta}_i}$ [45, 56]. In particular, the axis of the ellipse that describes this scattering in the space are given by $2\sqrt{\kappa_i \lambda_{i:1}}$, $2\sqrt{\kappa_i \lambda_{i:2}}$, where

$$\lambda_{i:1} \triangleq \frac{1}{2}\left[\sigma^2_{i:\mathrm{x}} + \sigma^2_{i:\mathrm{y}} + \sqrt{(\sigma^2_{i:\mathrm{x}} - \sigma^2_{i:\mathrm{y}})^2 + 4\sigma^2_{i:\mathrm{xy}}}\right], \tag{2.41}$$

$$\lambda_{i:2} \triangleq \frac{1}{2}\left[\sigma^2_{i:\mathrm{x}} + \sigma^2_{i:\mathrm{y}} - \sqrt{(\sigma^2_{i:\mathrm{x}} - \sigma^2_{i:\mathrm{y}})^2 + 4\sigma^2_{i:\mathrm{xy}}}\right]. \tag{2.42}$$

If $\sigma_{i:\mathrm{y}} > \sigma_{i:\mathrm{x}}$, then equations (2.41) and (2.42) in order to compute $\lambda_{i:1}$ and $\lambda_{i:2}$ are simply swapped.

The proportionality factor κ_i is related to the confidence interval C_i that target $\boldsymbol{\theta}_i$ is enclosed in the ellipse, is given by

$$\kappa_i = -2\ln(1 - C_i)\ . \tag{2.43}$$

It follows that the Fisher Ellipse for the i-th target $\boldsymbol{\theta}_i$ is described through the following equation [56]

$$\frac{[(x - p_{i:\mathrm{x}})\cos\gamma_i + (y - p_{i:\mathrm{y}})\sin\gamma_i]^2}{\kappa_i \cdot \lambda_{i:1}} + \frac{[(x - p_{i:\mathrm{x}})\sin\gamma_i - (y - p_{i:\mathrm{y}})\cos\gamma_i]^2}{\kappa_i \cdot \lambda_{i:2}} = 1\ , \tag{2.44}$$

where the *rotation angle* γ_i describes the offset between the principal axis for the ellipse and reference axis and it is defined as [1]

$$\gamma_i \triangleq \frac{1}{2}\arctan\left(\frac{2\sigma_{i:\mathrm{xy}}}{\sigma^2_{i:\mathrm{x}} - \sigma^2_{i:\mathrm{y}}}\right). \tag{2.45}$$

Figure 2.4 illustrates the level of accuracy of the reconstructed CRLBs $\bar{\varepsilon}$, as a function of the number of samples collected P using Nakagami distributed residual noise with b_{ij} uniformly selected between $0 - 4$ for NLOS and $\sigma = 0.5$ for both LOS and NLOS errors. To help the comparison, it has been added to the plot also a line representing the theoretical CRLB, i.e. computed with perfect knowledge of the statistic of the channel. Clearly the EE-reconstructed CRLB is much closer to the theoretical one than its GK alternative: the latter can not reach the accuracy of the former, even for a huge number of samples.

First, the minimum number of samples P required for obtaining relatively accurate results using the above derived CRLBs are analyzed. As it is illustrated in Figure 2.3, that the non-parametric estimators converges to the PDF with sufficient number of samples, therefore the estimated CRLB will converge to a stable value as P increases.

In Figure 2.5, for $P = 50$ samples collected per link, are now represented by their respective Fisher ellipses (theoretical and reconstructed with the two methods). Only those reconstructed with the EE almost perfectly match the theoretical PEB, with only a slight difference in the axis orientation. For $P = 250$ samples collected per link, the respective Fisher ellipses of the two reconstruction methods both have almost or matching axis orientation to the theoretical PEB with the EE method much closer in the axis lengths than the GK method.

[1] For $\sigma^2_{i:\mathrm{x}} = \sigma^2_{i:\mathrm{y}}$ then $\gamma_i = 0$.

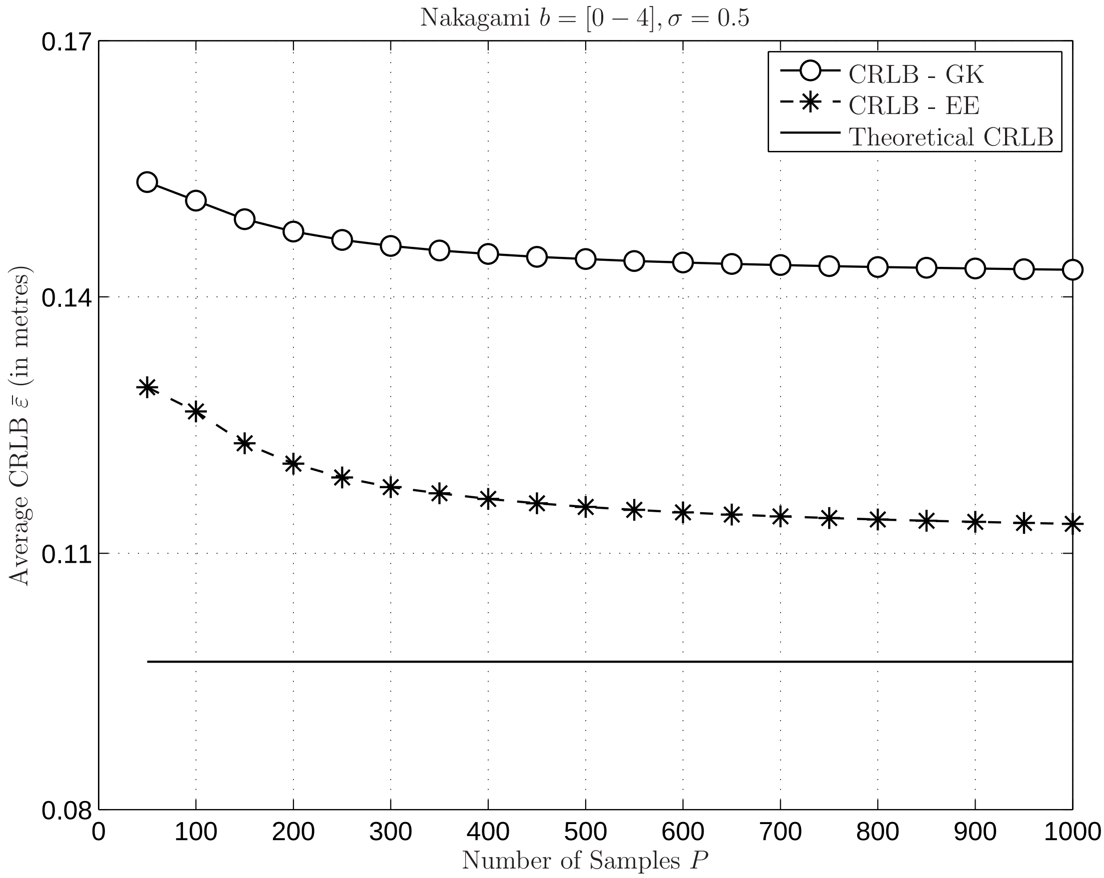

Figure 2.4: Average CRLB as a function of the number of samples.

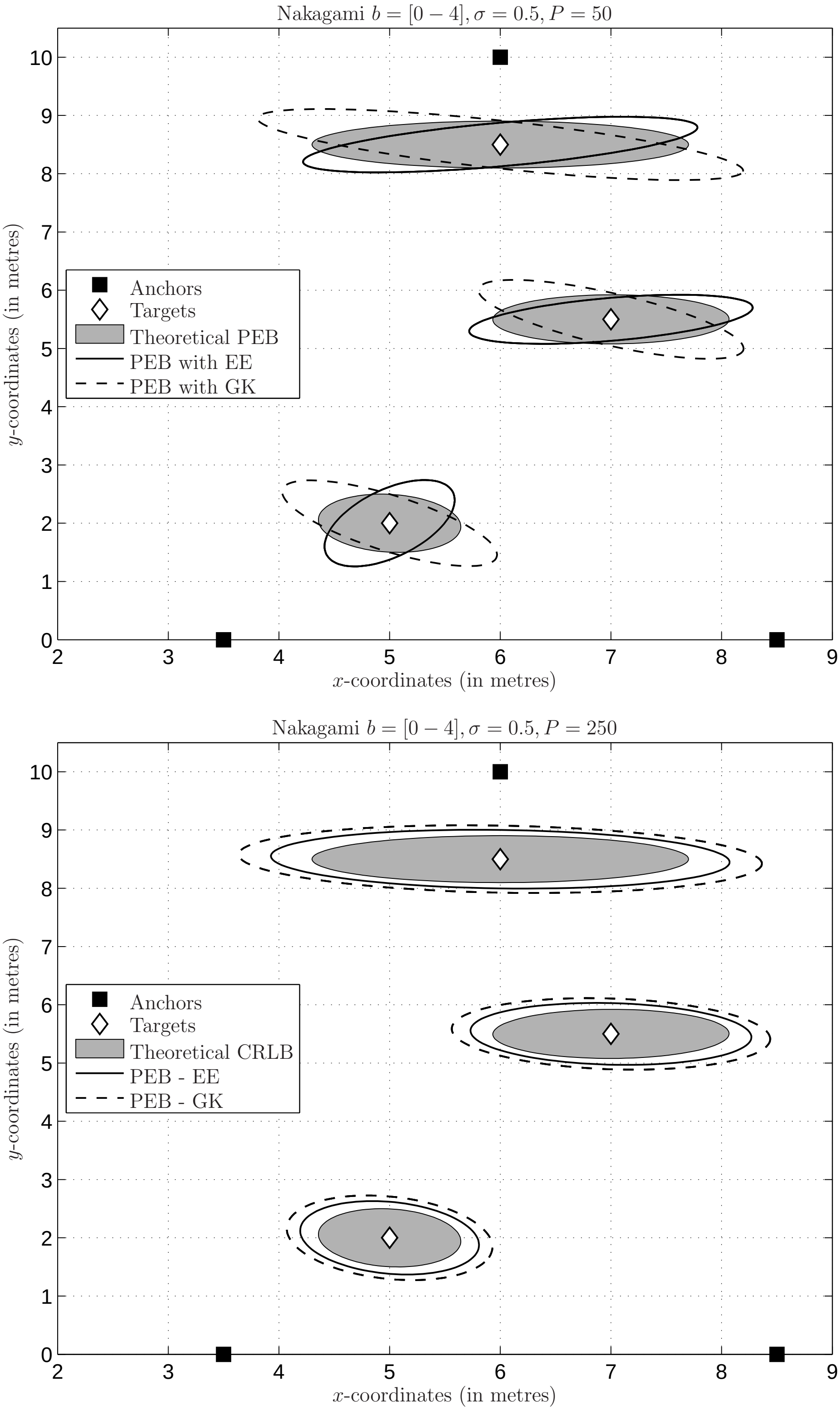

Figure 2.5: The 95% Fisher ellipses, theoretical, and estimated with $P = 50, 250$ samples collected per link.

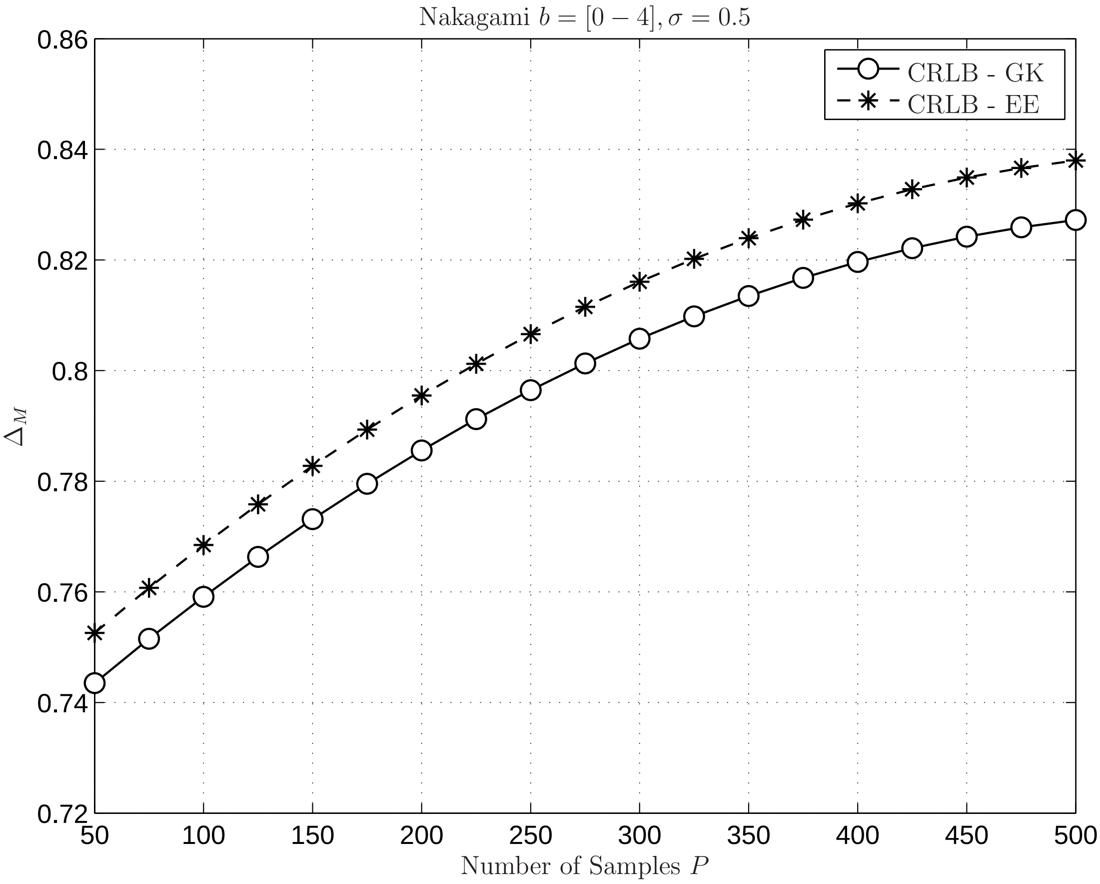

Figure 2.6: Δ as a function of the number of samples.

To better capture the differences in the PEB estimation, with respect to the theoretical PEB, Figure 2.6 illustrates, as a function of the number of samples, the position error bound inner product Δ, given as

$$\Delta \triangleq \frac{1}{N_t}\sum_{i=1}^{N_t}\frac{\langle \hat{A}_i \cdot A_i \rangle}{\sqrt{\hat{A}_i A_i}}, \tag{2.46}$$

where $\langle\cdot\rangle$ denotes the inner product, A is the area of the theoretical Fisher ellipse and $\hat{A}$ of the reconstructed methods (EE or GK method). It is seen that EE method performs much better than the GK method, which inherently implies that the reconstructed Fisher Ellipses of EE are closer in size and orientation to the theoretical Fisher Ellipses than that of GK, for all number of samples collected P as they both approach the maximum possible value 1.

2.6 Conclusions

The chapter focused on error analysis by estimating and reconstructing the statistics of the ranging error without a priori knowledge of the wireless channel. A well known method for non-parametric estimator, the Gaussian Kernel was used for the reconstruction of error distributions from samples and the corresponding error bound was derived.

We have proposed a new method, namely the Edgeworth Expansion, to reconstruct from samples the statistics of the measurement error by exploiting the power of moment convergence for Wireless Sensor Networks. This approach was proven to be valid both in Line-of-Sight and Non-Line-of-Sight conditions, and in conditions when it impossible to estimate a priori the statistics of the ranging error.

The two methods were compared against each other using two error bounds – the Cramèr-Rao Lower Bound and Position Error Bound, which were derived to evaluate their performance of the estimators. Results showed that the Edgeworth Expansion technique is more efficient and performs better than the Gaussian Kernel method, requiring much lesser number of samples to reach the same accuracy.

Chapter 3

Optimized Superresolution Ranging

3.1 Introduction

In wireless localization, loads of research have gone into determining the distance between devices using some of the widely known traditional techniques such as Received Signal Strength (RSS), Time of Arrival (ToA), Time Difference of Arrival (TDoA) and Phase-Difference of Arrival (PDoA) [20, 25, 57, 58].

The choice on selecting the technique that better fits the ranging needs, is usually based on a complicated trade off between precision, accuracy, costs, reliability as well as the network scenario. A ranging algorithm which can produce distance estimates from ranging measurements, irrespective of the technique is desirable in WSN. In this chapter, we seek to propose an efficient and accurate algorithm which is applicable to any ranging technique, as it only requires integer multiple measurements irrespective of the technique used as its input.

Taking into account a scenario in which the scarcity of LOS connections between devices is an important feature to be considered. Indoor scenario is a very common example of this, as a consequence, solutions based on AoA or RSS (known to be highly affected by multipath propagation and NLOS paths) are known to be suboptimal.

A possible alternative is the ToA, which is highly suited for indoor scenarios though multhipath propagation exists. One of the challenges in ranging is the accuracy, which critically depends upon the accuracy with which the arrival time is measured at the transmitting end. Various works have been proposed to accurately measure ToA [15,16], for simplicity, the Two-Way Ranging (TWR) technique is selected for analysis.

Here, we propose a ranging technique by applying and optimizing superresolution algorithms such as Multiple Signal Classification (MUSIC) and Root Multiple Signal Classification (RMUSIC) over ToA measurements using a sparse ruler/sequence. Superresolution algorithms are frequency estimation techniques which are subspace methods for direction-determining spectrum which are based on the eigendecomposition structure of the covariance (autocorralated) matrix for estimating the Direction of Arrival (DoA) of incoming source signals [59–61]. These techniques totally depend on the following properties of the covariance matrix of an incoming source signal, which are: the vector space spanned by its eigenvectors are partitioned into two orthogonal subspaces, the signal only subspace and the noise only subspace; the steering vectors corresponding to the direction of the incoming source signal are orthogonal to the noise only subspace assuming the incoming signals are uncorrelated. These subspace-based algorithms have received wide attention and usage because of their relatively high resolution and computational simplicity as well as their ability to reach the CRLB, provided the SNR of the incoming source signal is large enough to enable the resolution of distinct peaks in the estimated distance spectrum [62, 63].

The main parts of this chapter are standardized as follows: in Section 3.2 a brief mathematical description of the ToA-based TWR scheme and CRLB are given. Section 3.3 introduces the mathematical formulation of the proposed superresolution ranging algorithm and their optimized implementation for distance estimation. Result and comparison follow in Section 3.5, while conclusions remarks of the contributions of this chapter are presented in Section 3.6.

3.2 Time of Arrival-based Two-Way Ranging

Consider the problem of estimating the distance d between a reference node (anchor) A and a target node T based on ToA measurements. Using the standard TWR technique [15, 16], the estimate distance $\tilde{d}$ is given as

$$\tilde{d} = \left[(\tau_{\mathrm{RX:1}} - \tau_{\mathrm{TX:1}}) - \tau_{\mathrm{T}}\right] \cdot \frac{c}{2}\,, \tag{3.1}$$

where τ_{TX} is signal transmitted time, τ_{RX} is the signal received time, τ_{T} is the retransmission delay at device T and c is the speed of light.

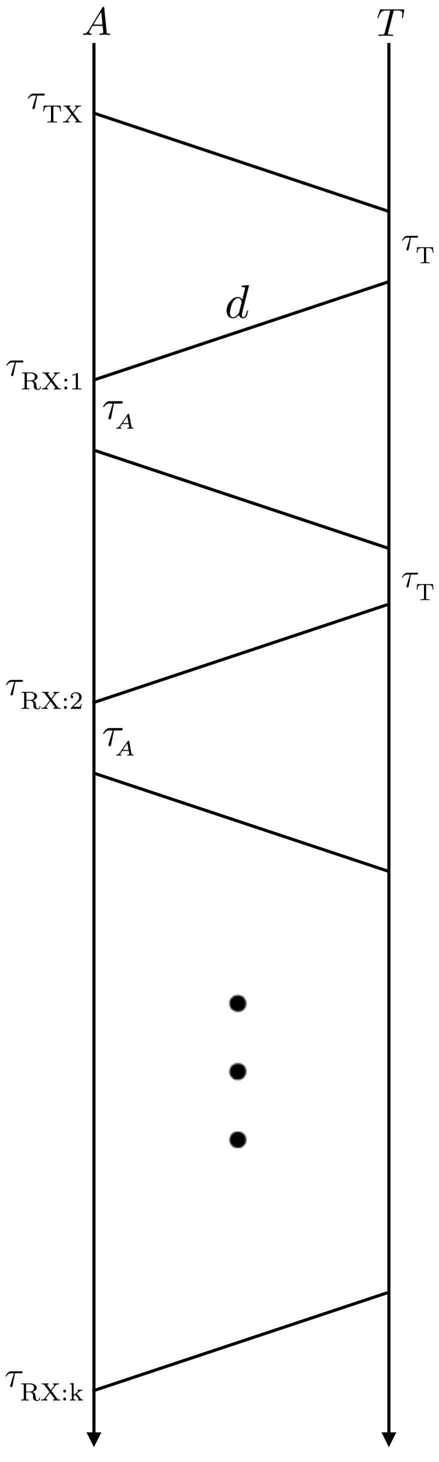

Figure 3.1: Multiple uniform Two-Way Ranging Model. A total of K measurements are performed starting at τ_{TX} up to $\tau_{\mathrm{RX:K}}$.

A single measurement is sufficient to estimate the distance between the devices, but this procedure can be repeated multiple times to obtain a more accurate estimate where the transmitted signal travels multiple round trip times as in Figure 3.1.

From the k-th round trip measurement obtained at receiver, the corresponding k-th distance estimate is given as

$$\begin{aligned} d_1 &= \left[(\tau_{\mathrm{RX}} - \tau_{\mathrm{TX}}) - \tau_t\right] \cdot \frac{c}{2}\,, \\ &\;\;\vdots \\ d_k &= \left[(\tau_{\mathrm{RX:k}} - \tau_{\mathrm{TX}}) - k\tau_{\mathrm{T}} - (k-1)\tau_{\mathrm{S}}\right] \cdot \frac{c}{2k}\,, \end{aligned} \tag{3.2}$$

where the distances are non-identical due to different round trip noises.

Without loss of generality (w.l.g.), τ_{S} and τ_{T} are assumed to be zero, since they serve no mathematical purpose, and therefore

$$kd_k = \frac{c(\tau_{\mathrm{RX:k}} - \tau_{\mathrm{TX}})}{2} = \frac{c\Delta\tau_k}{2}, \tag{3.3}$$

where $\Delta\tau_k$ is the Time of Arrival of the signal and $\frac{c\Delta\tau_k}{2}$ corresponds to integer distances (kd_k). This is to enable $\frac{c\Delta\tau_k}{2}$, which are then to be subject to Gaussian-distributed random variables with zero-mean and variance.

Therefore, $\frac{c\Delta\tilde{\tau}_k}{2}$ is modeled as a Gaussian distribution and its PDF is

$$\begin{aligned} P\Big(\frac{c\Delta\tilde{\tau}_k}{2}; \frac{c\Delta\tau_k}{2}, \sigma\Big) &= \frac{1}{\sqrt{2\pi}\sigma} \exp\left(-\frac{(\frac{c\Delta\tilde{\tau}_k}{2} - \frac{c\Delta\tau_k}{2})^2}{2\sigma^2}\right), \\ &= \frac{1}{\sqrt{2\pi}\sigma} \exp\left(-\frac{(k\tilde{d}_k - kd_k)^2}{2\sigma^2}\right). \end{aligned} \tag{3.4}$$

3.2.1 Cramér-Rao lower bound

From K samples of ToA measurements $\frac{c\boldsymbol{\Delta}\tilde{\boldsymbol{\tau}}}{2} \triangleq \{\frac{c\Delta\tilde{\tau}_1}{2}, \cdots, \frac{c\Delta\tilde{\tau}_K}{2}\}$ and using the PDF in equation (3.4), the likelihood function is given as

$$L\Big(\frac{c\Delta\tilde{\tau}_k}{2}; \frac{c\Delta\tau_k}{2}, \sigma\Big) = \prod_{k=1}^{K} \frac{1}{\sqrt{2\pi}\sigma} \exp\left(-\frac{(k\tilde{d}_k - kd_k)^2}{2\sigma^2}\right). \tag{3.5}$$

The log-likelihood function is given as

$$\begin{aligned}\ln L\Big(\frac{c\Delta\tilde{\tau}_k}{2};\frac{c\Delta\tau_k}{2},\sigma\Big) &= \ln\prod_{k=1}^{K}\frac{1}{\sqrt{2\pi}\sigma}\exp\left(-\frac{(k\tilde{d}_k-kd_k)^2}{2\sigma^2}\right),\\ &= \sum_{k=1}^{K}\left(\ln\frac{1}{\sqrt{2\pi}\sigma}-\frac{(k\tilde{d}_k-kd_k)^2}{2\sigma^2}\right).\end{aligned} \tag{3.6}$$

The gradient of the log-likelihood function is as follows

$$\begin{aligned}\frac{\partial\ln L\Big(\frac{c\Delta\tilde{\tau}_k}{2};\frac{c\Delta\tau_k}{2},\sigma\Big)}{\partial d} &= \frac{\partial}{\partial d}\sum_{k=1}^{K}\left(\ln\frac{1}{\sqrt{2\pi}\sigma}-\frac{(k\tilde{d}_k-kd_k)^2}{2\sigma^2}\right),\\ &= \sum_{k=1}^{K}\frac{k^2(\tilde{d}_k-d_k)}{\sigma^2}.\end{aligned} \tag{3.7}$$

The Hessian of the log-likelihood function is

$$\frac{\partial^2\ln L\Big(\frac{c\Delta\tilde{\tau}_k}{2};\frac{c\Delta\tau_k}{2},\sigma\Big)}{\partial d^2} = -\sum_{k=1}^{K}\frac{k^2}{\sigma^2}. \tag{3.8}$$

Finally, the Fisher Information J is given by

$$J = -\mathbb{E}\left[\frac{\partial^2\ln L(\frac{c\Delta\tilde{\tau}_k}{2};\frac{c\Delta\tau_k}{2},\sigma)}{\partial d^2}\right] = \sum_{k=1}^{K}\frac{k^2}{\sigma^2}, \tag{3.9}$$

where the key feature determining the Fisher information is $k = 1, \cdots, K$ and the CRLB is given as J^{-1}.

In the next sections, we present a standard and optimized implementation of two common superresolution algorithms used for reducing the SNR required for resolution.

3.3 Superresolution Ranging

Let us revisit the fundamental relationship between the Time of Arrival $\Delta\tau_k$ and distance estimate $\tilde{d}$ according to equation (3.3). Assume that a complete set of uniform round trip times ($\boldsymbol{\tau}_{\mathrm{RX}} = \{\tau_{\mathrm{RX:1}}, \cdots, \tau_{\mathrm{RX:K}}\}$) corresponding to ToA measurements are measured and collected,

$$\frac{c\boldsymbol{\Delta}\tilde{\boldsymbol{\tau}}}{2} \triangleq \left[\frac{c\Delta\tilde{\tau}_1}{2}, \cdots, \frac{c\Delta\tilde{\tau}_K}{2}\right]. \tag{3.10}$$

Taking the above vector $\frac{c\boldsymbol{\Delta}\tilde{\boldsymbol{\tau}}}{2}$ as the argument of the element-wise complex exponential function $g(x) = \exp(jx)$, we obtain

$$\begin{aligned} g\Big(\frac{c\boldsymbol{\Delta}\tilde{\boldsymbol{\tau}}}{2}\Big) &= [e^{\frac{jc\Delta\tilde{\tau}_1}{2}}, \cdots, e^{\frac{jc\Delta\tilde{\tau}_K}{2}}]^{\mathrm{T}} \\ &= [e^{j\tilde{d}}, \cdots, e^{jK\tilde{d}}]^{\mathrm{T}}. \end{aligned} \tag{3.11}$$

One can immediately recognize from equation (3.11), the similarity between the complex exponential vector $g(\frac{c\boldsymbol{\Delta}\tilde{\boldsymbol{\tau}}}{2})$ and the steering vector of a linear antenna array [59], which suggests that the parameter of interest (distance d), can be estimated using spectral superresolution techniques [60, 64] based on the concept of signal and noise subspaces for obtaining unbiased estimates of a single parameter.

3.3.1 Spectral MUSIC Approach

Multiple Signal Classification (MUSIC) algorithm is a very popular spectral search superresolution technique developed by R. O. Schmidt in [60] as a generalization and computation of Pisarenko harmonic decomposition [65]. The Pisarenko's method is a carrier frequency estimation technique, which assumes that a signal are composed of complex exponentials in the presence of additive white noise. This estimation scheme is quite limited as a priori knowledge of the number of complex exponentials is required.

Equally, the MUSIC algorithm as a frequency and also a DoA estimator can be applied to distance estimation problem, since the assumptions on the complex exponential vector $g(\frac{c\boldsymbol{\Delta}\tilde{\boldsymbol{\tau}}}{2})$ in equation (3.11) is that $\text{rank}(g(\frac{c\boldsymbol{\Delta}\tilde{\boldsymbol{\tau}}}{2})) = 1$ and the collected set of ToA measurements $\frac{c\boldsymbol{\Delta}\tilde{\boldsymbol{\tau}}}{2}$ are uniform.

The sample array covariance matrix $\mathbf{R}_{\mathrm{x}}$ is obtained as

$$\tilde{\mathbf{R}}_{\mathrm{x}} = g\Big(\frac{c\boldsymbol{\Delta}\tilde{\boldsymbol{\tau}}}{2}\Big) g\Big(\frac{c\boldsymbol{\Delta}\tilde{\boldsymbol{\tau}}}{2}\Big)^{\mathrm{H}}, \tag{3.12}$$

which has a fundamental property where the spanned space of the eigenvectors are partitioned into the two orthogonal subspaces – signal only subspace and noise only subspace.

The eigendecomposition of the sample covariance matrix $\tilde{\mathbf{R}}_{\mathrm{x}}$ yields

$$\tilde{\mathbf{R}}_{\mathrm{x}} = \underbrace{\tilde{\mathbf{e}}_{ss}\tilde{\mathbf{\Lambda}}_{ss}\tilde{\mathbf{e}}_{ss}^{\mathrm{H}}}_{\text{signal-subspace}} + \underbrace{\tilde{\mathbf{E}}_{ns}\tilde{\mathbf{\Lambda}}_{ns}\tilde{\mathbf{E}}_{ns}^{\mathrm{H}}}_{\text{noise-subspace}} \tag{3.13}$$

where the sample eigenvalues are sorted in descending order and the vector $\tilde{\mathbf{e}}_{ss} \triangleq [\tilde{\mathbf{e}}_1]_{K\times 1}$ and matrix $\tilde{\mathbf{E}}_{ns} \triangleq [\tilde{\mathbf{e}}_2, \cdots, \tilde{\mathbf{e}}_K]_{K\times K-1}$ contain in their columns the signal-subspace and noise-subspace eigenvectors of $\tilde{\mathbf{R}}_x$ respectively.

It is quite clear that the basis of noise-subspace $\tilde{\mathbf{E}}_{ns}$ formed by the $(K-1)$ eigenvectors associated with the $(K-1)$ smallest eigenvalues are orthogonal to the complex exponential vector $g(\frac{c\boldsymbol{\Delta}\tilde{\boldsymbol{\tau}}}{2})$ [60], and therefore

$$\begin{aligned} g\Big(\frac{c\boldsymbol{\Delta}\boldsymbol{\tau}}{2}\Big) &\perp \mathbf{E}_{ns} \\ g\Big(\frac{c\boldsymbol{\Delta}\boldsymbol{\tau}}{2}\Big)^{\mathrm{H}}\mathbf{E}_{ns}\mathbf{E}_{ns}^{\mathrm{H}}g\big(\frac{c\boldsymbol{\Delta}\boldsymbol{\tau}}{2}\big) &= 0, \end{aligned} \tag{3.14}$$

where $\perp$ depicts orthogonality between two vectors.

In view of the second part of equation (3.11), the spectral MUSIC estimates the distance $\tilde{d}$ between the pair of devices S and T from the maximum of the function

$$f(\tilde{d}) = \frac{1}{g\Big(\frac{c\boldsymbol{\Delta}\tilde{\boldsymbol{\tau}}}{2}\Big)^{\mathrm{H}}\tilde{\mathbf{E}}_{ns}\tilde{\mathbf{E}}_{ns}^{\mathrm{H}}g\Big(\frac{c\boldsymbol{\Delta}\tilde{\boldsymbol{\tau}}}{2}\Big)} \tag{3.15}$$

by searching over d using a fine grid as it exploits the orthogonality in equation (3.14).

3.3.2 Root MUSIC Approach

The Root MUSIC algorithm as an expansion of the spectral MUSIC minimizes its computational complexity by replacing the search of the minimum of $f(\tilde{d})$ by polynomial rooting, and its only solution is the distance estimate $\tilde{d}$ [64].

From the complex exponential vector in equation (3.11) is

$$\begin{aligned} \mathbf{g}(\tilde{d}) &= [e^{j\tilde{d}/a}, \cdots, e^{jK\tilde{d}/a}]^T \\ \mathbf{g}(z) &= [z^1, \cdots, z^K]^T, \end{aligned} \tag{3.16}$$

where $z \triangleq e^{j\tilde{d}/a}$ and a is introduced as the maximum possible estimate of the distance so as to avoid rotation due to the complex exponential function.

Similar to spectral MUSIC, the sample array covariance matrix $\tilde{\mathbf{R}}_{\mathrm{x}}$ and its eigendecomposition are obtained as shown in equations (3.12) and (3.13). From equation 3.15,

$$
\begin{aligned}
f(\tilde{d}) &= \mathbf{g}(z^{-1})^{\mathrm{T}}\tilde{\mathbf{E}}_{ns}\tilde{\mathbf{E}}_{ns}^{\mathrm{H}}\mathbf{g}(z) \triangleq f(z) \\
&= [z^{-1}, \cdots, z^{-K}] \begin{bmatrix} e_{11} & \cdots & e_{1K} \\ \vdots & \cdots & \vdots \\ e_{K1} & \cdots & e_{KK} \end{bmatrix} \begin{bmatrix} z^{1} \\ \vdots \\ z^{K} \end{bmatrix} \\
f(z) &= \sum_{l=-K+1}^{K-1} a_l z^l,
\end{aligned} \tag{3.17}
$$

where a_l is the sum of the lth diagonal entries of $\tilde{\mathbf{E}}_{ns}\tilde{\mathbf{E}}_{ns}^{\mathrm{H}}$ [64].

The polynomial $f(z)$ has $(2K-1)$ unitary modulus roots which form conjugate reciprocal pairs are

$$
z = e^{j\tilde{d}/a} \quad \text{and} \quad \bar{z} = e^{-j\tilde{d}/a}\ . \tag{3.18}
$$

Due to the presence of noise, the Root-Music computes all roots of $f(z)$ and estimates the distance $\tilde{d}$ by selecting the largest-magnitude root from those lying inside the circle.

Though the MUSIC and Root MUSIC algorithms are known to be very close to optimum for uncorrelated signals, they can be improved significantly. The problem is therefore not of the superresolution algorithms but how they are being used. Specifically, by optimizing the aperture of the collected set of ToA measurements.

3.4 Optimized Superresolution Ranging

For the optimization of the superresolution algorithm, nonuniform set of round trip times $\boldsymbol{\tau}_{\mathrm{RX}} = \{\tau_{\mathrm{RX:n}_1}, \cdots, \tau_{\mathrm{RX:n}_K}\}$ corresponding to ToA measurements are collected, by carefully and sparsely allocating the ranging slots/cycles according to a sparse ruler $\langle n_1, n_2, \cdots, n_K : n_1 = 0, n_K = L\rangle$.

The complete set of ToA measurements are

$$
\frac{c\boldsymbol{\Delta}\tilde{\boldsymbol{\tau}}}{2} \triangleq \left[\frac{c\Delta\tilde{\tau}_{n_1}}{2}, \cdots, \frac{c\Delta\tilde{\tau}_{n_K}}{2}\right]. \tag{3.19}
$$

as seen in Figure 3.2 with an added waiting time $\tau_{n_{K-1}} = (n_K - n_{K-1} - 1)\cdot(\tau_{\mathrm{RX:n}_1} - \tau_{\mathrm{TX}})$ at the source S for the elimination of some certain round trip times.

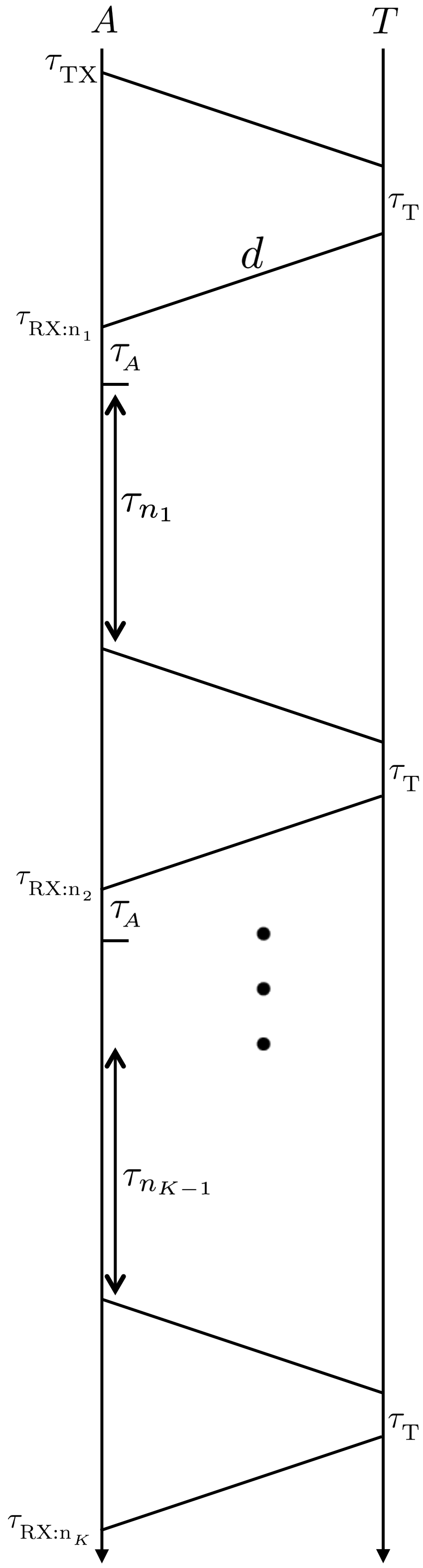

Figure 3.2: Multiple nonuniform two-way ranging Model. A total of K measurements are performed starting at τ_{TX} up to $\tau_{\mathrm{RX:n}_K}$

3.4.1 Features and Genetic Algorithm to Design a Sparse Ruler

As an undirected graph, a sparse ruler is a K-marks ordered sequence whose corresponding differences contain elements with little or no repetition [66]. The K-marks ruler consists of K distinct non-negative integers ($n_i < n_{i+1}$) such that there are $M = \frac{K(K-1)}{2}$ distance differences (unique/repeated)

$$n_j - n_i \quad (1 \leq i < j \leq K) \tag{3.20}$$

with no restrictions on its length N. There is no requirement that a sparse ruler should be able to measure all distances up to its length, when it does, it is called a perfect ruler which does not exists beyond four marks ($K = 4$) [67].

The design of a sparse ruler is a hard combinatorial problem and there is no general solution to its construction [68,69], nor can the known rulers be used in every application due features required. As a result, various heuristic techniques to design sparse rulers with specific features can therefore be found in the literature, including constraint programming, local search, and evolutionary or genetic algorithms [68, 70].

In the context of this section, the interest is to introduce sparse rulers so as to enable resource (time) optimization by carefully specifying that ranging cycles/frame $\boldsymbol{\tau}_{\text{RX}}$ are allocated in relation to a sparse ruler. To this end, we briefly describe a direct genetic algorithm to find sparse rulers with minimal or no repetition, which is a technique proposed by [71] through the steps below.

(i) Representation: Sparse rulers are exemplified by the markers and number of marks on the ruler. Another option of representation for sparse rulers is by the distance between successive markers of the ruler, which are known as the lengths of its segments. A sparse ruler can therefore be represented by the $K - 1$ distances indicating the lengths of its $K - 1$ segments that compose the K-mark ruler.

(ii) Initial Population: To ascertain the singleness of each segment length of a ruler, individuals or members in each segment sets of the initial population were chosen at random. This is done using a set of numbers 1 to $3K$ (maximum allowed segment in the length), then a monotonous sequence of random permutation between two individuals of the elements 2 through $3K$ is executed to assert segment length 1 is preserved among the elements of the segments in the ruler. Finally, the first $K - 1$ elements including segment length 1 are selected, and then randomized using this same swapping scheme.

(iii) Evaluation: Most genetic algorithms for obtaining sparse ruler are evaluated by minimizing fitness functions. For a ruler to be sparse, there exists two fitness criteria it must meet as well minimized, which are the overall length of the ruler (as short as possible) and number of repeats in the ruler (little similarity between distances it can measure). In most applications, the number of repeats is the most significant and must be as little as possible).

(iv) Mutation: There exist two kinds of mutation deployed in genetic algorithms: permutation and transmutation Permutation is the change in order between two segments while transmutation is the change in the segment lengths. Mutation is controlled for each segment element individually in the ruler through a mutation probability to determine if mutation occurs or not for each element. With the generation of the initial population, special preventative measures are taken to guarantee that segment length 1 is preserved in the ruler by restricting it to the permutation type of mutation as it was proven that all sparse rulers must have the segment of length 1 [68].

(v) Tournament Selection: This is used where a random number of individual rulers are selected from the population. Multiple parent rulers are chosen based on the individual rulers with the lowest fitness scores.

(vi) Crossover: A random number is compared to a crossover probability to determine if crossover will occur or not. If crossover is to be performed, it is done similar to partially mapped two point crossover, and if not, the two parents are also the two children. Before crossover the two parents are aligned with each other to reduce the prevent the possibility of crossover between two mirror images.

From different approaches studied, the best result is obtained corresponding to the exertion of a *high mutation and low crossover* genetic algorithm. A pseudo-code of the proposed genetic algorithm described above is given in Appendix A. In the next chapter, we introduce a new genetic algorithm for generating single optimal Golomb rulers as well as multiple sets of orthogonal Golomb rulers with more detailed explanation of the genetic algorithm.

With the use of a sparse ruler, the corresponding expanded ToA measurements differences

$$\frac{c\Delta\tilde{\tau}_{n_j}}{2} - \frac{c\Delta\tilde{\tau}_{n_i}}{2} \quad (1 \leq i < j \leq K) \tag{3.21}$$

are unique or with little repititions. The differences of the ToA measurements are

$$\frac{c\boldsymbol{\Delta}\tilde{\boldsymbol{\tau}}}{2} \triangleq \left[\frac{c\Delta\tilde{\tau}_{v_1}}{2}, \cdots, \frac{c\Delta\tilde{\tau}_{v_M}}{2}\right]., \tag{3.22}$$

where $[v_1, \cdots, v_M]$ denote the corresponding differences of the K-marks sparse ruler. With the aid of sparse ruler thinning, M ToA measurements have been obtained from measuring only K round trip times.

3.4.2 MUSIC and Root MUSIC Approach

The MUSIC and Root MUSIC algorithms can both be generally applied to all complete set of round trip times (uniform, nonuniform, and sparse), with the ToA measurements relating to integers ($v_m : m = 1, \cdots, M$).

From equation (3.22), the complex exponential vector becomes

$$\begin{aligned} g(\frac{c\boldsymbol{\Delta}\tilde{\boldsymbol{\tau}}}{2}) &= [e^{\frac{jc\Delta\tilde{\tau}_{v_1}}{2}}, \cdots, e^{\frac{jc\Delta\tilde{\tau}_{v_1}}{2}}]^T \\ &= [e^{jv_1\tilde{d}}, \cdots, e^{jv_M\tilde{d}}]^T. \end{aligned} \tag{3.23}$$

For MUSIC, the rest of the algorithm is similar to that of Subsection 3.3.1. For Root-MUSIC, the $M \times 1$ complex exponential vector is given as

$$\begin{aligned} \mathbf{g}(\tilde{d}) &= [e^{jv_1\tilde{d}/a}, \cdots, e^{jv_M\tilde{d}/a}]^T. \\ \mathbf{g}(z) &= [z^{v_1}, \cdots, z^{v_M}]^T, \end{aligned} \tag{3.24}$$

while the sample array covariance matrix $\tilde{\mathbf{R}}_{\mathrm{x}}$ and its eigendecomposition are estimated similarly as in equations (3.12) and (3.13).

From equation (3.15),

$$\begin{aligned} f(\tilde{d}) &= \mathbf{g}(z^{-1})^{\mathrm{T}}\tilde{\mathbf{E}}_{ns}\tilde{\mathbf{E}}_{ns}^{\mathrm{H}}\mathbf{g}(z) \triangleq f(z) \\ &= [z^{-v_1}, \cdots, z^{-v_M}] \begin{bmatrix} e_{v_1v_1} & \cdots & e_{v_1v_M} \\ \vdots & \cdots & \vdots \\ e_{v_Mv_1} & \cdots & e_{v_Mv_M} \end{bmatrix}, \begin{bmatrix} z^{v_1} \\ \vdots \\ z^{v_M} \end{bmatrix} \\ f(z) &= \sum_{l=-v_M+1}^{v_M-1} a_l z^l, \end{aligned} \tag{3.25}$$

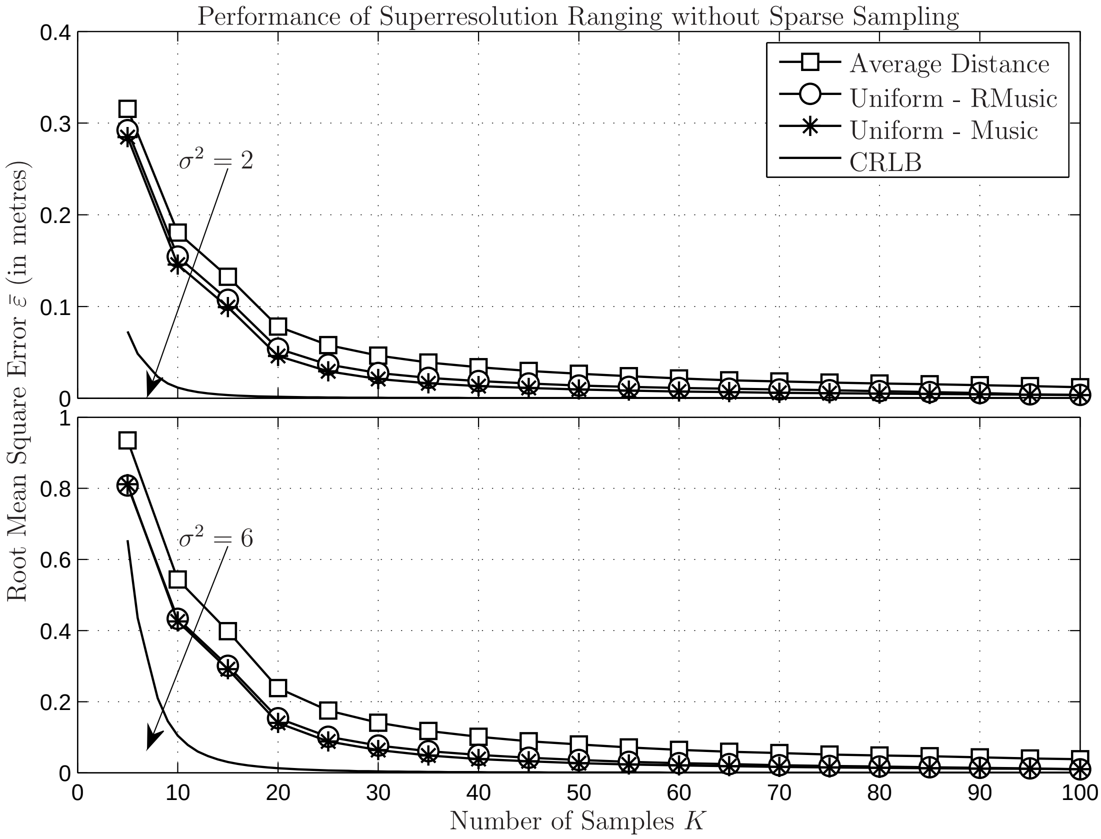

Figure 3.3: Performance of superresolution and average-based ranging algorithms as a function of the sample set sizes K, *without* Sparse-optimized sampling.

where a_l is the sum of the lth diagonal entries of $\tilde{\mathbf{A}}_{ns}\tilde{\mathbf{A}}_{ns}^{\mathrm{H}}$. The $v_M \times v_M$ matrix $\tilde{\mathbf{A}}_{ns}\tilde{\mathbf{A}}_{ns}^{\mathrm{H}}$ is formed as follows:

1. $\tilde{\mathbf{A}}_{ns}\tilde{\mathbf{A}}_{ns}^{\mathrm{H}}$ is firstly formed as a $v_M \times v_M$ zero matrix.
2. The (k_i, k_i) element of $\tilde{\mathbf{E}}_{ns}\tilde{\mathbf{E}}_{ns}^{\mathrm{H}}$ replace the corresponding (i, i) element of $\tilde{\mathbf{A}}_{ns}\tilde{\mathbf{A}}_{ns}^{H}$ for all $i = 1, \cdots, M$ i.e., the elements of $\tilde{\mathbf{E}}_{ns}\tilde{\mathbf{E}}_{ns}^{\mathrm{H}}$ replace the corresponding elements of $\tilde{\mathbf{A}}_{ns}\tilde{\mathbf{A}}_{ns}^{\mathrm{H}}$ of the same index.

The rest of the algorithm is similar to that of Subsection 3.3.2

3.5 Performance Evaluation

In this section, simulations were conducted so as to evaluate the performance of the spectral MUSIC and Root MUSIC superresolution algorithms using uniform and sparse ToA measurements, and compared against the Cramèr-Rao Lower Bound (CRLB) and averaging of distances obtained from ToA measurements, similar to equation (3.2) as a benchmark for the algorithms [72, 73].

The simulations were based on obtaining uniform or sparse sets of ToA measurements $\boldsymbol{\Delta\tilde{\tau}}$ (equations (3.10) and (3.19)) by adding Gaussian-distributed random variable with a zero mean and variance $\sigma^2 = 1, \cdots, 10$ to the integer distances (kd or $n_k d$) using equation (3.3). Considering the set of collected ToA measurements $\boldsymbol{\Delta\tilde{\tau}}$, the average distance estimates $\tilde{d}$ can be obtained as

$$\tilde{d} = \underbrace{\frac{1}{K}\sum_{k=1}^{K}\frac{c\Delta\tilde{\tau}_k}{2k}}_{uniform} \quad \text{or} \quad \underbrace{\frac{1}{K}\sum_{k=1}^{K}\frac{c\Delta\tilde{\tau}_{n_k}}{2n_k}}_{sparse}. \tag{3.26}$$

As seen in Figures 3.3 and 3.4, this technique is sub-optimum, as it requires a large n number of round trip times $\mathbf{T_{Rx}}$ to achieve a low RMSE and get close enough to the CRLB.

For uniformly collected ToA measurements, the superresolution algorithms perform much better than the average distance technique as their RMSE are much lower but still far off from CRLB, since they also require large K number of samples to achieve low RMSE in the Figures 3.3 and 3.4. The results of the superresolution algorithms using uniformly measured round trip times/ToA measurements are still sub-optimal.

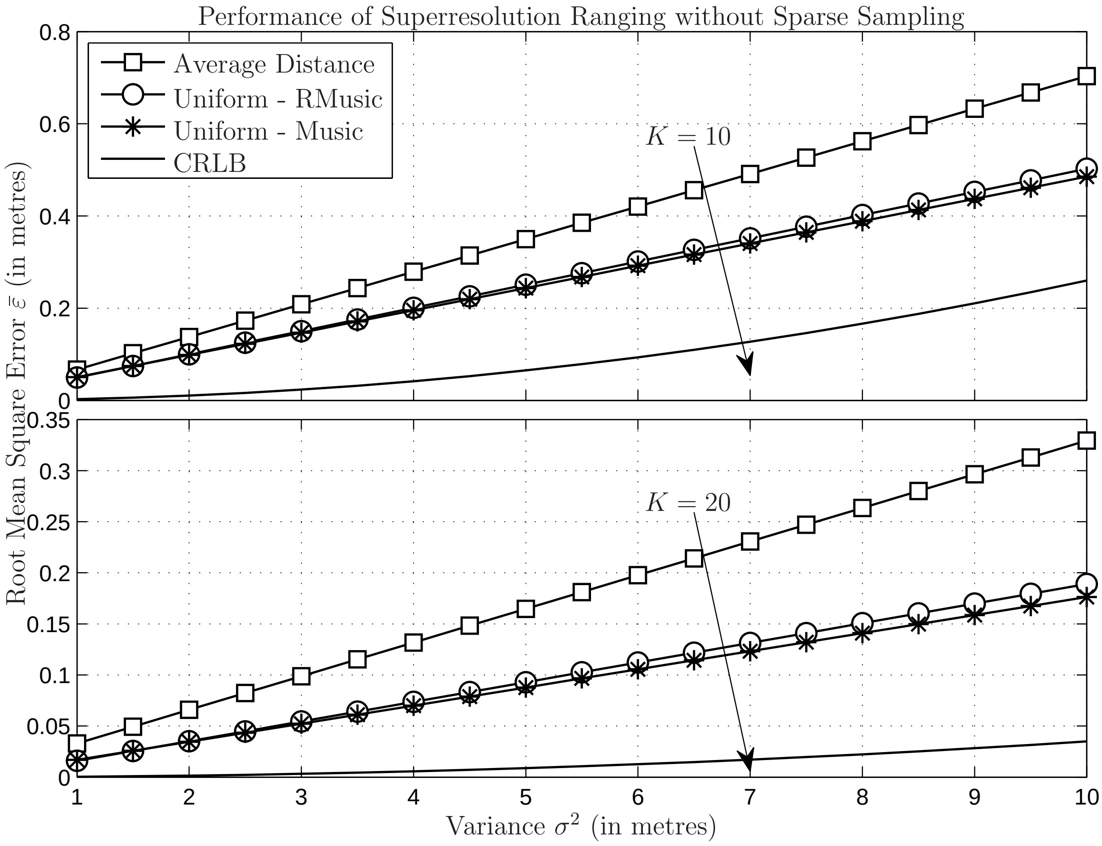

Figure 3.4: Performance of superresolution and average-based ranging algorithms as a function of the ToA error variance σ^2, *without* Sparse-optimized sampling.

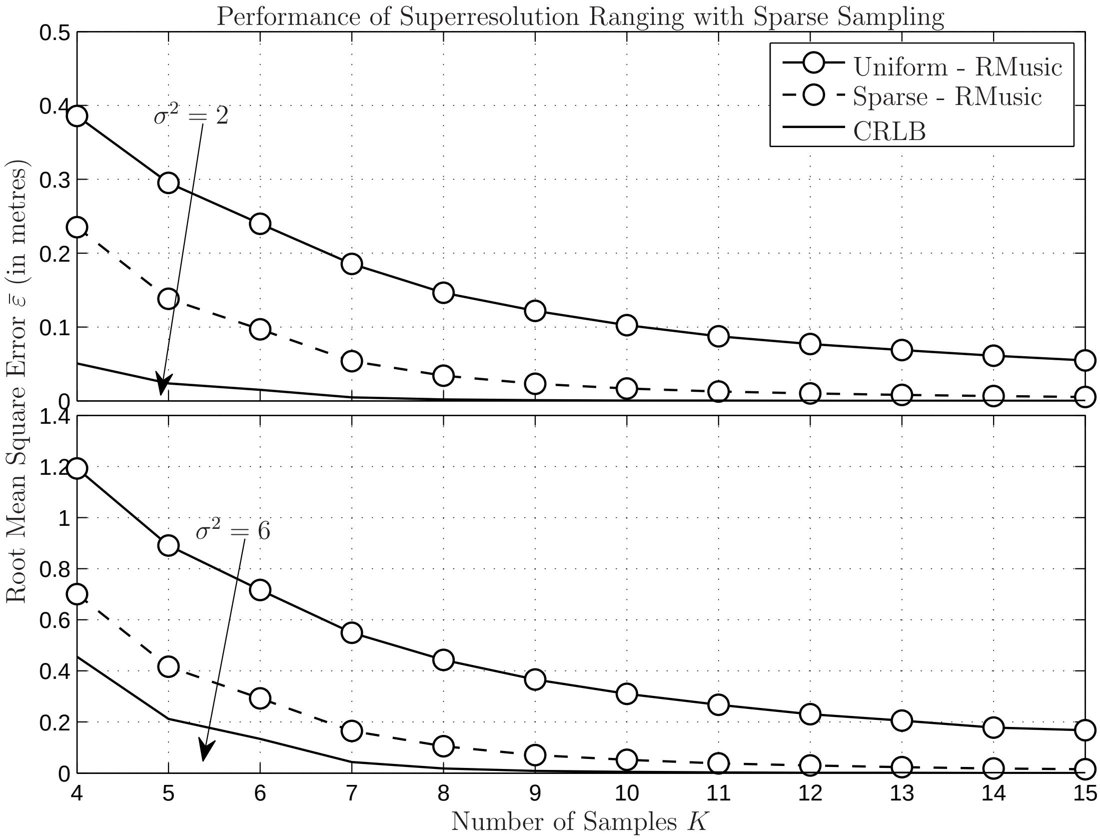

Figure 3.5: Performance of superresolution ranging algorithms as a function of the sample set sizes K, both *with* and *without* Sparse-optimized sampling.

Table 3.1: Examples of Optimal Golomb Rulers.

K	M	N	Optimal Sparse Rulers
4	6	6	0 1 4 6
5	10	11	0 1 4 9 11
6	15	17	1 2 5 11 16 18
7	21	25	1 2 5 11 19 24 26
8	28	34	1 2 5 10 16 23 33 35
9	36	44	1 2 6 13 26 28 36 42 45
10	45	55	1 2 7 11 24 27 35 42 54 56
11	55	72	1 2 5 14 29 34 48 55 65 71 73
12	66	85	1 3 7 25 30 41 44 56 69 76 77 86
13	78	106	1 3 6 26 38 44 60 71 86 90 99 100 107
14	91	127	1 5 7 21 36 53 60 78 79 87 90 100 123 128
15	105	151	1 5 21 31 58 60 63 77 101 112 124 137 145 146 152

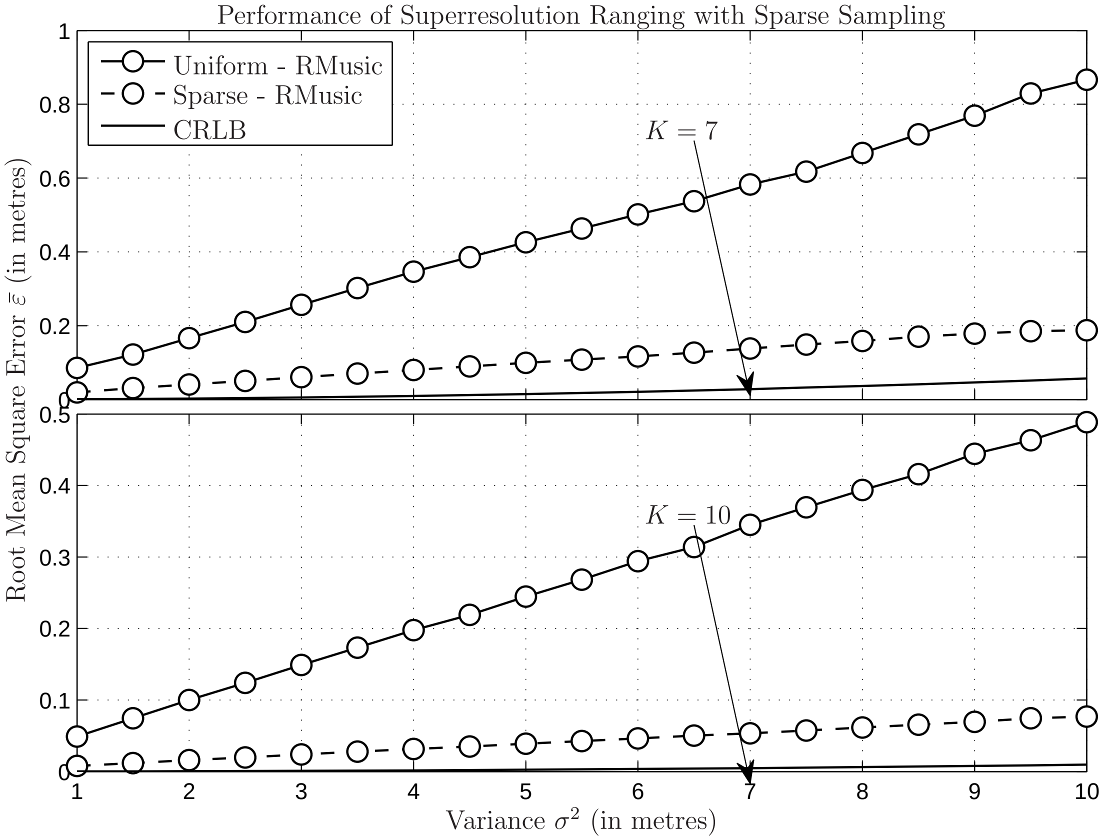

Figure 3.6: Performance of superresolution ranging algorithms as a function of the ToA error variance σ^2, both *with* and *without* Sparse-optimized sampling.

As mentioned, the MUSIC and Root MUSIC algorithms are known to be very optimum for uncorrelated signals, and since only one signal is being estimated, the correlation problem is totally avoided, and therefore their performance can be improved significantly. The problem is therefore not of the superresolution algorithms but how they are being used. The results of the superresolution algorithms were improved by optimizing the aperture of the collected set of ToA measurements $\boldsymbol{\Delta}\tilde{\boldsymbol{\tau}}$ as in Section 3.4 which eliminates redundancy. This was done using a K-marks sparse ruler whose difference triangles maps K ToA measurements $\{\boldsymbol{\Delta}\tilde{\boldsymbol{\tau}}_k\}_{k=1}^{K}$ to M ToA measurements $\{\boldsymbol{\Delta}\tilde{\boldsymbol{\tau}}_m\}_{m=1}^{M}$ with little or no repetition.

With the superresolution algorithms, optimal sparse rulers called K-marks Golomb rulers [69] in Table 3.1 were used for the simulations with varying lengths L and aperture. In this set-up, we achieved a far better performance with a much lower RMSE and got very close to the CRLB compared to any of the ranging techniques described above using uniformly collected ToA measurements as in Figures 3.5 and 3.6. Figure 3.5 shows that using $K = 8$ optimized set of ToA measurements, we achieve a lower RMSE than using $K = 15$ uniform set of ToA measurements for $\sigma = 0.2, 0.6$. While in Figure 3.6, a lower RMSE was obtained for the optimized set of ToA measurements at $\sigma = 0.5$ compared to using uniform set of ToA measurements at $\sigma = 0.1$ for $K = 7, 10$. By optimizing the collection of the K number of round trip times, we were able to improve greatly the accuracy of distance estimates $\tilde{d}$, as a result reduce their corresponding RMSE.

3.6 Conclusions

We proposed a new ranging technique, which combines superresolution algorithms popularly used in finding the direction of arrival of sources in antenna array systems such as MUSIC and Root MUSIC algorithms with the powerful mathematical notion of a sparse ruler obtained using genetic techniques, to perform efficient and accurate Time of Arrival-based ranging. The new optimized solution was proven to being more efficient with respect to the naive uniform version in terms of samples (ranging information) to be collected, and above all, to have performances very close to the fundamental limits depicted by the Cramèr-Rao Lower Bound.

Chapter 4

Multipoint Ranging via Orthogonally Designed Golomb Rulers

4.1 Introduction

Wireless localization is a fairly mature area of research, with a vast literature [20,21,27]. It is therefore paradoxical that despite the formidable effort put into the problem, wireless positioning is still shy of its potential as a truly ubiquitous technology [8,9,11].

Ubiquity requires the technology to be available in every environment, and it is well-known that wireless localization systems are still inaccurate and unreliable in places such as urban canopies and indoors, which are characterized by rich multipath and scarcity of LOS conditions. Furthermore, compared to the quality and omnipresence of satellite- and cellular-based systems in open outdoor spaces, indoor positioning solutions [74–76] are still relatively fragile, under-deployed and unconsolidated.

One explanation is that literature has provided a large number of building blocks to solve parts of the problem, but still does not harmoniously provide comprehensive solutions.

To qualify the above statement, consider the case of AoA positioning were a good number of AoA localization, and estimation algorithms [59, 60, 77] exists. Of particular relevance is the fact that simultaneous estimation of the AoA of multiple signals/sources is relatively easy to perform, which is of fundamental importance to reduce latency in indoor applications where the concentration of users is typically large.

Yet, AoA-based indoor positioning is not common today because: *a*) AoA-based localization algorithms are highly susceptible to NLOS conditions, such that accurate and robust AoA input is needed; and *b*) accurate and robust AoA estimation requires expensive multi-antenna systems and high computational capabilities, which are incompatible with typical indoor requirements of small, low-cost, low-power devices.

The limitations of the AoA-based approaches partially explain the predominance of range-based indoor localization systems proposed both by academia and industry [21, 27, 78, 130]. Indeed, various accurate robust distance-based localization algorithms exist, and distance estimates are relatively inexpensive to obtain from radio signals without requiring multiple antennas or significant additional RF circuitry. But again the deployment of this technology is short of its potential, which arguably is a result of the fact that since ranging quality is severely degraded by interference, positioning systems are required to carefully schedule the collection of ranging information, leading to low refreshing ratios and communication costs.

The above rationale points to a curious predicament. On one hand, many excellent AoA estimation algorithms exist, which however are not typically utilised for indoor positioning as multi-antenna systems are too expensive. On the other, many excellent distance-based positioning algorithms exist [27], which however can only be effectively employed for indoor positioning, if ranging information can be collected efficiently from multiple sources so as to reduce latency.

The work presented in this chapter is a proposal to solve the aforementioned impasse. Specifically, we offer a solution to the multipoint ranging problem based on the same superresolution techniques typically used for AoA estimation. As shall be explained, however, in this context the ability to handle multiple sources when employing superresolution methods does not stem from the separability of signals through the eigenproperties of mixed covariance matrices, but rather by a robustness to sampling sparsity which interestingly is not always enjoyed by such methods in the multi-antenna setting. The feature suggests that the collection of input data can be optimized by designing such sampling sparsity according to Golomb rulers [66, 67, 70, 71], which however must maintain mutual orthogonality. The latter is achieved by a new genetic algorithm – designed under the inspiration of the behaviour of prides of lions – which enables the construction of multiple orthogonal and equivalent[1] Golumb rulers.

The performance of the new algorithm to construct Golomb rulers is compared against the state of the art, and shown thereby to outperform all alternatives we could find. Furthermore, an original CRLB analysis of the new strategy is performed, which indicates that in addition to the advantage of enabling simultaneous multipoint ranging, the overall solution achieves remarkable gain in accuracy over current methods.

In summary, our contributions are as follows:

1) A new multipoint ranging algorithm obtained by adapting superresolution techniques for ToA [15, 16, 57, 79] and PDoA [17–19] ranging, under a unified mathematical framework and such that resources (time/frequency) can be optimized by employing allocation schemes dictated by purpose-designed Golomb rulers (Section 4.2);

2) A new genetic algorithm that not only outperforms the best known alternative to-date in both speed and efficacy, but also enables the simultaneous construction of multiple orthogonal sets of Golomb rulers of equivalent properties (Section 4.3);

3) A complete and specific CRLB analysis of the resulting method, which validates the proposed technique by demonstrating that it indeed nearly achieves the fundamental limit in terms of estimation error performance (Section 4.4).

4.2 Superresolution ToA and PDoA Ranging

There are three basic methods to estimate the distance between a pair of wireless devices using their signals: Received Signal Strength Indicator (RSSI), ToA and PDoA. Amongst these alternatives, RSSI-ranging is known to be the least accurate and least robust [13, 14]. In fact, after some early attention due mostly to its inherent low-power potential [80, 81], RSSI-ranging has since lost appeal thanks to the emergence of low-power physical layer standards such as 802.15.4g [82] and 802.11ac [83], which facilitate the implementation of low-power ToA and PDoA ranging mechanisms. In light of the above, we shall focus hereafter on the latter two forms for multipoint ranging.

[1] Equivalence will be defined more rigorously according to two different criteria.

4.2.1 ToA-based Two-Way Ranging Model

Consider the problem of estimating the distance d between a reference node (anchor) A and a target node T based on ToA measurements. Using the standard two-way ranging technique [15, 16], and assuming that the procedure is executed not a single but multiple times, the k-th distance estimate $\tilde{d}_k$ of d is computed by

$$\tilde{d}_k = \Big[\big(\tau_{\mathrm{RX}:k} - \tau_{\mathrm{TX}:k}\big) - k \cdot \tau_T\Big] \cdot \frac{c}{2} \tag{4.1}$$

where c is the speed of light; $\tau_{\mathrm{TX}:k}$ and $\tau_{\mathrm{RX}:k}$ are respectively the time stamps of the k-th packet at transmission and reception back at the anchor; and τ_T is a fixed and known waiting period observed by the target, for reasons that are beyond[2] the ranging process itself.

Since τ_T is known *a priori* by the anchor, it serves no mathematical purpose and therefore can be assumed to be zero[3] without loss of generality. Similarly, before the k-th ranging cycle the anchor may in practice hold for a (possibly unequal) waiting period $\tau_{A:(k-1)}$, which however can also be normalized to zero, without loss of generality.

Referring to Figure 4.1, and considering the latter assumptions on τ_T and $\tau_{A:i}$ for $i = \{1, \cdots, k-1\}$, equation (4.1) can then be rewritten as

$$\tilde{d}_k = \left[\underbrace{\big(\tau_{\mathrm{RX}:k} - \tau_{\mathrm{TX}:1}\big)}_{\Delta\tau_k} - k \cdot \cancelto{0}{\tau_T} - \sum_{i=1}^{k-1} \cancelto{0}{\tau_{A:i}}\right] \cdot \frac{c}{2k} \equiv \Delta\tau_k \cdot \frac{c}{2k}. \tag{4.2}$$

One way to interpret the model described by equation (4.2) is that in a ToA-based TWR scheme with multiple ranging cycles, the time-difference measurement $\Delta\tau_k$ obtained at the k-th cycle has a linear functional relationship with the cycle index k, with the proportionality factor determined by the distance d between the target and the anchor, *i.e.*,

$$\Delta\tau_k = \omega_d k, \quad \text{with} \quad \omega_d = \frac{2d}{c}. \tag{4.3}$$

The convenience of this interpretation of ToA-based TWR will soon become evident.

[2] For instance, τ_T may be imposed by the frame structure of the underlying communication system.

[3] Strictly speaking, τ_T could also be considered a source of ranging errors, since it is subject to jitter (imperfect time-keeping). In practice, however, jitter errors are several orders of magnitude below the timing errors involved in measuring $\tau_{\mathrm{RX}:k}$, and therefore can be effectively ignored.

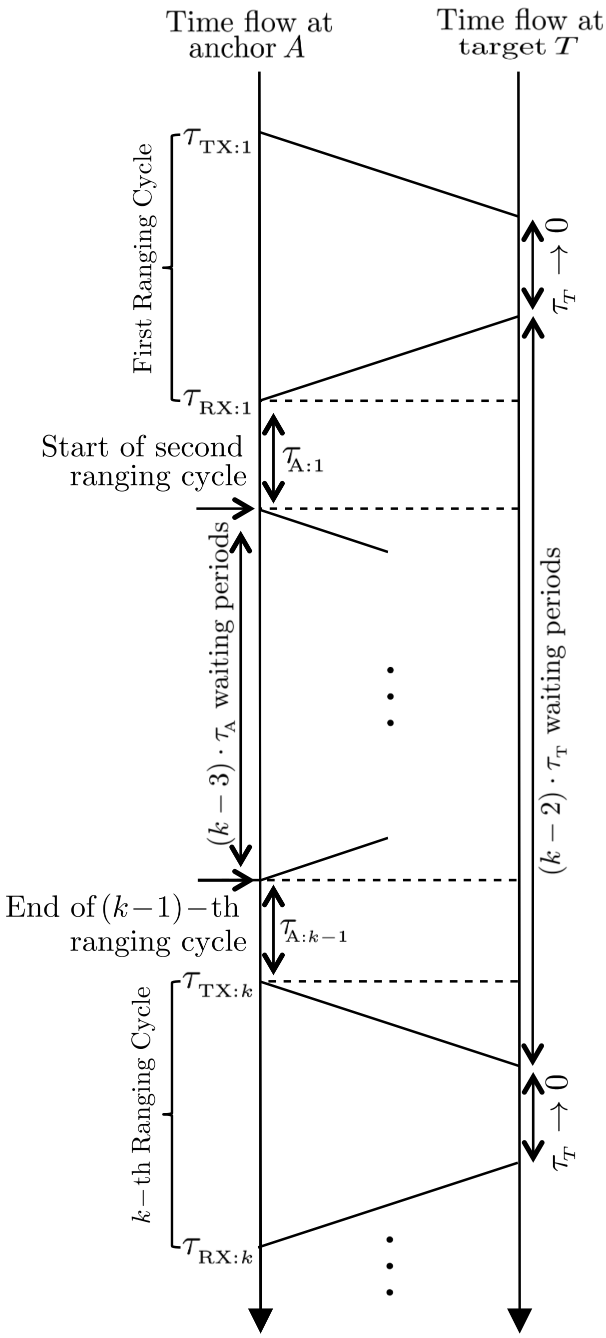

Figure 4.1: Illustration of the non-uniform TWR scheme. Multipoint ranging can be performed by intercalating different sources in different orthogonal (non-overlapping) slots (cycles).

ex

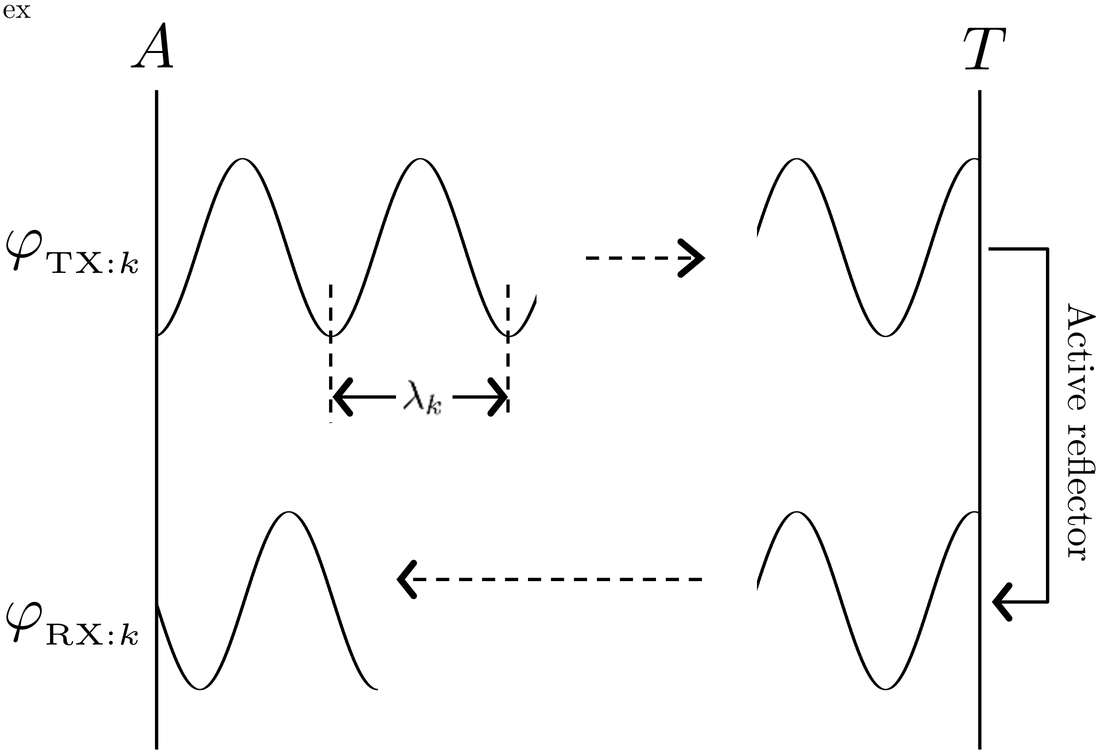

Figure 4.2: Illustration of PDoA ranging mechanism for a single frequency. Multipoint-point ranging can be performed by allocating different sources to different orthogonal carriers.

4.2.2 PDoA-based Continuous Wave Radar Ranging Model

Consider the problem of estimating the distance d between a reference node (anchor) A and a target node T based on the phases of the signals exchanged between the devices.

One possible mechanism, as illustrated in Figure 4.2, is that the anchor A emits a continuous sinusoidal wave $x(t) = A_0 \cos(2\pi f t + \varphi_{\mathrm{TX}})$ of frequency f with a known phase φ_{TX} and the target T acts as an active reflector, such that A can measure the phase φ_{RX} of the returned signal $y(t) = B_0 \cos(2\pi f t + \varphi_{\mathrm{RX}})$ [17–19]. In this case, the roundtrip distance $2d$ and the phases φ_{TX} and φ_{RX} are related by

$$\varphi = \varphi_{\mathrm{RX}} - \varphi_{\mathrm{TX}} = \frac{4\pi d}{c} f - 2\pi L, \tag{4.4}$$

where L is the integer number of complete cycles of the sinusoidal over the distance $2d$.

Obviously the distance d cannot be estimated directly based on equation (4.4) since the quantity N is unknown. However, taking the derivative of equation (4.4) with respect to f one obtains

$$\frac{\mathrm{d}\varphi}{\mathrm{d}f} = \frac{4\pi d}{c}. \tag{4.5}$$

Let there be a set of equi-spaced frequencies $\mathbb{F} = \{f_0, \cdots, f_K\}$ such that $\Delta f = f_{k+1} - f_k$ for all $0 \leq k < K$, and assume the roundtrip phases φ_k for all f_k are measured. Then, thanks to the linear relationship between f and d described by equation (4.5), it follows that

$$\Delta\varphi_k = \omega_d k, \quad \text{with} \quad \omega_d = \frac{4\pi \Delta f d}{c}, \tag{4.6}$$

where $\Delta\varphi_k \triangleq \varphi_k - \varphi_0$ for all $1 \leq k < K$.

Comparing equations (4.3) and (4.6), we conclude that both the ToA-based TWR and the PDoA-based Continuous Wave Radar Ranging (CWRR) methods are mathematically equivalent, in the sense that the measured quantities, respectively $\Delta\tau_k$ and $\Delta\varphi_k$, have a linear relationship with a counter k, governed by a slope coefficient ω_d that is directly and unequivocally related to the desired information d.

4.2.3 Linearity of Ranging Models and Applicability of Golomb Rulers

In light of the models described above, we shall consider for simplicity that we are able to measure quantities Δ_k, such that

$$\Delta_k = \omega_d \cdot k, \tag{4.7}$$

where ω_d is a coefficient with a constant relationship with d.

Obviously the desired parameter d can be estimated directly from each measured Δ_k, but the resulting estimation errors can be very large, especially if the hardware utilized to that end are low power radios, not purpose-built for ranging purposes (*e.g.* Bluetooth devices or ZigBee sensors).

As shall be demonstrated in the sequel, such error performances can be significantly improved by taking not a single, but multiple measurements of Δ_k, and utilizing superresolution techniques. In so doing, however, it is also desired to keep the total number of measurements of Δ_k to a minimum, in order to minimize power consumption as well as delay, which incidentally may also impact estimation accuracy since devices are typically mobile. For the same reasons, it is furthermore desirable to perform such measurements with respect to multiple points simultaneously.

We therefore seek a strategy to design the sequence of measurements of Δ_k, that can be used to improve the accuracy of multipoint ranging efficiently. To this end, first notice that trivially due to the linearity of the relationship described by equation (4.7), we have, for any pair of integers (k, q), with $k > q$,

$$\Delta_k - \Delta_q = \omega_d \cdot (k - q) = \Delta_{k-q}. \tag{4.8}$$

This simple property has a remarkable consequence. Indeed, consider an ascending sequence of non-negative integers $\mathcal{N} = \{n_1, \cdots, n_K\}$ and the associated set of input measurements $\mathbb{\Delta}_{\mathcal{N}} = \{\Delta_{n_1}, \cdots, \Delta_{n_K}\}$. By virtue of equation (4.8), the set $\mathbb{\Delta}_{\mathcal{N}}$ can be expanded into $\mathbb{\Delta}_{\mathcal{V}} = \{\Delta_{n_2} - \Delta_{n_1}, \cdots, \Delta_{n_K} - \Delta_{n_1}, \cdots, \Delta_{n_K} - \Delta_{n_{K-1}}\} = \{\Delta_{n_2-n_1}, \cdots, \Delta_{n_K-n_{K-1}}\} = \{\Delta_{\nu_1}, \cdots, \Delta_{\nu_M}\}$, where the cardinality M of $\mathbb{\Delta}_{\mathcal{V}}$ is obviously upper bounded by $M \leq K\frac{K-1}{2}$.

Other than the much larger cardinality, the sequences $\mathbb{\Delta}_{\mathcal{V}}$ and $\mathbb{\Delta}_{\mathcal{N}}$ have, as far as the purpose of distance estimation is concerned, fundamentally the same nature since both carry samples of the quantities Δ_k. In other words, the model described in subsection

4.2.2 allows for large input sets of cardinality N to be obtained from a significantly smaller number K of actual measurements, by carefully designing the feedback intervals or the carrier frequencies required to perform ranging estimates. Furthermore, the linearity between the measured quantities Δ_k and the corresponding indexes k is so that such design can be considered directly in terms of the relationship between the integer sequences $\mathcal{N} \to \mathcal{V}$.

Sparse rulers or sequences $\mathcal{N}$ that generate optimally expanded equivalents $\mathcal{V}$ are known as *Golomb rulers* and their design under the constraints of our problem is the subject in Section 4.3. Here, however, let us proceed by demonstrating how the aforementioned model enables the straightforward application of superresolution algorithms for ToA and PDoA ranging.

4.2.4 Multipoint Ranging via Superresolution Algorithms

Straightforwardly, assume that a set of input measurements between the target node and an anchor A is collected according to a Golomb ruler $\mathbb{\Delta}_{\mathcal{N}_A}$, from which the associated expanded set $\mathbb{\Delta}_{\mathcal{V}_A}$. Likewise, let sample sets to another anchor B be collected according to another ruler $\mathbb{\Delta}_{\mathcal{N}_B}$, which after expansion yields $\mathbb{\Delta}_{\mathcal{V}_B}$.

Dropping the subscripts A and B for notational simplicity, consider the following complex vector that can be built for any of these two anchors[4],

$$\mathbf{x} = [e^{j\Delta_{\nu_1}}, e^{j\Delta_{\nu_2}}, \cdots, e^{j\Delta_{\nu_M}}]^{\mathrm{T}} \equiv [e^{j\omega_d}, e^{j\nu_2\omega_d}, \cdots, e^{j\nu_M\omega_d}]^{\mathrm{T}}, \tag{4.9}$$

where $^{\mathrm{T}}$ denotes transposition and we have normalized $\nu_1 = 1$, without loss of generality.

Notice that as long as no element in $\mathbb{\Delta}_{\mathcal{N}_A}$ belongs also to $\mathbb{\Delta}_{\mathcal{N}_B}$, the two sequences are orthogonal, meaning that the collection of ranging data from A and B can be conducted without interference. This is regardless of the fact that the corresponding vectors, constructed according to equation (4.9) would most certainly *not* be (in general) orthogonal.

One can immediately recognize from equation (4.9) the similarity between the vector $\mathbf{x}$ and the steering vector of a linear antenna array [59,60,64], with inter-element spacings governed by $\mathbb{\Delta}_{\mathcal{V}}$. An estimate of the parameter of interest ω_d can therefore be recovered from the covariance matrix $\mathbf{R}_{\mathbf{x}} \triangleq \mathbb{E}[\mathbf{x} \cdot \mathbf{x}^{\mathrm{H}}]$. Specifically, under the assumption that each measurement Δ_{ν_m} is subject to independent and identically distributed (iid) white

[4]Obviously the concept generalizes to an arbitrary number of anchors.

noise with variance σ^2, the covariance matrix $\mathbf{R_x}$ can be eigen-decomposed to

$$\mathbf{R_x} = \mathbf{U} \cdot \mathbf{\Lambda} \cdot \mathbf{U}^{\mathrm{H}}, \tag{4.10}$$

with

$$\mathbf{U} = \left[\mathbf{u_x} \,\vdots\, \mathbf{U}_0,\right] \quad \text{and} \quad \mathbf{\Lambda} = \left[\begin{array}{c:c} 1+\sigma^2 & \mathbf{0} \\ \hdashline \mathbf{0} & \sigma^2\mathbf{I} \end{array}\right], \tag{4.11}$$

where $\mathbf{U}_0$ is the K-by-$(K-1)$ null-space of $\mathbf{R_x}$.

Given the above properties, many superresolution algorithms can be employed to obtain ranging estimates from ToA and PDoA measurements [84–87]. Since our focus in this article is to demonstrate such possibility, discuss the resulting opportunities to optimize resources, and analyze the corresponding implications on the achievable ranging accuracies, we shall limit ourselves to two explicit classical examples, for the sake of clarity.

One way to obtain an estimate $\hat{\omega}_d$ of ω_d is via the classic spectral MUSIC algorithm [60–62], where a search for the smallest vector projection onto the noise subspace of $\mathbf{R_x}$ is conducted, namely

$$\hat{\omega}_d = \arg\max_{\omega_d} \frac{1}{\|\mathbf{e}^{\mathrm{H}} \cdot \mathbf{U}_0\|^2} \quad \text{with} \quad \mathbf{e} \triangleq [e^{j\omega_d}, e^{j\nu_2\omega_d}, \cdots, e^{j\nu_M\omega_d}]^{\mathrm{T}}. \tag{4.12}$$

Alternatively, $\hat{\omega}_d$ can be obtained using the root MUSIC algorithm [59, 64, 88], which makes use of the fact that the projection square norm $\|\mathbf{e}^{\mathrm{H}} \cdot \mathbf{U}_0\|^2$ defines an equivalent polynomial in $\mathbb{C}$ with coefficients fully determined by the Grammian matrix of the null subspace of $\mathbf{R_x}$. Specifically, define the auxiliary variable $z \triangleq e^{j\omega}$ such that $\mathbf{e} = [z, z^{\nu_2}, \cdots, z^{\nu_M}]^{\mathrm{T}}$, and the two zero-padded vectors $\mathbf{e}_{\mathrm{L}} = [z^{-1}, 0, \cdots, 0, z^{-\nu_2}, 0, \cdots, 0, z^{-\nu_3}, 0, \cdots, \cdots, 0, z^{-\nu_M}]$ and $\mathbf{e}_{\mathrm{R}} = [z, 0, \cdots, 0, z^{\nu_2}, 0, \cdots, 0, z^{\nu_3}, 0, \cdots, \cdots, 0, z^{\nu_M}]$. Then we may write

$$P(z) \;= \|\mathbf{e}^{\mathrm{H}} \cdot \mathbf{U}_0\|^2 = \mathbf{e}_{\mathrm{L}} \cdot \mathbf{G} \cdot \mathbf{e}_{\mathrm{R}}^{\mathrm{T}} \equiv \sum_{\nu=0}^{2\nu_M-2} \mathrm{tr}(\mathbf{G};\nu) \cdot z^{\nu}, \tag{4.13}$$

where the last equivalence sign alludes to the multiplication by z^{ν_M} required to take the algebraic function into a polynomial; $\mathbf{G}$ is a Gramian matrix constructed by zero-padding the matrix $\mathbf{U}_0 \cdot \mathbf{U}_0^{\mathrm{H}}$, such that the (m,ℓ)-th element of $\mathbf{U}_0 \cdot \mathbf{U}_0^{\mathrm{H}}$ is the (ν_m, ν_ℓ)-th element of $\mathbf{G}$; and $\mathrm{tr}(\mathbf{G};\nu)$ denotes the m-th trace of the matrix $\mathbf{G}$ – *i.e.*, the sum of the k-th diagonal of $\mathbf{M}$, counting from the the bottom-left to the upper-right corner.

The estimate $\tilde{\omega}_d$ can then be obtained by finding the only unit-norm root of $P(z)$, *i.e.*,

$$\tilde{\omega}_d = \arg\text{sol}\left\{P(z) = 0 \;\middle|\; |z| = 1\right\}. \tag{4.14}$$

Whatever the specific method used to extract the distance information (embedded in $\tilde{\omega}_d$) from the vectors constructed as shown in equation (4.9), the superresolution algorithms described are all:

- Superimposable: Thanks to the expansions $\mathcal{N} \rightarrow \mathcal{V}$, measurement intervals or frequencies corresponding to multiple sources can be superimposed without harm. To exemplify, consider the case of two sources A and B and the measurements from both sources be collected continuously according to the sequence $\mathcal{N} = \{1, 3, 4, 5, 6, 7, 8, 10\}$, but such that the sources A and B are only active according to the orthogonal (*i.e.*, non-overlapping) sequences $\mathcal{N}_A = \{1, 3, 6, 7\}$ and $\mathcal{N}_B = \{4, 5, 8, 10\}$. The samples in $\mathcal{N}_A$ can, however, be transformed into the sequence $\mathcal{V}_A = \{3-1, 6-1, 7-1, 6-3, 7-3, 7-6\} \equiv \{1, 2, 3, 4, 5, 6\}$, which contains 6 samples. Furthermore and likewise, $\mathcal{N}_B \rightarrow \mathcal{V}_B = \{5-4, 8-4, 10-4, 8-5, 10-5, 10-8\} \equiv \{1, 2, 3, 4, 5, 6\}$. In other words, each source collects only 4 samples, sharing orthogonal slots of a frame (ToA), or different frequencies in a band (PDoA), without interference. Each such set of 4 collected samples are then transformed into 6 equivalent measurements which are subsequently fed to the superresolution ranging algorithm.

- Unambiguous: In the case of AoA estimation using antenna arrays, the elements of the steering vectors are complex numbers whose arguments are *periodic functions* of the desired parameter, which in turn gives rise to aliasing (ambiguity) of multiple parameter values that lead to the same set of measurements [89–92]. In contrast, in the context hereby the quantities Δ_k are *linear functions*[5] of the desired parameter d, such that no such ambiguity occurs.

- Separable: Thanks to the fact that sample collection is orthogonalized by design via the utilization of Golomb rulers without overlapping marks, superresolution

[5]Ambiguity typically occurs in superresolution methods applied to AoA estimation [92–96] due to a combination of the circularity of the arguments of the complex exponentials *and* the periodicity such functions exhibit on the estimated parameter. It can be easily demonstrated that in the case of interest here, where Δ_{ν_k} are linear functions of d, such ambiguity can be avoided by arbitrary scaling. Furthermore, for the applications of interest (indoor localization) unambiguity holds in practical terms also without scaling.

multipoint ranging can be carried without interference using orthogonal non-uniform sample vectors, each processed by a separate estimator. In other words, the vectors $\mathbf{x}$ constructed according to equation (4.9) depend only the signal from a single source. Consequently, issues such as correlation amongst multiple signals, which commonly affects superresolution algorithms [92–96], do not exist in the context hereby. If implemented that way, the application of superresolution algorithms to multipoint ranging are more closely related to Pisarenko's original harmonic decomposition algorithm [65], than to derivative methods such as MUSIC. Obviously, however, multiple sample vectors pertaining to different sources can also be decorrelated and processed jointly to save computational complexity.

4.3 Optimization of ToA and PDoA Range Sampling via Golomb Rulers

Under the mathematical model described in Section 4.2, the optimization of ranging resources amounts to allocating ranging cycles or frequency pairs to multiple sources, respectively, which is directly related to that of designing Golomb rulers [66].

Indeed, referring to the example offered in the previous section on the fact that Golomb rulers are superimposable (if so-designed), and given the general objective of reducing the total number of cycles/frequencies required to perform multipoint ranging, we shall now turn our attention to the design of sets of mutually-orthogonal Golomb rulers.

Golomb rulers are sets of integer numbers that generate, by means of the difference amongst their elements, larger sets of integers, without repetition. The problem was first studied independently by Sidon [97] and Babcock [98], but these special sets are named after Solomon W. Golomb [99] as he was the first to popularize their application in engineering. Before we discuss the design of Golomb rulers for the specific application of interest, it will prove useful to briefly review some of their basic characteristics and features.

4.3.1 Basic Characteristics and Features of Golomb Rulers

Consider a set of ordered, non-negative integer numbers $\mathcal{N} = \{n_1, n_2, \cdots, n_K\}$, with $n_1 = 0$ and $n_K = N$, without loss of generality[6]. This set has cardinality (or *order*) K,

[6]Since Golomb rulers are invariant to translation, we consider without loss of generality, that the first element is 0 and the last is N. That is slightly different from the representation adopted in

and it will prove convenient to define the *length* of the set by its largest element N. Next, consider the corresponding set $\mathcal{V}$ of all possible pairwise differences

$$\nu_{k\ell} = n_k - n_\ell \quad (1 \leq \ell < k \leq K). \tag{4.15}$$

If the differences $\nu_{k\ell}$ are such that $\nu_{k\ell} = \nu_{pq}$ if and only if (iff) $k = p$ and $\ell = q$, then the set $\mathcal{N}$ is known as a *Golomb ruler*. Such sets are thought of as *rulers*, as their elements can be understood as *marks* of a ruler, which can thus *measure* only the lengths indicated by any pair of marks. In analogy to the latter, we henceforth refer to the set $\mathcal{V}$ as the *measures* set.

It follows from the definition that the number of distinct lengths that can be measured by a Golomb ruler – in other words, the order of $\mathcal{V}$ – is equal to $K\frac{K-1}{2}$. The first key feature of a Golomb ruler is therefore that if $\mathcal{N}$ has order K, then $\mathcal{V}$ has order $K\frac{K-1}{2}$.

A simple example of a Golomb ruler is $\mathcal{N} = \{0, 1, 4, 6\}$, which generates the Measures $\mathcal{V} = \{1, 2, 3, 4, 5, 6\}$. In this particular example, $\mathcal{V}$ is *complete*, as it contains all positive integers up to its length, so that the Golomb ruler of order 4 is said to be *perfect*. In other words, a perfect ruler allows for *all lengths* to be measured, up to the length of the ruler itself.

Unfortunately, no perfect Golomb ruler exists [67] for $K > 4$. It is therefore typical to focus on designing rulers that retain another feature of the order-4 Golomb ruler, namely, its compactness or *optimality* in the following senses: *a*) no ruler shorter than $N = 6$ can exist that yields $K\frac{K-1}{2} = 6$ distinct measures; and *b*) no further marks can be added to the ruler, without adding redundancy. In general, these two distinct optimality criteria are defined as

a) *Length optimality*: Given a certain order K, the ruler's length N is *minimal* ($N = N_{\text{opt}}$);

b) *Density optimality*: Given a certain length N, the ruler's order K is *maximal* ($K = K_{\text{opt}}$).

The design of optimum Golomb rulers of higher orders is an NP-hard problem [70, 100, 101]. To illustrate the computational challenge involved, the Distributed.net project [102], which has the largest computing capacity in the world, has since the year 2000 dedicated a large share of its computing power to finding optimum Golomb rulers of

subsection 4.2.4, but will prove convenient hereafter.

various sizes. The project took 4 years to compute the optimal Golomb ruler of order 24, and is expected to take 7 years to complete the search for the optimal order-27 ruler!

Therefore, we quickly review some known relevant methods used to construct Golomb rulers.

4.3.1.1 Algebraic Methods

Various algebraic methods exist for obtaining Golomb rulers, the best known being the Singer, Bose-Chowla and Ruzsa constructions [100, 103], which utilize the structure of finite fields to produce Golomb rulers. In general, these algebraic methods yield near-optimal rulers, although in a few cases some of the generated rulers were proved to be optimal.

A drawback of these approaches is that they only apply to the design of rulers of order K, where K is either a prime or power of a prime number, although it has been demonstrated that by truncating rulers of more markers, one can construct near-optimal Golomb rulers of smaller orders.

4.3.1.2 Exact Methods

The most efficient exact method to find Golomb rulers was proposed by J. Shearer [121] and used to generate optimal GRs with $K = 14$ to 16. This method is based on the combination of branch-and-bound algorithm with a backtracking algorithm and an upper bound set to the length of the best known solution which influenced the results and performance positively by avoiding divergence. This heuristic technique is used in large parallel schemes such as the Distributed.net project mentioned in Section 4.1. The drawback of the technique is that it requires an exhaustive search, demanding several months or years to obtain results, even with high computational power.

4.3.1.3 Evolutionary Approaches

Due to the enormous computations required, evolutionary approaches have been developed to find optimal and near-optimal GRs in feasible time.

Soliday et al [71] presented an efficient approach based on genetic principle, which applies for arbitrary orders. In such method, the GRs are represented sequencea of

$K-1$ unique segments. Feeney [69] studied hybridized genetic algorithms with/without local search and possible combination with baldwanian/lamarckian learning.

Although, these approaches achieved better results, the best result obtained corresponded to the execution of a genetic algorithm alone. Specifically, between orders $K = 10$ to 16, it was found that the relative distance error to the known optimal GRs are between 9.7 and 36.5% for Soliday, and 6.8 and 20.3% for Feeney.

In the context of this paper, our interest is to design *orthogonal* Golomb rulers, that also come as close as possible to satisfying the length and density of the optimality criteria described so as to optimise resources. Although a few good algorithms to generate Golomb rulers do exist, none of the methods discovered so far are capable of outputting rulers adhering to a specific optimality criterion. Notice moreover that the optimality criteria described above are not necessarily sufficient to satisfy the needs of specific applications. In addition, the orthogonality requirement adds the demand that rulers be designed out of a predefined set of available integers $\mathcal{W}$, which to the best of our knowledge is an *unsolved* problem in the literature.

4.3.2 Genetic Algorithm to Design Orthogonal Golomb Rulers

Due to the aforementioned reasons, we shall take an evolutionary approach to design Golomb rulers adhering to specific features. In the next subsection, we therefore describe a new genetic algorithm to design the required rulers. The algorithm is a modified version of the technique first proposed in [71], and inspired on the behaviour of wild animals that live in small groups, such as *prides of lions*, and incorporate the following components.

4.3.2.1 Representation

Following the framework proposed in [71], Golomb rulers will be represented not by their marks, but by the differences of *consecutive marks*. That is, let $\mathcal{N} = \{n_1, n_2, \cdots, n_K\}$. Then this set will be represented by $\mathcal{S} = \{s_1, \cdots, s_{K-1}\}$, where

$$s_i = n_{i+1} - n_i \quad \forall \quad i = \{1, \cdots, K-1\}. \tag{4.16}$$

4.3.2.2 Initial Population

In order to initialize the genetic algorithm an *initial population* of segment sets is needed. Let $s_{\max}$ be a design parameter describing the largest possible segment in the desired rulers, and consider the *primary set* of segments $\mathcal{S}^* \triangleq \{1, 2, \cdots, s_{\max}\}$, where $s_{\max}= \{K-1, \cdots, 3K\}$. Then, each member $\mathcal{S}_p$ of the initial population is given by an $(K-1)$-truncation of a uniform random permutation of $\mathcal{S}^*$. In other words, each member $\mathcal{S}_p$ of the initial population $\mathbb{P}$ is a set with $K-1$ segments randomly taken without repetition from $\mathcal{S}^*$.

Notice that $s_{\max}$ must be larger than the order K of the desired rulers, and that the larger the difference $s_{\max} - K$, the larger the degrees of freedom available to construct suitable rulers.

An initial population $\mathbb{P}$ of cardinality P can then be defined as a set[7] of P non-equal segment sets $\mathcal{S}_p$, that is, $\mathbb{P} \triangleq \{\mathcal{S}_p\}_{p=1}^{P}$, with $\mathcal{S}_p \neq \mathcal{S}_q$ for all pairs (p, q).

4.3.2.3 Fitness Function

Once an initial population $\mathbb{P}$ is selected, each of the candidate rulers $\mathcal{S}_p$ are evaluated according to a fitness function [70, 71, 104, 105] designed to capture how closely the candidate ruler $\mathcal{S}_p$ approaches the prescribed features of the desired rulers.

Specifically, in the application of interest Golomb rulers must have:

a) length N_p as small as possible for a given order (see optimality criteria in subsection 4.3.1), so as to minimize the duration/bandwidth of the ranging systems;

b) all marks belonging to a certain set of admissible marks $\mathcal{W}$, that is, $F_p = 0$, such that multiple orthogonal rulers can be generated successively;

c) no repeated measures, that is, $R_p = 0$, so as to maximize the expansion from $\mathcal{N}_p$ to $\mathcal{V}_p$.

In order to define a suitable fitness function with basis on these criteria, let us denote the set of marks and the measure set corresponding to $\mathcal{S}_p$ respectively by $\mathcal{N}_p$ and $\mathcal{V}_p$.

[7]Hereafter, whenever self-evident, we shall omit the lower and upper limits from our set of sets notation, in the name of notational simplicity. For instance, $\mathbb{P} \triangleq \{\mathcal{S}_p\}_{p=1}^{P}$ and $\mathbb{P} \triangleq \{\mathcal{S}_p\}$ should be understood as equivalently.

Next, let the scalars N_p and F_p respectively denote the length and the minimum number of marks[8] in the ruler $\mathcal{N}_p$ that are not in the set of admissible marks $\mathcal{W}$. Finally, let R_p be the number of repeated elements in $\mathcal{V}_p$. Then, the fitness function is defined as

$$f(\mathcal{S}_p) \triangleq N_p \times (R_p + F_p + 1). \tag{4.17}$$

Notice that since randomly selected candidate rulers $\mathcal{S}_p$ are by construction suboptimal, $N_p \geq N_{\text{opt}}$ for all p. Furthermore, the sum $R_p + F_p$ is a non-negative integer, assuming the value 0 only when no repetitions occur in $\mathcal{V}_p$ and no marks outside $\mathcal{W}$ can be found in $\mathcal{N}_p$, *simultaneously*. In other words, the *minimum* value of the fitness function is exactly N and is achieved if and only if the respective candidate is indeed a Golomb ruler satisfying all the conditions required.

4.3.2.4 Mutations

Although the fitness function has the desired property of being minimized only at optimum choices of $\mathcal{S}_p$, the underlying optimization procedure is not analytical, but combinatorial, due to the discreteness of the optimization space (specifically, the space of all sets of segment sequences with $K-1$ elements). Therefore, in order to optimize $f(\mathcal{S}_p)$ one needs to search the vicinity of $\mathcal{S}_p$, which is achieved by performing *mutations* over the latter.

There are two distinct types of elementary mutations that can be considered: *transmutation* and *permutation*. The first refers to the case where one element of $\mathcal{S}_p$ is changed to another value[9], while the second refers to a permutation between two segments.

Both types of mutation have similar effects in increasing or decreasing the quantities R_p, and F_p but different effects on N_p as transmutation leads to a change while permutation keeps it constant. But since a candidate sequence $\mathcal{S}_p$ is by definition already a Golomb ruler if $R_p = 0$, mutation is applied to $\mathcal{S}_p$ only if $R_p > 0$. And in that case, only one of the two types of elementary mutations is applied, randomly and with equal probability.

The elementary mutation operator will be hereafter denoted $\mathcal{M}(\cdot)$, and a version of $\mathcal{S}_p$ subjected to a single elementary mutation is denoted $\mathcal{S}_p^\dagger$ such we may write $\mathcal{S}_p^\dagger = \mathcal{M}(\mathcal{S}_p)$. A sequence $\mathcal{S}_p$ is replaced by $\mathcal{S}_p^\dagger$ if and only if $f(\mathcal{S}_p^\dagger) < f(\mathcal{S}_p)$. The mutation step

[8] Notice that in order to count F_p, all shifts (or translations) of $\mathcal{N}_p$ within the range $[\min(\mathcal{W}), \max(\mathcal{W})]$ must be considered, since Golomb rulers are invariant to shifts/translation.

[9] Since a segment of length 1 is always required in a Golomb ruler [68], $s_i = 1$ is never subjected to transmutation [68].

is repeated for every p until an improved replacement of $\mathcal{S}_p$ is found. The mutation procedure is further iterated over the population $\mathbb{P}$ repeatedly until at least on candidate sequence $\mathcal{S}_p$ is Golomb, $R_p = 0$. If no ruler can be found out of the initial population after a certain number of mutation iterations, the algorithm is restarted with an increased primary set $\mathcal{S}^* \triangleq \{1, 2, \cdots, s_{\max} + 1\}$. This process is repeated until a mutated population $\mathbb{P}^\dagger$ is found, which contains at least one Golomb ruler.

4.3.2.5 Selection

As a result of the mutation process described above, $\mathbb{P}^\dagger$ certainly contains one or more Golomb rulers. Such rulers, however, may still violate the prescribed set of admissible marks $\mathcal{W}$ – that is, may still have $F_p > 0$ – and may not have the shortest length desired – *i.e.*, $N_p > N$.

The optimized Golomb ruler will be obtained via the *evolutionary* process to be described in the sequel, which in turn requires the classification the rulers in the population according to their function. Specifically, all sequences $\mathcal{S}_p$ with $R_p = 0$ will be referred to as a *male sequence*, such that the one with the smallest score $f(\mathcal{S}_p)$ will be hereafter referred to as the *dominant male* sequence and denoted $\mathcal{S}_{♂}$. In other words, define the set of sequences $\mathcal{S}_p$ with no repetition, denoted by $\mathbb{P}^\dagger_{♂} \triangleq \{\mathcal{S}_p | R_p = 0\}$, then

$$\mathcal{S}_{♂} = \{\mathcal{S}_p \in \mathbb{P}^\dagger_{♂} | f(\mathcal{S}_p) < f(\mathcal{S}_q) \; \forall \, q \neq p\}. \tag{4.18}$$

In turn, all the other remaining sequences will be designated as *female* sequences. We shall therefore denote[10] $\mathbb{P}^\dagger_{♀} \triangleq \mathbb{P}^\dagger \setminus \mathcal{S}_{♂}$.

4.3.2.6 Evolution

The evolution of the sequences occurs based on the Darwinian principle of variation via reproduction and selection by survival of the fittest. Here, reproduction refers to the construction of new sequences via random crossover between the male sequence and any of the female ones, where crossover amounts to the swap of a block of adjacent "genes" from $\mathcal{S}_{♂}$ and $\mathcal{S}_{♀}$.

Let us denote the crossover operator as $\mathcal{C}(\cdot, \cdot)$, such that a child of $\mathcal{S}_{♂}$ and the i-th female $\mathcal{S}_{♀:i}$ in the population, generated via a single elementary crossover, can be

[10] Notice that this implies that "male" sequences in $\mathbb{P}^\dagger_{♂}$, but do not have the smallest score are thereafter relabelled "female".

described as $\mathcal{C}(\mathcal{S}_{♂}, \mathcal{S}_{♀:i})$. Then, the population evolves according to the following behaviour:

- The dominant male reproduces with all females generating the children $\mathcal{C}(\mathcal{S}_{♂}, \mathcal{S}_{♀:i})$;
- If any element in $\mathcal{C}(\mathcal{S}_{♂}, \mathcal{S}_{♀:i})$ appears more than once, a reconstruction is applied to such element by attributing it a new different element from the segments $\mathcal{S}^*$.
- If there are any children with no repetition ($R_i = 0$) and with fitness function lower than that of $\mathcal{S}_{♂}$, then the child with the lowest score amongst those takes the place of the dominant male, that is

$$\mathcal{S}_{♂} \leftarrow \{\mathcal{C}(\mathcal{S}_{♂}, \mathcal{S}_{♀:i}) \mid R_i = 0 \quad \text{and} \quad f(\mathcal{C}(\mathcal{S}_{♂}, \mathcal{S}_{♀:i})) < f(\mathcal{S}_{♂})\}; \tag{4.19}$$

- All other sequences are considered female, and out of original females and their children, only the best $P - 1$ sequences, *i.e.* the ones with the lowest scores, remains in $\mathbb{P}^{\dagger}$.

A pseudo-code of the genetic algorithm described above is given in Appendix A. Due to the "pride of lions" evolutionary approach employed in the proposed algorithm, convergence to desired rulers is significantly faster then that achieved with the "giant octopus[11]" approach taken in [71], where both parent sequences are destroyed during the crossover process.

Let us first remark that the computational complexity of the ruler design technique is not relevant for the application in question (multipoint ranging), because that process occurs **off-line**. For example, in a ToA-based system, a specific frame structure is set and fixed, such that the number of slots available for ranging is known and invariable. Similarly, for PDoA systems a given set of frequencies is used which cannot be changed due to other constraints originating form the communications usage of the radios.

4.3.2.7 Efficiency of the Genetic Algorithm

In order to evaluate the performance of the proposed genetic algorithm, a set of simulations conducted for order $K = 5$ to 15 was performed. In the simulations, the initial population size was $P = 100$ and the maximum number of mutations and crossovers were both set to $G = C = 50$, respectively.

[11] It is known that both the female and male Pacific giant octopuses parish shortly after the hatching of their eggs [106].

The results achieved after 10 runs are compiled in Table 4.1, where a comparison against Golomb rulers obtained using Soliday's and Feeney's algorithm [69, 71] is shown. The comparison is based on the average relative errors, defined as

$$\eta \triangleq \mathbb{E}\left[\frac{N - N_{\text{opt}}}{N_{\text{opt}}}\right], \tag{4.20}$$

where N_{opt} is the length of the shortest-known (optimal) ruler with the same cardinality.

The Table illustrates that the proposed genetic algorithm finds **multiple orthogonal** optimal and near optimal Golomb rulers for $K = 9$ to $K = 16$, all the while outperforming the algorithms proposed by Soliday and Feeney.

Table 4.1: Comparison of Average Relative Error of Golomb Rulers

K	N_{opt}	Soliday [71]	Feeney [69]	Proposed (P=4)	Proposed (P=7)
5	11	0.0%	0.0%	0.0%	0.0%
6	17	0.0%	0.0%	0.0%	0.0%
7	25	0.0%	0.0%	0.0%	0.0%
8	34	2.94%	0.0%	0.0%	0.0%
9	44	0.0%	6.8%	0.0%	0.0%
10	55	12.7%	12.7%	9.1%	7.27%
11	72	9.7%	11.1%	8.33%	6.94%
12	85	21.2%	18.8%	14.1%	10.59%
13	106	17.0%	15.1%	15.1%	12.26%
14	127	32.2%	15.0%	17.3%	13.39%
15	151	36.4%	18.9%	19.9%	16.56%

It is found that even if the population considered during the evolution process is maintained to the minimum, replacing parents only by better offsprings tends to improve results as K grows. More importantly, a substantial and consistent improvement is achieved if $P > 2$, such that the best (male) ruler can "reproduce" with multiple females.

Thanks to the modified fitness function (see equation (4.17) compared to [71, Eq. (4)]), which not only includes a direct term (*i.e.*, F_p) to account for the utilization of forbidden marks, but also is only minimized when sequences are in fact Golomb rulers, the algorithm here proposed is capable of generating any desired number of orthogonal Golumb rulers, provided that $s_{\max}$ is sufficiently large. This is achieved by subsequent executions of the algorithm, each time with $\mathcal{W}$ reduced by the marks of the rulers already generated.

4.3.3 Explicit Example

For the sake of clarity, let us provide an example of how the proposed genetic algorithm described in the preceding subsection works. To this end, consider that we seek to obtain a few mutually orthogonal Golomb rulers of order $K=10$, with marks admissible within $\mathcal{W} = \{0, 1, 2, \cdots, 99\}$ and largest segment $s_{\max} = 3K$.

Following step 1), the algorithm works not with the rulers themselves, but with sets given by the corresponding consecutive segments. And since the desired rulers must have K marks, the sets of segments $\mathcal{S}_p$ must have each $K-1$ elements, such that the complete population of segment sets is given by all possible distinct combinations of $K-1$ numbers out of $\mathcal{S}^* \triangleq \{1, 2, \cdots, s_{\max}\}$.

Clearly this is much too large a number of sequences to be considered. We therefore start instead with a much smaller initial population sample $\mathbb{P}$, of a chosen cardinality, say $P = 50$. In order to obtain $\mathbb{P}$ according to step 2), we then construct 50 sets $\mathcal{S}_p$, each being a set with $K-1$ segments randomly taken without repetition from $\mathcal{S}^* \triangleq \{1, 2, \cdots, 3K\}$. For instance, $\mathbb{P} = \{\{1, 10, 7, 8, 25, 3, 14, 6, 4\},\ \{9, 15, 5, 3, 1, 14, 26, 2, 4\}, \cdots\}$ would be an example of the first few members of the initial population.

Next, following steps 3) and 4), the population $\mathbb{P}$ undergoes mutation (transmutation or permutation) and ranking according to their fitness scores, until one or more mutated sequences $\mathcal{S}_p$ with $R_p = 0$ emerge. The sequence with $R_p = 0$ and the lowest score is selected as the dominant male sequence, and all other sequences are referred to as female, as described in step 5). Recall that male sequences are such that the corresponding rulers are Golomb, since they do not yield measure repetition.

To provide an explicit example of the result of the mutation process, it can be seen that after a slight mutation the first member of the initial population shown above can be transformed[12] to $\mathcal{S}_{♂} = \{1, [14], (13), [3], 25, (28), (12), 6, 4\}$, while the first female sequence can mutate to $\mathcal{S}_{♀:1} = \{[8], 15, 5, 3, 1, 14, [28], (4), (2)\}$.

The sequence $\mathcal{S}_{♂}$ above is indeed associated with a Golomb ruler ($R_{♂} = 0$), namely, $\mathcal{N}_{♂} = \{0, 1, 15, 28, 31, 56, 84, 96, 102, 106\}$, while the ruler associated with $\mathcal{S}_{♀:1}$, given by $\mathcal{N}_{♀:1} = \{0, 8, 23, 28, 31, 32, 46, 74, 78, 80\}$, is not Golomb as $R_{♀:1} = 9$.

[12]In order to ease visualization of which "genes" have mutated, we highlight permuted and transmuted "genes" respectively with $[\cdot]$ and $(\cdot)$.

Notice that both rulers adhere to the design constraint of $K = 10$. However, it can also be seen that the ruler $\mathcal{N}_{♂}$ contains two forbidden marks ($F_p = 2$), namely, 102 and 106, which do not belong to $\mathcal{W}$. Therefore, this sequence does not minimize the fitness score and the algorithm proceeds to the evolutionary stage.

Within the evolutionary stage, cross-breading between the male sequence and all female sequences occur, as described in step 6), typically generating an improved male sequence in each iteration, until eventually a male sequence emerges that has both $R_{♂} = 0$ and $F_{♂} = 0$, minimizing the fitness score and stopping the process.

As for example, it can be seen that the segment set $\mathcal{S}_{♂} = \{1, (15), (5), 3, 25, (14), 12, 6, 4\}$, can be obtained from the cross-over of genes $14 \leftrightarrow 15$, $13 \leftrightarrow 5$ and $28 \leftrightarrow 14$ between the previous male and female sequences. This latter set is associated with the ruler $\mathcal{N}_{♂} = \{0, 1, 16, 21, 24, 49, 63, 75, 81, 85\}$, which appears on the left column of Table 4.2.

As a result of all the above, the algorithm outputs a first Golomb ruler with the desired constraints, specifically, $K = 10, N \leq 99$. Next, subtracting the marks already allocated from the permissible set of marks, we obtain a new set $\mathcal{W} = \{2, \cdots, 15, 17, \cdots, 20, 22, 23, 25, \cdots, 48, 50, \cdots, 62, 64, \cdots, 74, 76, \cdots, 80, 82, \cdots, 84, 86, \cdots, 99\}$.

The genetic algorithm is initialized again with the same order $K = 10$ and same primary set of segments $\mathcal{S}^* \triangleq \{1, 2, \cdots, 3K\}$, but with the updated set of admissible marks $\mathcal{W}$. A new initial population is selected randomly according to step 2, yielding for example $\mathbb{P} = \{\{1, 8, 21, 13, 11, 4, 12, 6, 14\}, \{1, 11, 4, 13, 9, 10, 14, 7, 18, 6\}, \cdots\}$ and all other steps are executed subsequently as described earlier.

A possible outcome of this second run is the ruler $\mathcal{N}_{♂} = \{2, 3, 11, 32, 45, 56, 60, 72, 78, 92\}$, which is (by design) orthogonal to the one obtained earlier and is also listed in Table 4.2. Repeating this process three more times resulted in the other rulers shown on the left column of Table 4.2, all of which are mutually orthogonal by design.

Before we conclude this section, let us remark that the above is only one of two distinct ways to run the proposed genetic algorithm. Specifically, notice that by fixing $K = 10$ we obtain mutually orthogonal rulers of different lengths, but one could instead allow K to vary in order to satisfy a prescribed length N.

This approach is motivated by the fact that the corresponding array-like vectors (see equation (4.9)) will have the same aperture, which in turn is directly related to the accuracy of the corresponding distance estimation via superresolution algorithms. This choice is referred to as Equivalent[13] Resource Quality (ERQ) grouping.

The other possibility discussed previously, in which the Golomb rulers with the same cardinality K are generated, is motivated by the fact that, in the context hereby, each marker in the ruler corresponds to a measurement that is taken, so that such rulers imply that the same number of ranging cycles/frequencies by all pairs. This approach is therefore referred to as Fair Resource Allocation (FRA).

Examples of Golomb rulers obtained with the algorithm described above and grouped according to the ERQ and FRA criteria are listed in Table 4.2. It can be observed that, as desired and by design, no two identical numbers can be found in two different rulers within the same group, such that the rulers in the same group are mutually orthogonal.

To illustrate the importance of this feature, multipoint ranging between a source and 5 different anchors can be carried out simultaneously within a block of no more than 100 cycles/frequencies by taking only 50 ToA/PDoA measurements according to the rulers displayed in Table 4.2. Furthermore, this can be achieved either with equivalent ranging quality using the group of ERQ rulers, or with fairly allocated resources using the group of FRA rulers, respectively.

Table 4.2: Examples of Golomb Rulers with FRA and ERQ Designs.

K	Fair Resource Allocation	N	M	K	Equivalent Resource Quality	N	M
10	0,1,16,21,24,49,63,75,81,85	85	45	9	0,1,7,10,30,41,45,63,87	87	36
10	2,3,11,32,45,56,60,72,78,92	90	45	9	2,3,6,32,37,49,56,76,89	87	36
10	5,9,15,29,42,51,68,80,91,96	91	45	10	4,5,16,20,33,42,52,66,73,91	87	45
10	6,13,17,19,33,43,61,62,84,93	87	45	11	8,9,18,21,38,46,53,72,77,93,95	87	55
10	12,14,22,27,28,46,66,73,77,94	82	45	11	12,13,17,25,31,47,68,70,79,96,99	87	55

4.4 Error Analysis and Comparisons

In this section, we analyse the performance of the multipoint ranging approach described above, both with PDoA and ToA measurements. To this end, we first derive the Fisher Information Matrices and associated Cramer-Rao Lower Bounds (CRLB) corresponding to the algorithms and later offer comparisons with simulated results. Since related material on ToA can be found more easily [72, 73], we shall consider first

[13] As shall be demonstrated in Section 4.4, unequal Golomb rulers with the same K and N, may still have different CRLBs.

the PDoA case and offer only a synthesis of the ToA counterpart.

4.4.1 Phase-Difference of Arrival

Start by recognising that phase difference measurements subject to errors are circular random variables. The Central Limit Theorem (CLT) over circular domains establishes that the most entropic (*i.e.*, least assuming) model for circular variables with known mean and variance is the von Mises or Tikhonov distribution [107]. Indeed, it is well-known [108–110] that phase estimation errors of first and second-order phase-locked loops (PLLs) are Tikhonov-distributed. Following such classic results, phase measurements are modeled as

$$\tilde{\Delta}\varphi \sim P_{\mathcal{T}}(x; \Delta\varphi, \kappa) \tag{4.21}$$

with

$$P_{\mathcal{T}}(x; \Delta\varphi, \kappa) \triangleq \frac{1}{2\pi I_0(\kappa)} \cdot \exp(\kappa \cos(x - \Delta\varphi)), \quad -\pi \leq x \leq \pi, \tag{4.22}$$

where $I_n(\kappa)$ is the n-th order modified Bessel function of the first kind and κ is a shape parameter which in the case of phase estimates is in fact given by the signal-to-noise-ratio (SNR) of input signals [108, Eq. (37)], and that relates to the error variance by

$$\sigma^2_{\Delta\varphi} = 1 - \frac{I_1(\kappa)}{I_0(\kappa)} \xrightarrow[\kappa>>1]{} \frac{1}{2\kappa+1} \approx \frac{1}{2\kappa}. \tag{4.23}$$

Consider then that a set of K independent measurements $\{\Delta\varphi_k\}_{k\in\mathcal{N}}$ is collected according to a Golomb ruler $\mathcal{N}$, such that the samples can be expanded into and augmented set of M samples $\{\Delta\varphi_m\}_{m\in\mathcal{V}}$, with

$$\Delta\varphi_m = \Delta\varphi_k - \Delta\varphi_\ell = \omega_d(k-\ell) = \omega_d\nu_m, \quad \text{for} \quad k > \ell \quad \text{and} \quad (k,\ell) \to m, \tag{4.24}$$

where each index m corresponds to a pair (k, ℓ) with $k > \ell$ with ascending differences[14], and we commit a slight abuse of notation compared to equation (4.6), since ν_m is a positive integer obtained from a the difference $k - \ell$, such that $\nu_m \neq m$.

At this point it is worthy of mention that although the expanded samples $\Delta\varphi_m$ are actually differences of phase differences, these quantities not only preserve the linear relationship with the parameter of interest but also their independence. As a result of

[14]Notice that this is ensured without ambiguity thanks to the fact that $\mathcal{N}$ is a Golomb ruler.

the double-differences, however, the SNR of $\Delta\varphi_m$ from equation (4.24) is half that of $\Delta\varphi_k$ from equation (4.6). In light of the asymptotic relationship, it follows that the shape parameter κ associated with $\Delta\varphi_m$'s are twice as small.

Using the model above, and incorporating the optimized sampling via Golomb ruler, the likelihood function associated with M independent measurements as per equation (4.6) becomes,

$$L_{\mathcal{T}}(\tilde{d};\Delta f,\kappa) = \prod_{m=1}^{M} P_{\mathcal{T}}(x;\Delta\varphi_m,\kappa) = \frac{1}{(2\pi I_0(\kappa/2))^M}\prod_{m=1}^{M}\exp\left[\frac{\kappa}{2}\cos\left(\frac{4\pi\Delta f}{c}\nu_m\cdot(\tilde{d}-d)\right)\right], \tag{4.25}$$

where $\nu_m \in \mathcal{V}$ and we have slightly modified the notation in order to emphasize the quantity and parameter of interest d.

For future convenience, let us define $\alpha = \frac{4\pi\Delta f}{c}$. Then the associated log-likelihood function is

$$\ln L_{\mathcal{T}}(\tilde{d};\Delta f,\kappa) = -M\ln 2\pi I_0(\kappa/2) + \frac{\kappa}{2}\sum_{m=1}^{M}\cos\left(\alpha\cdot\nu_m\cdot(\tilde{d}-d)\right), \tag{4.26}$$

and its Hessian becomes

$$\frac{\partial^2 \ln L_{\mathcal{T}}(\tilde{d};\Delta f,\kappa)}{\partial d^2} = -\frac{\alpha^2\kappa}{2}\sum_{m=1}^{M}\nu_m^2\cos\left(\alpha\cdot\nu_m\cdot(\tilde{d}-d)\right). \tag{4.27}$$

The Fisher Information is the negated expectation of the Hessian, thus,

$$J(\mathcal{V};\Delta f,\kappa) = -\mathbb{E}\left[\frac{\partial^2 \ln L_{\mathcal{T}}(\tilde{d};\Delta f,\kappa)}{\partial d^2}\right] = \frac{\alpha^2\kappa}{2}\sum_{m=1}^{M}\nu_m^2\mathbb{E}\left[\cos\left(\alpha\cdot\nu_m\cdot(\tilde{d}-d)\right)\right], \tag{4.28}$$

where the notation alludes to the fact that the key input determining the Fisher Information is the set of measures $\mathcal{V} = \{\nu_1,\cdots,\nu_M\}$.

Next, recognise that each term $\alpha\cdot\nu_m\cdot(\tilde{d}-d)$ is in fact a centralized circular variate with the same distribution $P_{\mathcal{T}}(x;0,\kappa/2)$, regardless of m. Then, substituting $\alpha\cdot\nu_m\cdot(\tilde{d}-d)$

with θ, we obtain

$$\begin{aligned} J(\mathcal{V};\Delta f,\kappa) &= \frac{\alpha^2\kappa}{2}\sum_{m=1}^{M}\nu_m^2\mathbb{E}\left[\cos\theta\right] = \frac{\alpha^2\kappa}{2}\sum_{m=1}^{M}\frac{\nu_m^2}{I_0(\kappa/2)}\underbrace{\frac{1}{\pi}\int_0^{\pi}\cos\theta\exp\left(\frac{\kappa}{2}\cos\theta\right)\mathrm{d}\theta}_{I_1(\kappa/2)} \\ &= \frac{\alpha^2\kappa}{2}\frac{I_1(\kappa/2)}{I_0(\kappa/2)}\sum_{m=1}^{M}\nu_m^2, \end{aligned} \tag{4.29}$$

where the integration limits in the integral above follow from evenness of the function $\cos(\theta)\exp(\frac{\kappa}{2}\cos\theta)$, and the last equality results from the integral solution found in [111, Eq. 9.6.19, pp. 376].

Since the above Fisher Information is a scalar, the CRLB is obtained directly by taking its inverse, *i.e.*,

$$\mathrm{CRLB}_{\mathrm{PDoA}}(\mathcal{V};\Delta f,\kappa) = \frac{1}{J(\mathcal{V};\Delta f,\kappa)}. \tag{4.30}$$

As stated earlier in this chapter, our objective is two-fold, namely, to reduce the amount of resources required to perform accurate distance estimation **and** at the same time enable multi-point ranging to be carried out in a more sensible way than simply ranging in a point-to-point fashion sequentially, as systems do today.

This obviously requires reducing the number of samples as well an intercalation of ranging cycles/frequencies amongst the various ranging pairs. Now, from a sheer information theoretical point of view, sacrificing samples incur in loss of information, and consequently in (theoretically achievable!) performance degradation. To clarify, a system in which a number M of **optimally** taken samples are available can always (in principle) outperform another with only $K < M$ samples.

The questions, however, are: a) how to optimally take such samples and b) if a reduction is required, how to do so sacrificing performance as little as possible, as one may recognize that **both** problems are solved in this chapter. Specifically, if one desires only to optimize the performance of a ranging system under the constraint that M samples are to be taken, then, our answer is that such samples must be taken according to a Golomb ruler **if** M is sufficiently large, which would be demonstrated soon.

Before proceeding to the ToA case, some analytical discussion and results on the statements offered above are in order. First, let us emphasize that given a set of phase difference measurements $\{\Delta\varphi_{n_k}\}_{k=1}^{K}$, with $n_k \in \mathcal{N}$, one always has the *option* of either exploit the properties of the Golomb ruler $\mathcal{N}$ and expand to a set of measurements

$\{\Delta\varphi_{\nu_m}\}_{m=1}^{M}$, or not. In case such option is *not* adopted, the associated Fisher Information and CRLB can obviously be obtained exactly as done above, but with κ replacing $\kappa/2$ and $\mathcal{N}$ replacing $\mathcal{V}$. That is,

$$J(\mathcal{N};\Delta f,\kappa) = \alpha^2\kappa\frac{I_1(\kappa)}{I_0(\kappa)}\sum_{k=1}^{K} n_k^2 \iff \mathrm{CRLB}_{\mathrm{PDoA}}(\mathcal{N};\Delta f,\kappa) = \frac{1}{J(\mathcal{N};\Delta f,\kappa)}. \quad (4.31)$$

Comparing these expressions, it can be readily seen that the choice of adopting the Golomb approach on the one hand subjects the resulting double-phase-differences to twice the noise, but on the other hand expands the number terms in the summation. In principle, the optimum choice between these options therefore depends on the ruler $\mathcal{N}$ and its order K, and the associated $\mathcal{V}$ and M, as well as κ.

Let us define the Fisher Information ratio

$$R_J(\mathcal{N},\mathcal{V};\Delta f,\kappa) \triangleq \frac{J(\mathcal{N};\Delta f,\kappa)}{J(\mathcal{V};\Delta f,\kappa/2)}, \quad (4.32)$$

such that $R_J(\mathcal{N},\mathcal{V};\Delta f,\kappa) < 1$ indicates that expansion from $\mathcal{N}$ to $\mathcal{V}$ is advantageous. Plots of $R_J(\mathcal{N},\mathcal{V};\Delta f,\kappa)$ as a function of $\sigma^2_{\Delta\varphi}$ are shown in Figure 4.3. As can be seen thereby, the ruler $\mathcal{N} = \{0,1,4,6\}$, for instance, yields superior results compared to its associated measure set $\mathcal{V} = \{1,2,3,4,5,6\}$, because the loss of 3dB (implied by $\kappa \to \kappa/2$) incurred by the latter is not compensated by the increase gained in the sum of squares achieved by using $\mathcal{V}$ instead of $\mathcal{N}$.

For larger rulers, however, the advantage of expanding the rulers quickly becomes significant, thanks to the geometric increase of M with respect to K. A ruler of order $K = 6$, *e.g.*, $\mathcal{N} = \{0,1,4,10,12,17\}$, already achieves better performance expanded into $\mathcal{V} = \{1,\cdots,17\}$ than otherwise, for $\sigma_{\Delta_\varphi} \leq 0.22$. Likewise, the expanded version of the order-10 ruler $\mathcal{N} = \{0,1,16,21,24,49,63,75,81,85\}$ is superior up to $\sigma_{\Delta_\varphi} \leq 0.65$ – which incidentally defines essentially the entire range of interest – and finally the expanded ruler of order-20 is always superior, for any σ_{Δ_φ}.

In summary, it can be said that applying the Golomb expansion leads to superior results, as long as the ruler is large enough and σ_{Δ_φ} is in the region of interest.

4.4.2 Time of Arrival

Due to the similarity of the ToA and PDoA ranging models described in Section 4.2, the Fisher Information and CRLB for ToA-ranging with Golomb rulers are very similar to those given above for the PDoA case. For the sake of brevity, we therefore offer here only a succinct derivation.

Assuming that the error on the time of arrival estimates are Gaussian-distributed, were have

$$\hat{\Delta\tau} \sim P_{\mathcal{G}}(x; \Delta\tau, \sigma^2_{\Delta\tau}) = \frac{1}{\sqrt{2\pi}\sigma_{\Delta\tau}} \exp\left(-\frac{(x-\Delta\tau)^2}{2\sigma^2_{\Delta\tau}}\right), \tag{4.33}$$

such that the likelihood function, the log-likelihood function, its Hessian and the Fisher Information, considering already the expansion $\mathcal{N} \to \mathcal{V} \Rightarrow \sigma^2_{\Delta\tau} \to 2\sigma^2_{\Delta\tau}$ and emphasizing the quantities of interest, becomes

$$L_{\mathcal{G}}(\tilde{d}; \sigma^2_{\Delta\tau}) = \prod_{m=1}^{M} P_{\mathcal{G}}(\tilde{d}; \Delta\tau_m, 2\sigma^2_{\Delta\tau}) = \frac{1}{(4\pi\sigma^2_{\Delta\tau})^{M/2}} \prod_{m=1}^{M} \exp\left(-\frac{\nu_m^2}{c^2\sigma^2_{\Delta\tau}}(\tilde{d}-d)^2\right),$$

$$\ln L_{\mathcal{G}}(\tilde{d}; \sigma^2_{\Delta\tau}) = -\tfrac{M}{2}\ln 4\pi\sigma^2_{\Delta\tau} - \frac{1}{c^2\sigma^2_{\Delta\tau}} \sum_{m=1}^{M} \nu_m^2(\tilde{d}-d)^2,$$

$$\frac{\partial^2 \ln L_{\mathcal{G}}(\tilde{d}; \sigma^2_{\Delta\tau})}{\partial d^2} = -\frac{2}{c^2\sigma^2_{\Delta\tau}} \sum_{m=1}^{M} \nu_m^2 \quad \Longrightarrow \quad J(\mathcal{V}; \sigma^2_{\Delta\tau}) = \frac{2}{c^2\sigma^2_{\Delta\tau}} \sum_{m=1}^{M} \nu_m^2. \tag{4.34}$$

As discussed above, if the measurements taken according to the Golomb markers are, however, used without taking their differences, the associated noise process has half the variance such that

$$J(\mathcal{N}; \sigma^2_{\Delta\tau}) = \frac{4}{c^2\sigma^2_{\Delta\tau}} \sum_{m=1}^{M} \nu_m^2. \tag{4.35}$$

Similarly as the PDoA case, the Fisher Information ratio

$$R_J(\mathcal{N}, \mathcal{V}; \sigma^2_{\Delta\tau}) \triangleq \frac{J(\mathcal{N}; \sigma^2_{\Delta\tau})}{J(\mathcal{V}; 2\sigma^2_{\Delta\tau})}, \tag{4.36}$$

such that $R_J(\mathcal{N}, \mathcal{V}; \sigma^2_{\Delta\tau}) < 1$ indicates that expansion from $\mathcal{N}$ to $\mathcal{V}$ is superior.

Plots of $R_J(\mathcal{N}, \mathcal{V}; \sigma^2_{\Delta\tau})$ as a function of $\sigma_{\Delta\tau}$ are shown in Figure 4.4. As can be seen in the figure, the ruler $\mathcal{N} = \{0, 1, 4, 6\}$, for instance, yields superior performance expanded into $\mathcal{V} = \{1, 2, 3, 4, 5, 6\}$ than otherwise, for $\sigma_{\Delta\tau} \leq 0.58$, because the loss of 3dB (implied by $\sigma^2_{\Delta\tau} \to 2\sigma^2_{\Delta\tau}$) incurred by the latter is compensated by the increase gained in the sum of squares achieved by using $\mathcal{V}$ instead of $\mathcal{N}$ up until $\sigma_{\Delta\tau} > 0.58$.

For larger rulers, however, the advantage of expanding the rulers becomes much more significant, thanks to the geometric increase of M with respect to K. It is seen that the expanded ruler of order $K = 6$, order $K = 6$ and order $K = 6$ are always superior, for any $\sigma_{\Delta\tau}$.

In summary, it can be said that applying the Golomb expansion leads to superior results, as long as the ruler is large enough and $\sigma_{\Delta\tau}$ is in the region of interest.

4.4.3 Simulations and Comparison Results

Let us finally study the performance of the proposed multipoint ranging technique by means of simulations and comparisons with the corresponding CRLBs derived above. For the sake of brevity, we will consider only PDoA ranging as all results obtained with the ToA approach are equivalent and similar to those in Section 3.5.

First, consider Figure 4.5, where the performances of two classic superresolution algorithms – namely the Music and Root Music algorithms of briefly described in Subsection 4.2.4 – are compared against the CRLB derived in Subsection 4.4.1. Plots are shown both as a function of K for various $\sigma^2_{\Delta\varphi}$ and vice-versa, and for the sake of having a practical reference, we include also results obtained by simply averaging the distance estimates corresponding to all independent samples.

We emphasize that in this Figure no Golomb ruler is used. Instead, a sequence of K consecutive samples is collected for each range estimate, as typically assumed in existing work [112, 113].

One fact learned from these plots – and is particularly visible in Figure 4.5(a) – is that without the efficient use of samples made possible by the Golomb ruler approach here proposed, superresolution algorithms require a large number of samples in order to reach the CRLB, which is a problem since resources such as energy consumption and latency are directly related to the number of samples collected.

Another fact of relevance that can be learned, however, is that although supperresolution methods do improve on a "naive" average-based estimator, that gain in itself is not that significant unless the number of samples K is rather large. This is highlighted in Figure 4.5(b), where it is seen that with $K = 10$, the simple average-based algorithm has essentially the same performance of MUSIC.

These results emphasize the significance of our contribution, by demonstrating that the efficient utilisation of samples is fundamental to reap from superresolution algorithms their true potential performance. This is further illustrated in Figure 4.6(a), where it can be seen that thanks to the Golomb sampling superresolution algorithms with a relatively small number of samples come much closer to the CRLB.

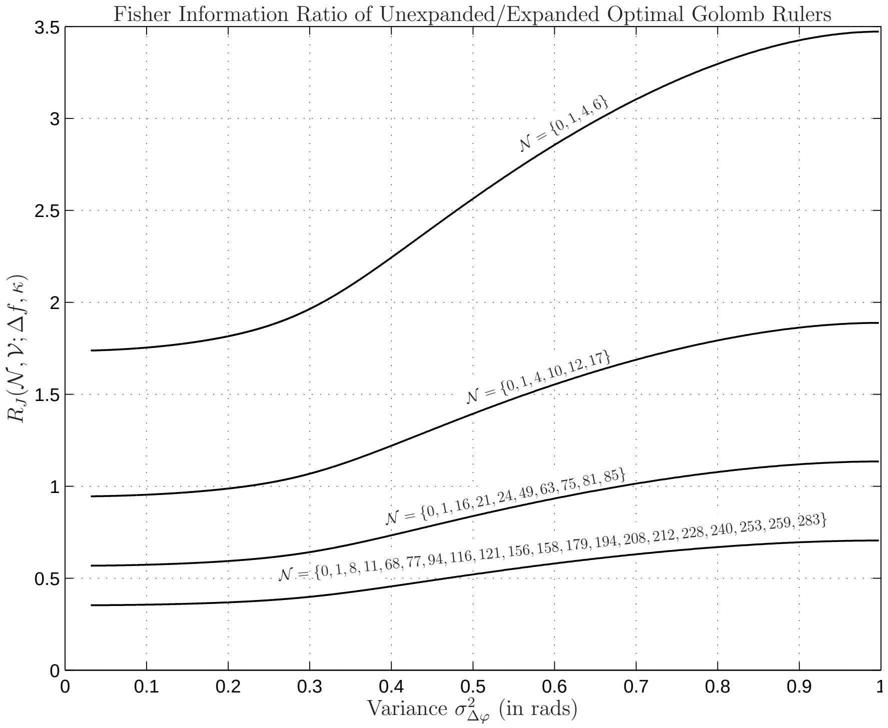

Figure 4.3: Evolution of Fisher Information ratio $R_J(\mathcal{N},\mathcal{V};\Delta f,\kappa)$ as a function of the phase error variance $\sigma^2_{\Delta\varphi}$, associated with different rulers $\mathcal{N}$.

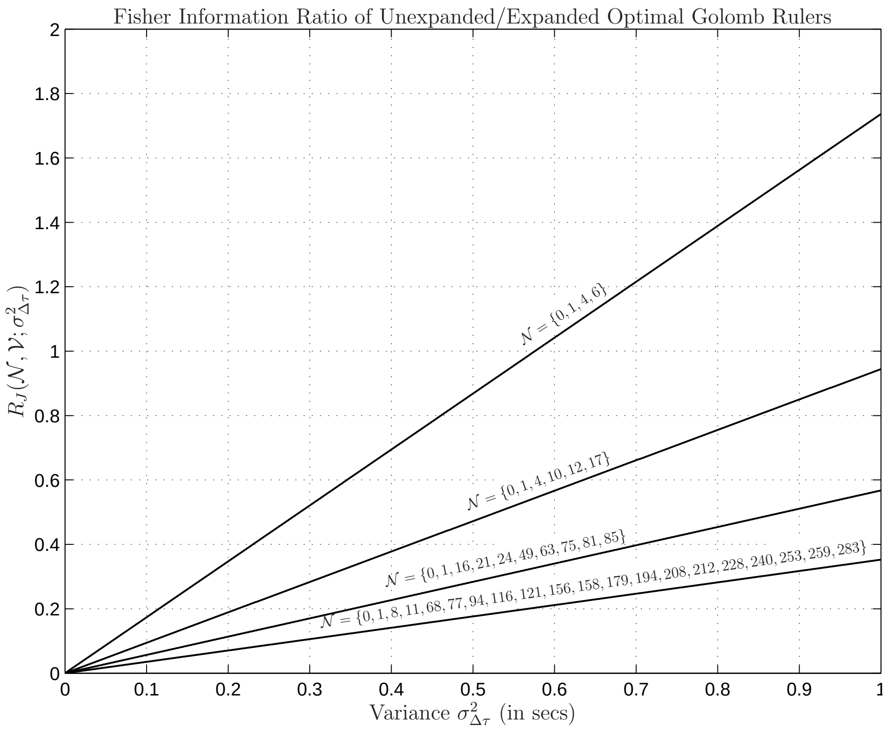

Figure 4.4: Evolution of Fisher Information ratio $R_J(\mathcal{N},\mathcal{V};\Delta f,\sigma^2_{\Delta\tau})$ as a function of the time of arrival error variance $\sigma^2_{\Delta\tau}$, associated with different rulers $\mathcal{N}$.

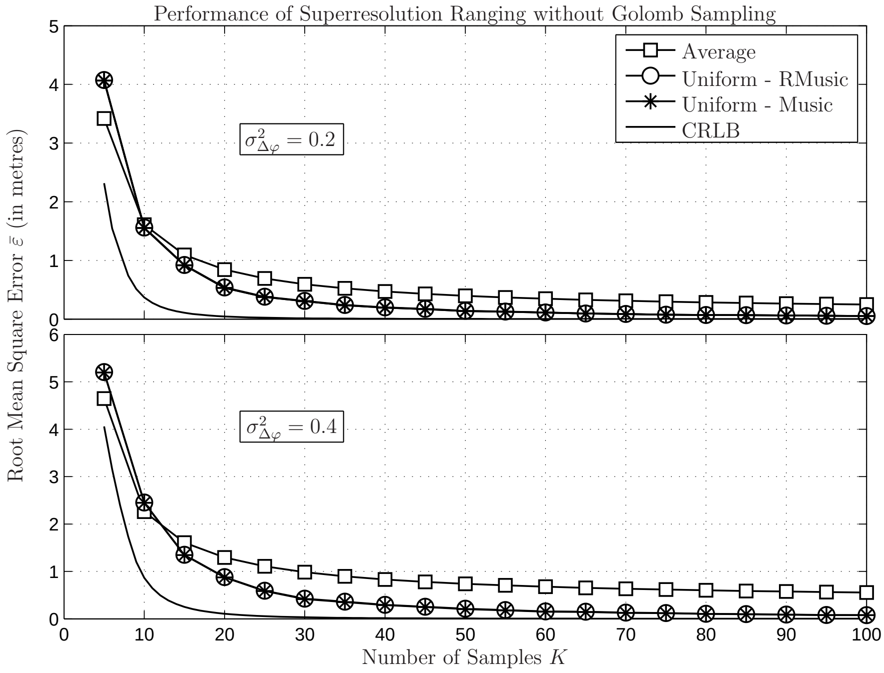

(a) As function of K, for different $\sigma^2_{\Delta\varphi}$.

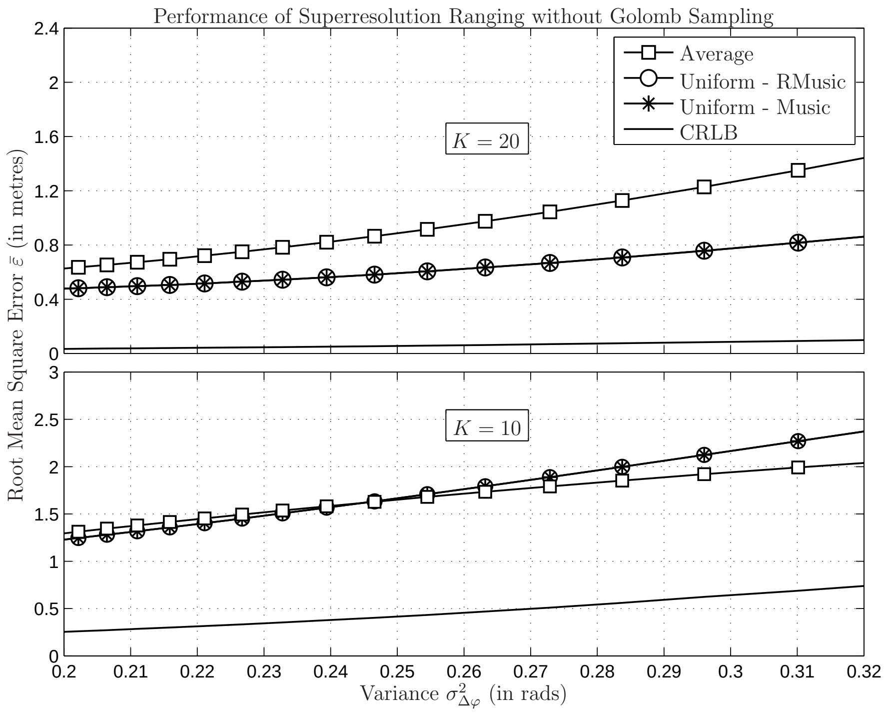

(b) As function of $\sigma^2_{\Delta\varphi}$, for different K.

Figure 4.5: Performance of superresolution and average-based ranging algorithms as a function of the sample set sizes K and the phase error variance $\sigma^2_{\Delta\varphi}$, *without* Golomb-optimized sampling.

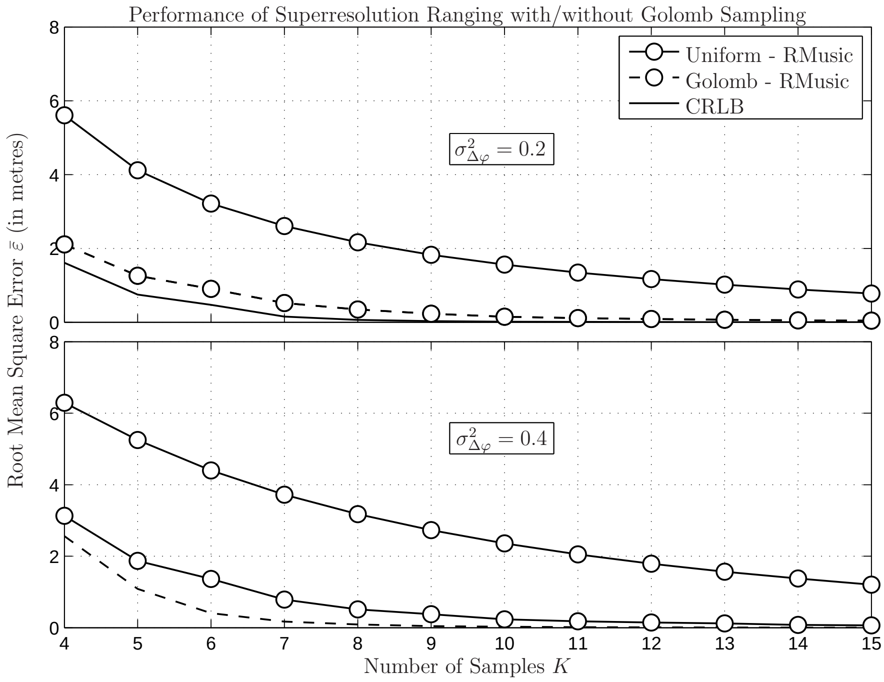

(a) As function of K, for different $\sigma^2_{\Delta\varphi}$.

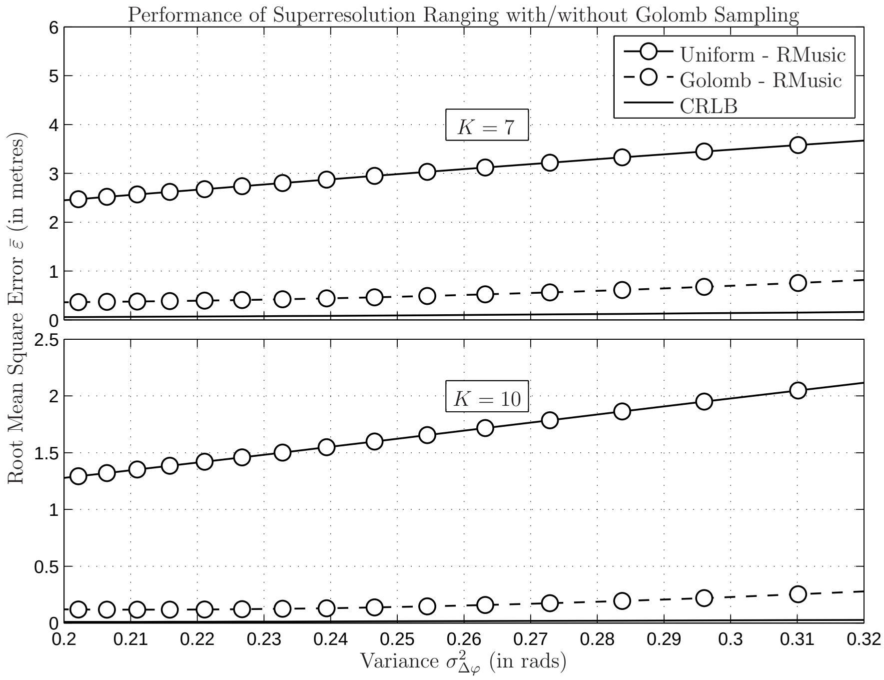

(b) As function of $\sigma^2_{\Delta\varphi}$, for different K.

Figure 4.6: Performance of superresolution ranging algorithms as a function of the sample set sizes K and the phase error variance $\sigma^2_{\Delta\varphi}$, both *with* and *without* Golomb-optimized sampling.

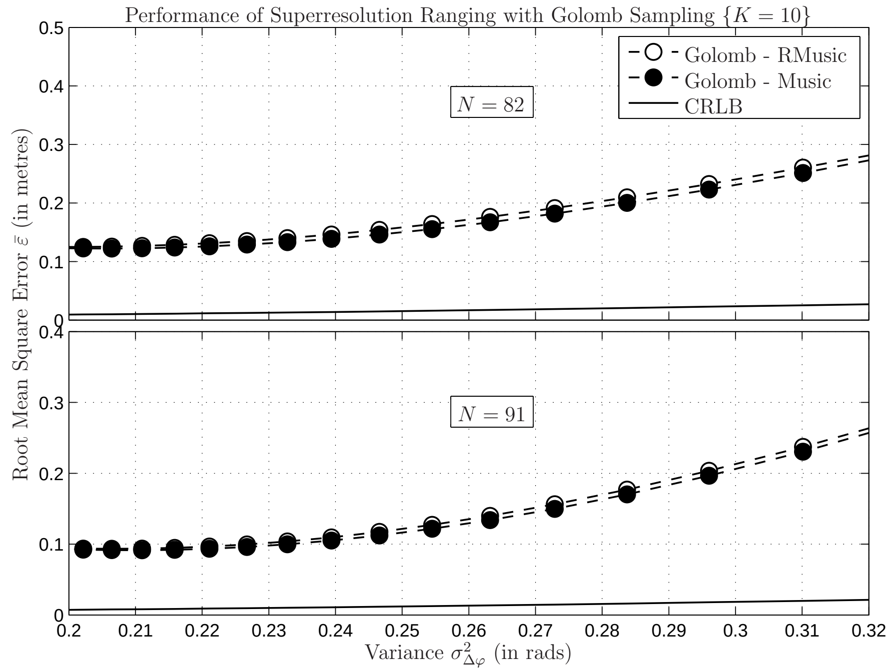

(a) As function of $\sigma^2_{\Delta\varphi}$, for the same K but different N.

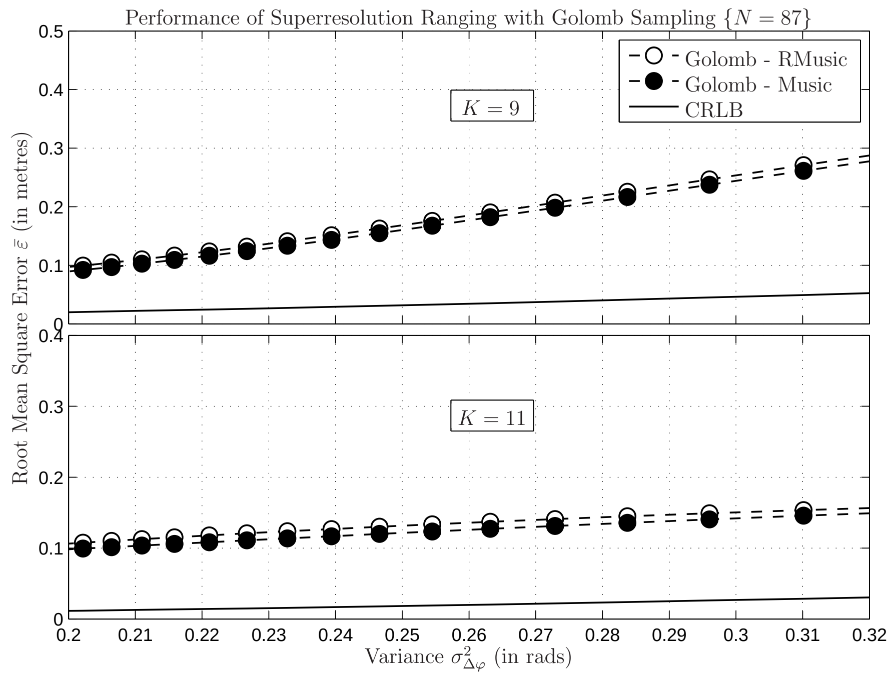

(b) As function of $\sigma^2_{\Delta\varphi}$, for the same N but different K.

Figure 4.7: Performance of superresolution ranging algorithms as a function of the sample set sizes K and length N, and the phase error variance $\sigma^2_{\Delta\varphi}$, both *with* Golomb-optimized sampling.

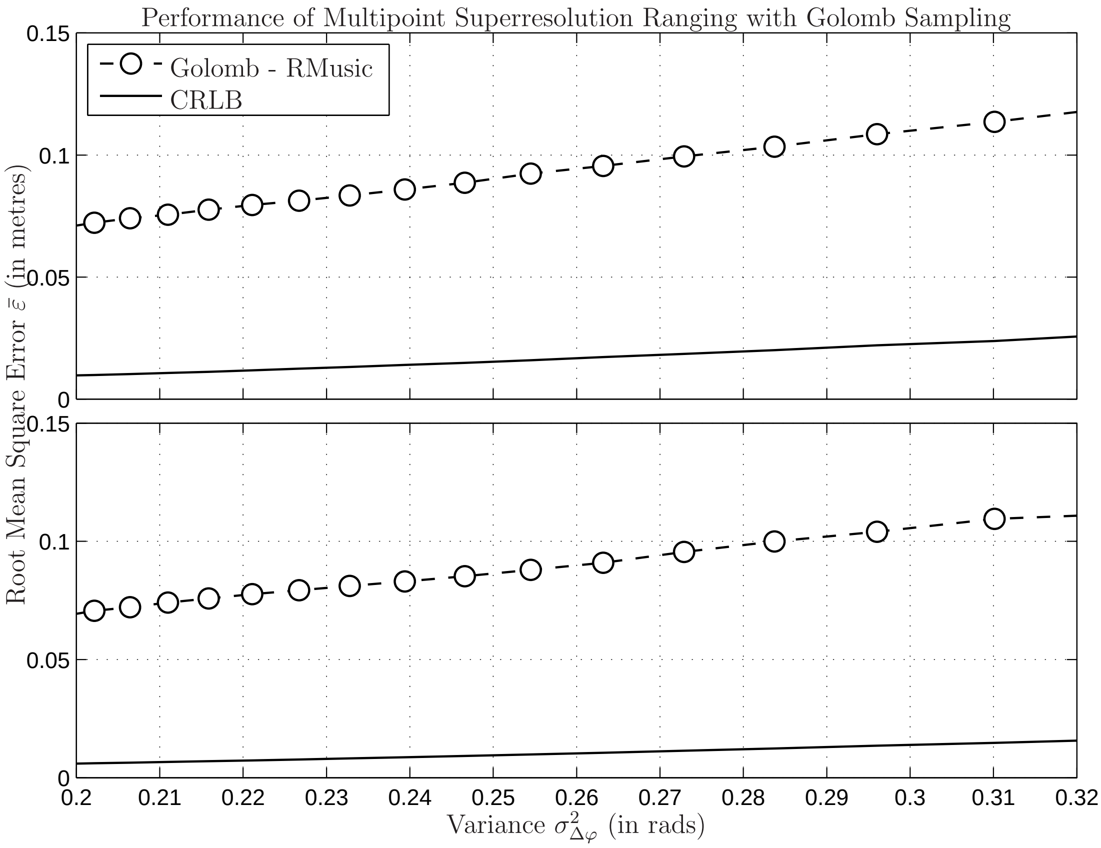

Figure 4.8: Performance of Golomb-optimized superresolution multipoint ranging with ERQ and FRA ruler allocation approaches.

Considered in coordination with the results of Figure 4.3, it can be generally said that a Golomb-optimized scheme with a total of 10 samples, taken at frequencies corresponding to an accordingly Golomb ruler $\mathcal{N}$ expanded into the associated measure set $\mathcal{V}$, followed by MUSIC estimation is an excellent choice for PDoA ranging.

Also, Golomb rulers are individually analysed for ranging so as to shed more light on their choice in relation to its sample set size K and length N. As seen in Figure 4.7(a), the Golomb ruler with a larger sample set length $N = 91$ performs better than the ruler with length $N = 82$ for an equal sample set size $K = 10$. Similarly also in Figure 4.7(b), for an equal sample set length $N = 87$, obviously the Golomb ruler with a larger sample set size $K = 11$ performs better than the ruler with size $K = 9$.

In fact, as illustrated by Table 4.2, such a choice also allows for an easy design of various orthogonal Golomb rulers, such that multipoint ranging can be efficiently performed. But since in this case a choice also can be made between the ERQ and FRA ruler allocation approaches, a fair question to ask in this context is what are the performances of corresponding choices.

This is addressed in Figure 4.8, where the average performances of an ERQ and an FRA multipoint ranging schemes employing the rulers shown in Table 4.2 are compared against corresponding CRLBs. The figure shows that in fact both approaches have similar performances relative to one another and relative to the CRLBs.

4.5 Conclusions

We offered an efficient and accurate solution to the multipoint ranging problem, based on an adaptation of superresolution techniques, with optimized sampling. Specifically, using as examples the specific cases of Time of Arrival and Phase-Difference of Arrival, unified under the same mathematical framework, we constructed a variation of the MUSIC and Root MUSIC algorithm to perform distance estimation over sparse sample sets determined by Golomb rulers. The design of the mutually orthogonal sets of Golomb rulers required by the proposed multipoint ranging method – a problem that founds no solution in current literature – was shown to be achievable via a new evolutionary genetic algorithm, which was also shown to outperform the best known alternative when used to generate optimal rulers. A Cramèr-Rao Lower Bound analysis of the overall optimized multipoint ranging solution was performed, which compared to simulated results quantified the substantial gains achieved by the proposed technique.

Chapter 5

Application for Indoor Wireless Localization

5.1 Introduction

Wireless localization is a very mature area of research, with plenty of work done in recent years both in academia and industry [21, 27]. Despite the amount of effort put into this problem, wireless positioning systems are still far off their potential as an ubiquitous and real-time locating technology [8, 9, 11].

Ubiquity requires the technology to be available in every environment, while real-time technology implies automatic identification and tracking within an environment. It is well-known that wireless localization systems are still inaccurate and unreliable in places such as urban cities and indoors, which are characterized by high multipath propagation and scarcity of LOS conditions. In comparison to the quality and omnipresence of satellite- and cellular-based systems (GPS and Mobile networks) in open outdoor spaces, indoor positioning systems [74–76] are still quite fragile and under-deployed.

For currently deployed indoor positioning systems, performance is mostly evaluated in terms of accuracy in target location and tracking, which is not sufficient in evaluating positioning systems. An indoor positioning system which satisfies performance measures and solves open challenges in wireless localization such as accuracy, precision, efficiency, complexity, robustness and cost is necessary. Therefore, we seek to present ranging and trilateration techniques (utilizing simulation and a positioning evaluation kit for range measurements acquisition) which satisfy some of the necessary performance metrics required for wireless localization.

To enable the implementation of some of the techniques described in this thesis, an indoor positioning system which allows the estimation of a target's position using PDoA ranging (based on its advantage over other traditional ranging techniques) is required. As a result, the ZigBee-based (IEEE 802.15.4 complaint) positioning evaluation kit developed by ZIGPOS GmbH [75] based on Atmel's phase measurement ranging technology [114] was purchased for this research. This technology is already an energy efficient, scalable and low cost real-time location system which offers the flexibility to modify its radio transceiver parameter configuration, ranging measurement and network parameter configuration to obtain Phase Measurement Units (PMU) according to the uniform and non-uniform ranging models described in Subsection 4.2.2 and shown in Figure 4.2.

In this chapter, we present two accurate ranging techniques to obtain multiple measured distances from a single realization of phase measurements by – 1) applying superresolution techniques to different permuted set of phase measurements with an outliers detection technique, and 2) a new slope sampling algorithm utilizing a resolution tolerance and confidence threshold peak search on the obtained spectrum of the residues. The acquired multiple distances are used to estimate the position of the target position using the most accurate state-of-the-art localization algorithm – SMDS evaluated in Chapter 1 which requires an initial target estimate. The initial target estimate will be obtained from the intersections of measured distances (estimates obtained from ranging algorithms) and the target position from the previous realization of phase measurements. These techniques seek to solve some very important performance measures in indoor positioning system (efficient, accuracy, precision and robustness) in two different network localization scenarios (inside and outside of the anchors) for target localization. It is important to mention that we are not providing a technology, rather proposing and implementing algorithms and techniques for an accurate wireless localization.

For the rest of this chapter: in Section 5.2, a brief description of the ZIGPOS positioning kit with descriptions and specifications are provided. Then, we introduce the system model for ranging and positioning as well as different network localization scenarios, which is followed by proposing new ranging techniques as well as trilateration techniques for target localization in Section 5.3. Results and performance evaluation of the proposed techniques for target localization are provided in Section 5.4, while conclusions are presented in Section 5.5.

(a) The REB233SMAD-EK hardware platform [114].

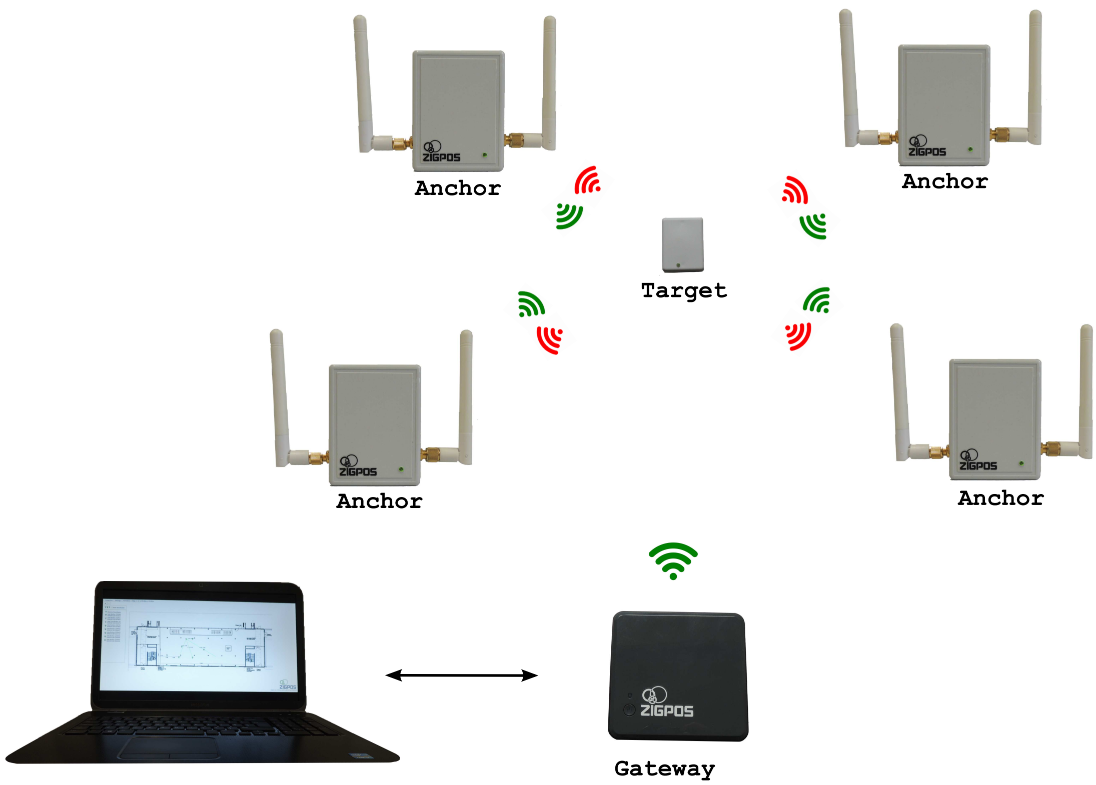

(b) The positioning kits and RTLS toolbox evaluation application and kit [32].

Figure 5.1: The ZIGPOS-RTLS Positioning Evaluation Technology.

5.2 ZIGPOS Positioning Evaluation Kit

The ZIGPOS positioning evaluation kit is a ZigBee-based (built on the IEEE 802.15.4[1] low-rate, wireless personal area networks (LoWPAN) standard) set of devices which were developed by ZIGPOS gGmbH in cooperation with Dresden elektronik [32, 75] for an easy to use, energy efficient, scalable and low cost indoor and outdoor real-time location system based on Atmel's phase measurement ranging technology (only indoor environment will be considered for evaluation in wireless localization).

The evaluation kit contains the easy to use ZIGPOS-RTLS toolbox evaluation application, a powerful software used to obtain the PMUs, multiple anchors (FFDs) and tags or targets (RFDs) as well as a coordinator or a gateway (FFD) which interfaces to a terminal application (computer system) for evaluating the performance of the technology in different applications [32]. From an engineeering and technical approach, the RTLS toolbox evaluation application is operated on an 8-bit Atmel Microcontroller Base Board with a recently developed REB233SMAD-EK hardware platform shown in Figure 5.1(a). The REB233SMAD-EK is a brand new state of the art device containing a unique set of the 2.4GHz RF transceiver AT86RF233 combined with the prominent microcontroller base board is able to evaluate radio transceiver PMUs, and modify functionality features such as transceiver radio, ranging measurement and network parameter configuration, and commands to automate ranging measurements [115].

The REB233SMAD-EK comprises two components – Radio Extender Board and Controller Base Board along with a USB port to enable connectivity with the PC terminal. The Radio Extender Board modules are assembled based on AT86RF233 radio transceiver which support IEEE 802.15.4 and ZigBee compatible communications with two SubMiniature version A (SMA) antennas to demonstrate an hardware-based antenna diversity attribute so as to improve the robustness of the radio link in harsh RF channels [115] and obtain accurate phase measurement add-on units, thereby enabling low cost and energy efficient combination of radio communication and position

[1]The IEEE 802.15.4 physical layer approves three different radio bands which are the 2.4GHz ISM band with 16 channels and 250Kbps data rate (Worldwide), 915MHz ISM band with 10 channels and 40Kbps data rate (Americas) and finally, the 868MHz band with one channel and 20Kbps data rate (Europe). The transmission range of a ZigBee-based device is between 1 and 100 meters. The ZigBee standard defines two devices which are Full Function Devices (FFDs) and Reduced Function Device (RFDs). FFDs serve as a regular wireless device and can as a network coordinator or gateway, enabling communication with any other device. RFDs are utilized for simpler applications and can only communicate with FFDs. A ZigBee-based network is known to scale up to over 65,000 nodes while utilizing a trust center-based authentication with a 128-bit Advanced Encryption Standard cryptography for security [82].

estimation of a wireless sensor node. The connection between the two REB233SMAD-EK components, form a completely functional and battery enabled wireless device.

Using the evaluation positioning kits in Figure 5.1(b), our input is reduced to developing and implementing ranging and trilateration techniques and algorithms for wireless localization capable in indoor and outdoor environments. This kit provides comprehensive monitoring, control and commissioning of network capabilities as well as ranging parameters such as frequency correction, antenna diversity, start and stop frequencies, frequency step, distance offset, and transmit power to easily deploy various network parameters and conditions. With the use of the graphical user interface, little or no in-depth knowledge in programming and IEEE 802.15.4 standards are required to evaluate the positioning kit.

In the next section, we present a system model for ranging and positioning with the two different network localization scenarios, and provide a detailed description of presented ranging techniques and algorithms, which are implemented to improve the accuracy of distance estimation followed by proposing new trilateration techniques implemented for a robust, accurate and precise target wireless localization.

5.3 Ranging and trilateration techniques

5.3.1 System Model

Consider a network of N nodes in an η-dimensional Euclidean space, out of which devices indexed $1, \cdots, N_t$ are *target* nodes which have no knowledge of their location (sometimes called sources), while devices indexed $N_t+1, \cdots, N_t+N_a$ are *anchor* nodes, i.e. reference devices of *a priori* known location. For comprehensibility, we will therefore consider the case of when $\eta = 2$, with the remark that the analysis to follow can be straightforwardly extended towards $\eta > 2$.

The localization problem consists of estimating the location of target nodes, given the knowledge on the location of anchors, and a set of measured distances amongst these various devices, which are typically affected by noise and bias [42].

To elaborate, let the coordinates of the i-th target be denoted by (x_i, y_i), and let us append the ordinates of all targets into the vector $\boldsymbol{\theta_x}$, and the corresponding abscises into the vector $\boldsymbol{\theta_y}$, such that the targets' coordinate vector to be estimated can be described by

$$\boldsymbol{\Theta} \triangleq [\boldsymbol{\theta_x}, \boldsymbol{\theta_y}] = [x_1, \cdots, x_{N_t}, y_1, \cdots, y_{N_t}]. \tag{5.1}$$

Likewise, the coordinates of the j-th anchor can be denoted as (x_j, y_j) and therefore, we describe all anchors' coordinate vector by

$$\boldsymbol{\Phi} \triangleq [\boldsymbol{\phi}_x, \boldsymbol{\phi}_y] = [x_{N_t+1}, \cdots, x_{N_t+N_a}, y_{N_t+1}, \cdots, y_{N_t+N_a}]. \tag{5.2}$$

It is assumed that when a pair of devices are able to communicate with one another, they can measure the mutual distance between each other, a process which is hereafter referred to as *ranging*. Ranging measurements are, however, customarily affected by noise and often not conducted over a LOS link between communicating devices. In NLOS and multipath conditions, additional ranging error in the form of a positive deviation from the true distance appears, which is referred to as *bias*. For simplicity, however, we will combine the ranging errors for both noise and bias. Under these assumptions, the ranging model applicable to a pair of devices i-th and j-th is given by

$$\tilde{d}_{ij} = d_{ij} + v_{ij} \equiv \sqrt{(x_i - x_j)^2 + (y_i - y_j)^2} + v_{ij}, \tag{5.3}$$

where $\tilde{d}_{ij}$ is the measured distance, d_{ij} is the true distance and the so-called *residual noise* v_{ij} is the ranging error resulting from both noise and bias in the wireless channel either in LOS or NLOS conditions.

In the next subsection, we provide a description of the different possible network localization scenarios for ranging and positioning.

5.3.2 Network Localization Scenarios

Two different and common network localization scenarios are possible as a result of the connection between a target and multiple anchors in a wireless network. The network localization scenarios are such that the targets $\boldsymbol{\Theta}$ are either inside the convex hull $\mathcal{C}(\boldsymbol{\Phi})$ of the anchors or outside the convex hull $\mathcal{C}(\boldsymbol{\Phi})$ of the anchors, where the $\mathcal{C}(\boldsymbol{\Phi})$ is the *convex hull* of $\boldsymbol{\Phi}$, i.e., the smallest convex set comprising the anchors as seen in Figure 5.2. The inside the convex hull scenario is the default scenario in indoor wireless localization originating from cellular and mobile networks, where anchors or base stations surround the target or mobile user, while the unpopular outside the convex hull scenario does occur mostly in situations where targets encounter communication and ranging difficulties with anchors, and also when targets are located in the corridor of a building while anchors are inside the rooms or offices.

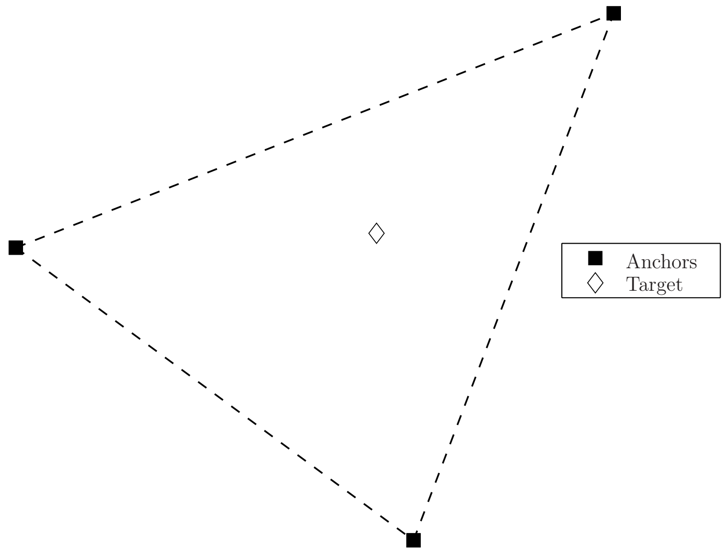

(a) Target inside $\mathcal{C}(\mathbf{\Phi})$.

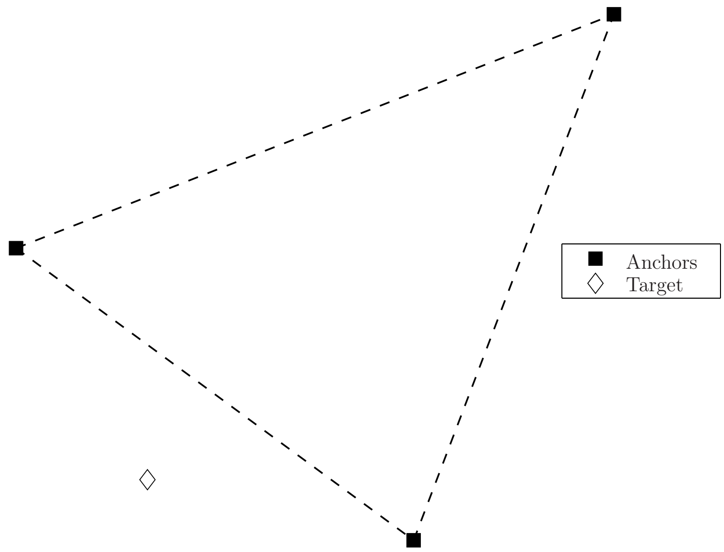

(b) Target outside $\mathcal{C}(\mathbf{\Phi})$.

Figure 5.2: Network Localization Scenarios.

5.3.3 Ranging Techniques

For an accurate estimation of the mutual distance between a pair of devices *e.g.* an anchor and a target, robust and accurate ranging techniques are necessary. Therefore, we seek to present accurate ranging techniques to be applied on Phase-Difference of Arrival (PDoA) measurements computed from Phase Measurement Units (PMU), which are to be obtained from the ZIGPOS positioning kit. Therein, let us quickly describe the steps involved in obtaining PMUs.

For the computation of PMUs, as illustrated in Figure 4.2, an anchor A acting as an initiator emits a continuous sinusoidal wave of frequency f with a known PMU and the target T acts as an active reflector, such that A can measure the PMU of the received (reflected) signal. In this thesis, the carrier frequencies to be used for emitting the continuous sinusoidal waves are from the free unlicensed $2.4 - 2.5$GHz Industrial, Scientific and Medical (ISM) radio bands channels available worldwide. The PMUs are obtained using a specified set of carrier frequencies $\mathbb{F} = \{f_{n_1}, \cdots, f_{n_K}\}$ such that the minimum frequency difference $\Delta f = \min \left[f_{n_{k+1}} - f_{n_k} \middle| \, k = 1, \cdots, K-1 \right]$ so as to optimize resources (frequencies and time), where $\mathcal{N} = \{n_1, \cdots, n_K\}$ is a Golomb ruler.

The REB233SMAD-EK hardware platform of the positioning kit operates on an 8-bit microcontroller board, which results in PMUs having integer values between 0 and 255 as seen in Figure 5.3. It is easy to note a few of the ranging configuration parameters used in obtaining PMUs on the first row such as the timestamps, start frequencies = 2403.0MHz, frequency step = 0.5MHz etc. Subsequently from the second row, entailed in its first column are the carrier frequencies $\mathbb{F} = \{2403.0, 2408.5, \cdots, 2483.0\}$MHz and the remaining columns are the known PMUs of the transmitted signal, PMUs of the reflected signal and a zero vector ($\mathbf{0}$). Each of the transmitted and reflected PMUs, for a given frequency, have an equal number of snapshots S

$$S = \frac{\text{number of columns} \;-\; 2}{2},$$

which is the number of transmitted or received PMU measurements in each frequencies.

The transmitted and reflected PMUs are converted to transmitted and reflected phases utilizing

$$\tilde{\varphi} \triangleq \frac{2\pi \cdot \text{PMU}}{2^8}, \quad 0 \le \tilde{\varphi} \le 2\pi, \tag{5.4}$$

```
fec:n/a, freqSet: 2, startFreq: 2403.0, beaconNum: 82, beaconSlot:
0, timestamp: 1386944874862
2403.0, 92, 94, 97, 66, 18, 6, 60, 255, 0, 46, 117, 255, 127, 9, 2,
255, 13, 13, 14, 17, 19, 29, 26, 25, 32, 34, 36, 40, 37, 47, 50, 49,
0
2408.5, 6, 11, 12, 103, 103, 107, 108, 105, 109, 113, 114, 116, 127,
122, 124, 132, 119, 120, 125, 132, 135, 136, 131, 139, 138, 138,
134, 148, 148, 145, 154, 157, 0
2410.0, 53, 59, 60, 15, 19, 19, 20, 30, 23, 28, 32, 28, 36, 40, 40,
48, 155, 160, 162, 163, 159, 170, 169, 176, 172, 182, 175, 184, 184,
183, 183, 195, 0
2410.5, 48, 53, 59, 65, 68, 68, 69, 71, 73, 78, 77, 80, 84, 95, 90,
95, 152, 149, 142, 154, 158, 155, 160, 163, 168, 167, 169, 169, 182,
174, 176, 183, 0
2415.0, 197, 195, 207, 56, 58, 64, 67, 68, 72, 73, 77, 74, 73, 81,
89, 78, 0, 3, 255, 5, 7, 8, 16, 16, 19, 22, 22, 25, 31, 31, 35, 33,
0
2425.5, 19, 28, 27, 210, 208, 209, 206, 214, 219, 217, 219, 224,
229, 233, 235, 233, 235, 233, 235, 232, 236, 244, 233, 248, 251, 2,
253, 1, 254, 2, 6, 8, 0
2433.5, 66, 72, 70, 32, 24, 28, 33, 42, 39, 47, 42, 45, 46, 57, 47,
52, 178, 189, 196, 194, 193, 196, 197, 204, 204, 213, 210, 217, 215,
213, 221, 221, 0
2445.0, 178, 182, 187, 75, 78, 82, 84, 85, 86, 86, 84, 104, 100, 99,
100, 107, 154, 158, 166, 162, 166, 167, 174, 176, 170, 178, 180,
185, 193, 186, 192, 192, 0
2454.5, 237, 240, 241, 182, 193, 198, 199, 192, 200, 200, 200, 206,
213, 215, 218, 224, 115, 121, 113, 123, 133, 127, 125, 132, 137,
136, 139, 142, 144, 148, 147, 150, 0
2463.0, 65, 63, 65, 236, 236, 247, 252, 249, 250, 255, 5, 8, 5, 8,
9, 12, 117, 125, 127, 127, 130, 136, 133, 135, 144, 146, 151, 144,
144, 152, 160, 158, 0
2465.5, 152, 160, 150, 66, 68, 70, 72, 73, 73, 74, 83, 85, 88, 87,
95, 100, 174, 183, 185, 188, 184, 185, 195, 198, 198, 203, 197, 209,
207, 211, 210, 216, 0
2469.0, 89, 88, 86, 152, 158, 165, 160, 160, 164, 173, 173, 173,
171, 179, 176, 179, 53, 52, 52, 51, 54, 55, 57, 68, 63, 66, 80, 82,
78, 75, 83, 81, 0
2479.0, 20, 20, 27, 89, 90, 96, 98, 95, 100, 105, 102, 106, 113,
121, 123, 115, 145, 157, 160, 154, 160, 161, 168, 171, 176, 169,
166, 182, 184, 178, 182, 186, 0
2482.0, 143, 138, 146, 26, 32, 34, 37, 31, 36, 42, 52, 47, 49, 51,
55, 60, 255, 3, 5, 1, 12, 11, 12, 22, 21, 23, 28, 23, 28, 36, 33,
36, 0
2483.0, 176, 181, 181, 149, 147, 148, 148, 151, 156, 162, 162, 164,
168, 171, 177, 174, 30, 32, 31, 40, 35, 44, 45, 46, 47, 47, 58, 61,
60, 57, 58, 63, 0
```

Figure 5.3: A single realization of measured PMUs from the ZIGPOS positioning kit [32].

$$\begin{bmatrix} \tilde{\varphi}_{\text{TX}_1 f_{n_1}} & \cdots & \tilde{\varphi}_{\text{TX}_S f_{n_1}} & | & \tilde{\varphi}_{\text{RX}_1 f_{n_1}} & \cdots & \tilde{\varphi}_{\text{RX}_S f_{n_1}} \\ \tilde{\varphi}_{\text{TX}_1 f_{n_2}} & \cdots & \tilde{\varphi}_{\text{TX}_S f_{n_1}} & | & \tilde{\varphi}_{\text{RX}_1 f_{n_2}} & \cdots & \tilde{\varphi}_{\text{RX}_S f_{n_2}} \\ & \vdots & & \cdots & & \vdots & \\ \tilde{\varphi}_{\text{TX}_1 f_{n_K}} & \cdots & \tilde{\varphi}_{\text{TX}_S f_{n_1}} & | & \tilde{\varphi}_{\text{RX}_1 f_{n_K}} & \cdots & \tilde{\varphi}_{\text{RX}_S f_{n_K}} \end{bmatrix}, \tag{5.5}$$

and the resulting measured phases by taking all possible pairwise differences between the transmitted phases $[\tilde{\varphi}_{\text{TX}_1 f_{n_k}}, \cdots, \tilde{\varphi}_{\text{TX}_S f_{n_k}}]$ and reflected phases $[\tilde{\varphi}_{\text{RX}_1 f_{n_k}}, \cdots, \tilde{\varphi}_{\text{RX}_S f_{n_k}}]$ for each frequencies $\mathbb{F} = \{f_{n_1}, \cdots, f_{n_K}\}$ using equation (4.4) is

$$\tilde{\boldsymbol{\Phi}} \triangleq \tilde{\boldsymbol{\Phi}}_{\text{RX}} - \tilde{\boldsymbol{\Phi}}_{\text{TX}} = [\tilde{\boldsymbol{\varphi}}_{\mathcal{N}:1}, \cdots, \tilde{\boldsymbol{\varphi}}_{\mathcal{N}:S^2}]$$

$$\tilde{\boldsymbol{\Phi}} = \begin{bmatrix} \tilde{\boldsymbol{\varphi}}_{n_1} \\ \tilde{\boldsymbol{\varphi}}_{n_2} \\ \vdots \\ \tilde{\boldsymbol{\varphi}}_{n_K} \end{bmatrix} = \begin{bmatrix} \tilde{\varphi}_{n_1:1} & \cdots & \tilde{\varphi}_{n_1:S^2} \\ \tilde{\varphi}_{n_2:1} & \cdots & \tilde{\varphi}_{n_2:S^2} \\ \vdots & \cdots & \vdots \\ \tilde{\varphi}_{n_K:1} & \cdots & \tilde{\varphi}_{n_K:S^2} \end{bmatrix}, \quad -2\pi \leq \tilde{\varphi} \leq 2\pi, \tag{5.6}$$

Next, we take a look at the phase measurements $\tilde{\boldsymbol{\Phi}}$ as a function of the frequencies $\mathbb{F}$, then estimate the phase errors and their distribution. Finally, we present new ranging techniques along with algorithms already described in previous chapters to improve phase measurements and compute accurate measured distances.

5.3.3.1 Phase Measurements

A common constraint encountered in phase measurements obtained from a wireless environment, is that the measured phases $\tilde{\boldsymbol{\Phi}}$ are quantized between -2π and 2π as plotted in Figure 5.4(a), which results in $\tilde{\boldsymbol{\Phi}}$ not increasing linearly across all frequencies $\mathbb{F}_{\mathcal{N}}$ as depicted by equation (4.5). This problem becomes evident in the fact that the computation of $\tilde{d}$ is directly dependent on the gradient $\frac{\Delta\varphi}{\Delta f}$ as seen in equation (3.1). The plot of measured phases $\tilde{\boldsymbol{\Phi}}$ against frequencies $\mathbb{F}$ should be a smooth straight line, which is not the case in Figure 5.4(a). Therefore, this is achieved using an unwrap algorithm which corrects $\tilde{\boldsymbol{\varphi}}_{\mathcal{N}:s}$ across all frequencies $\mathbb{F}$ for a given snapshot s by adding multiples of $\pm 2\pi$ when the absolute jumps between consecutive elements of $\tilde{\boldsymbol{\varphi}}_{\mathcal{N}:s}$ are greater than or equal to the jump tolerance of π.

A pseudo-code of the unwrap algorithm is given in Appendix A, with the result of the unwrap algorithm on the measured phases $\tilde{\boldsymbol{\Phi}}$ shown in Figure 5.4(b). For a given true distance d, the resulting true phases $\boldsymbol{\varphi}$ are obtained using equation (4.4) as

$$\boldsymbol{\varphi} \triangleq \boldsymbol{\varphi}_{\mathrm{RX}} - \boldsymbol{\varphi}_{\mathrm{TX}} = \frac{4\pi d}{c}\mathbb{F} - 2\pi L, \tag{5.7}$$

where $L = \mathrm{floor}(d \cdot \frac{\mathbb{F}}{c})$ denotes the number of complete sinusoidal cycles.

The objective of the unwrap algorithm is to achieve smoothness of the phase measurements $\tilde{\boldsymbol{\varphi}}$, and also enable the easy estimation of measured distance $\tilde{d}$ using a simple algorithm. Due to this smoothness, $\tilde{d}$ can be accurately estimated from a single snapshot s using the average ranging technique in equation (4.5)

$$\tilde{d} = \nabla \cdot \frac{c}{4\pi} = \frac{\sum_{k=1}^{K} f_{n_k} \cdot \tilde{\boldsymbol{\varphi}}_{n_k:s} - \frac{1}{K}\sum_{k=1}^{K} f_{n_k} \cdot \sum_{k=1}^{K} \tilde{\boldsymbol{\varphi}}_{n_k:s}}{\sum_{k=1}^{K} f_{n_k}^2 - \frac{1}{K}\Big(\sum_{k=1}^{K} f_{n_k}\Big)^2} \cdot \frac{c}{4\pi}, \tag{5.8}$$

where $\nabla = \frac{\Delta\varphi}{\Delta f}$ is the gradient the measured phases as a function of frequencies in Figure 5.4(b) which directly determines $\tilde{d}$.

For the average ranging technique, results showed that the measured distances $\tilde{d}$ have errors ranging between 11cm and 31cm as the measured phase measurement units were evaluated in LOS channel conditions. This confirms that in a clean wireless channel, the simple average technique is an adequate algorithm for measuring the distance between communicating devices using PDoA measurements with multiple carrier frequencies.

Taking a closer look at the measured phases[2], the errors are said to be subject to independent and identically distributed Tikhonov random errors as stated in Subsection 4.4.1. To put this in perspective, we estimate the error on the phase measurements by taking the difference between the measured phases $\tilde{\boldsymbol{\varphi}}_{\mathcal{N}:s}$ and its corresponding estimated phases $\hat{\boldsymbol{\varphi}}_{\mathcal{N}:s}$, for a single snapshot s. The estimated phases $\hat{\boldsymbol{\varphi}}_{\mathcal{N}:s}$ of $\tilde{\boldsymbol{\varphi}}_{\mathcal{N}:s}$ for a single snapshot s are given by

$$\hat{\boldsymbol{\varphi}}_{\mathcal{N}:s} = \nabla \cdot \mathbb{F} + \frac{1}{K}\sum_{k=1}^{K} \tilde{\varphi}_{n_k:s} - \nabla \cdot \frac{1}{K}\sum_{k=1}^{K} f_{n_k}, \tag{5.9}$$

and the phase measurement errors $\boldsymbol{\varepsilon}_{\tilde{\varphi}}$ on the measured phases $\tilde{\boldsymbol{\varphi}}_{\mathcal{N}:s}$ as

$$\boldsymbol{\varepsilon}_{\tilde{\varphi}} = \angle\left(\frac{\exp(j\tilde{\boldsymbol{\varphi}}_{\mathcal{N}:s})}{\exp(j\hat{\boldsymbol{\varphi}}_{\mathcal{N}:s})}\right), \tag{5.10}$$

where $\angle(-)$ returns the phase angles in radians of the complex elements (-).

[2] Subsequently, all measured phases $\tilde{\boldsymbol{\varphi}}$ are unwrapped.

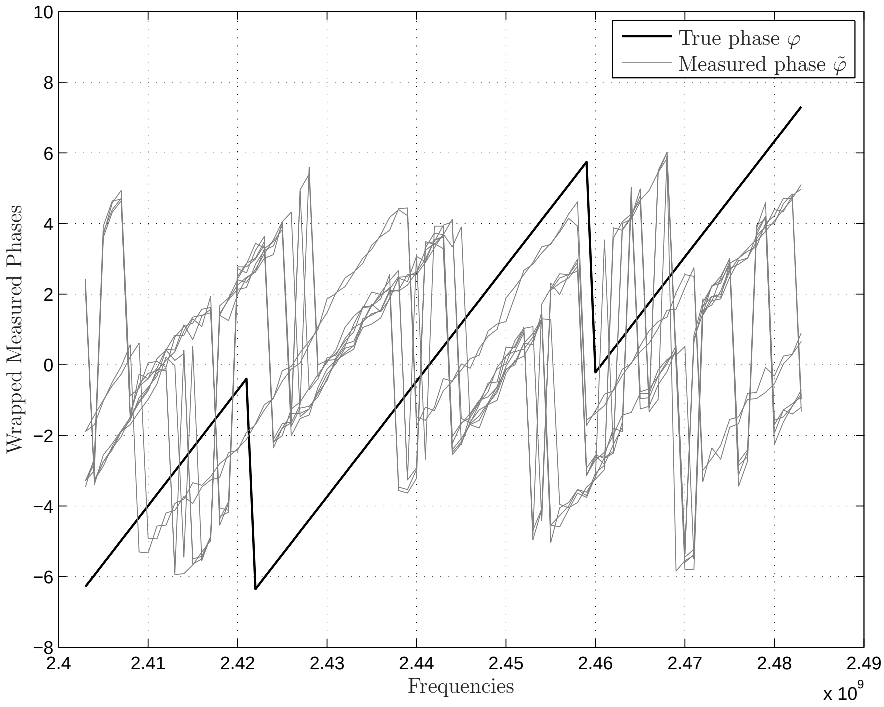

(a) Wrapped $\boldsymbol{\varphi}$ and $\tilde{\boldsymbol{\varphi}}$ as a function of frequencies $\mathbb{F}$.

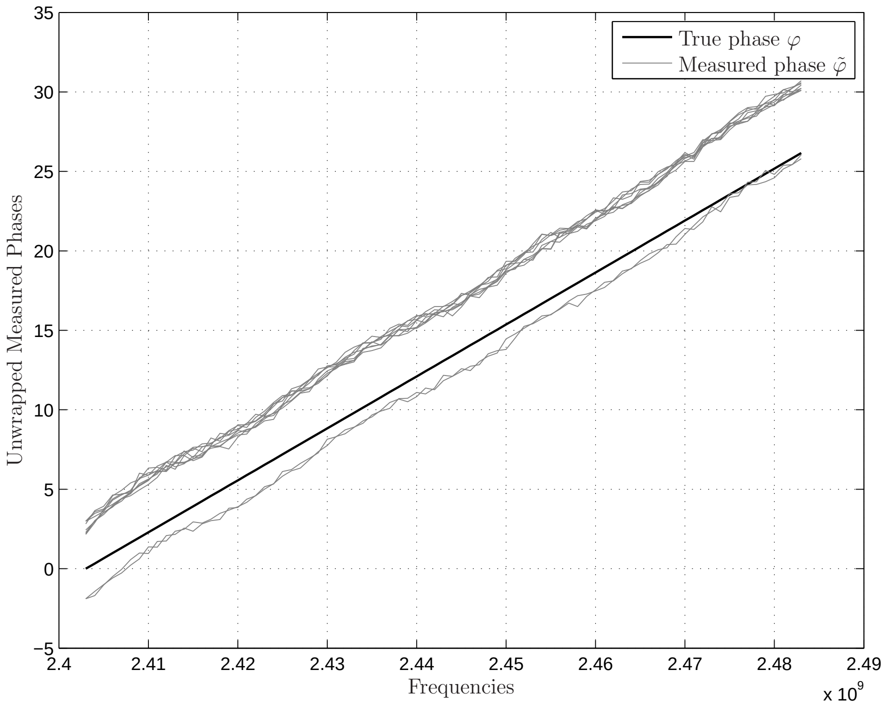

(b) Unwrapped $\boldsymbol{\varphi}$ and $\tilde{\boldsymbol{\varphi}}$ as a function of frequencies $\mathbb{F}$.

Figure 5.4: The true and measured phases and their unwrapped versions as a function of their corresponding frequencies in LOS conditons.

An histogram of the phase measurement errors $\boldsymbol{\varepsilon}_{\tilde{\boldsymbol{\varphi}}}$ for a given frequency f_{n_k} is shown in Figure 5.5 with a theoretical fit on the phase errors using equations (4.22) and (4.23) to obtain the necessary Signal-to-Noise Ratio (SNR) κ from the error variance $\sigma_{\tilde{\varphi}}^2$ of the phase errors and the PDF of the Tikhonov distribution. This confirms that phase measurements errors for a given frequency in a close-loop communication system (a system where the receiver is enabled with either a first or second-order phase-lock loop, which when locked tracks the phase of the received signal so as to compensate the effects of the phase errors) follows the Tikhonov or Von Mises distribution using collected insitu phase measurements [108–110]. As seen, the phase measurement errors $\boldsymbol{\varepsilon}_{\tilde{\varphi}}$ are mainly between -1 and 1 with an error variance of $\sigma_{\tilde{\varphi}}^2 = 0.3$ due to phase measurements units having been collected in LOS conditions.

As it is well-known that indoor wireless localization is performed in environments, which are characterized by high interferences from other devices and technologies sharing the $2.4 - 2.5$GHz ISM Band channels such as mobile phones and WiFi routers, rich multipath propagations from reflectors and absorbers and scarcity of LOS. Therefore, phase measurements evaluated in indoor environments are highly inaccurate and perturbed as seen in Figure 5.6, where there exists noise in the form of interferences and multhipaths in the upper bands of the selected frequencies channels. Due to these large errors in the measured phases $\tilde{\boldsymbol{\varphi}}$, the application of the unwrap algorithm did not fully achieve smoothness of the measured phases, which leads to poor and inaccurate measured distances $\tilde{d}$ using the average ranging technique in equation 5.8 ($d = 9.7$m and $\tilde{d} = 9.13\text{m}, 11.03\text{m}, 4.52\text{m}, 3.40\text{m}$ and 5.34m for the measured phases $\tilde{\boldsymbol{\varphi}}$ in Figure 5.6).

To mitigate against these interferences and multipath propagations in NLOS conditions, two different ranging techniques are presented - 1) by applying the superresolution techniques in Chapters 3 and 4 to different permuted set of phase measurements with an outliers detection technique, and 2) a new slope sampling algorithm utilizing a resolution tolerance and confidence threshold peak search on the spectrum of the obtained residues from the sampling algorithm. These ranging techniques will be applied on a single snapshot s of the measured phases $\tilde{\boldsymbol{\varphi}}_{\mathcal{N}:s}$ to compute multiple measured distances $\tilde{\mathbf{d}}$, resulting from different multipath signals in the measured phases, which will then be used for target localization with trilateration techniques to be introduced in the following subsection.

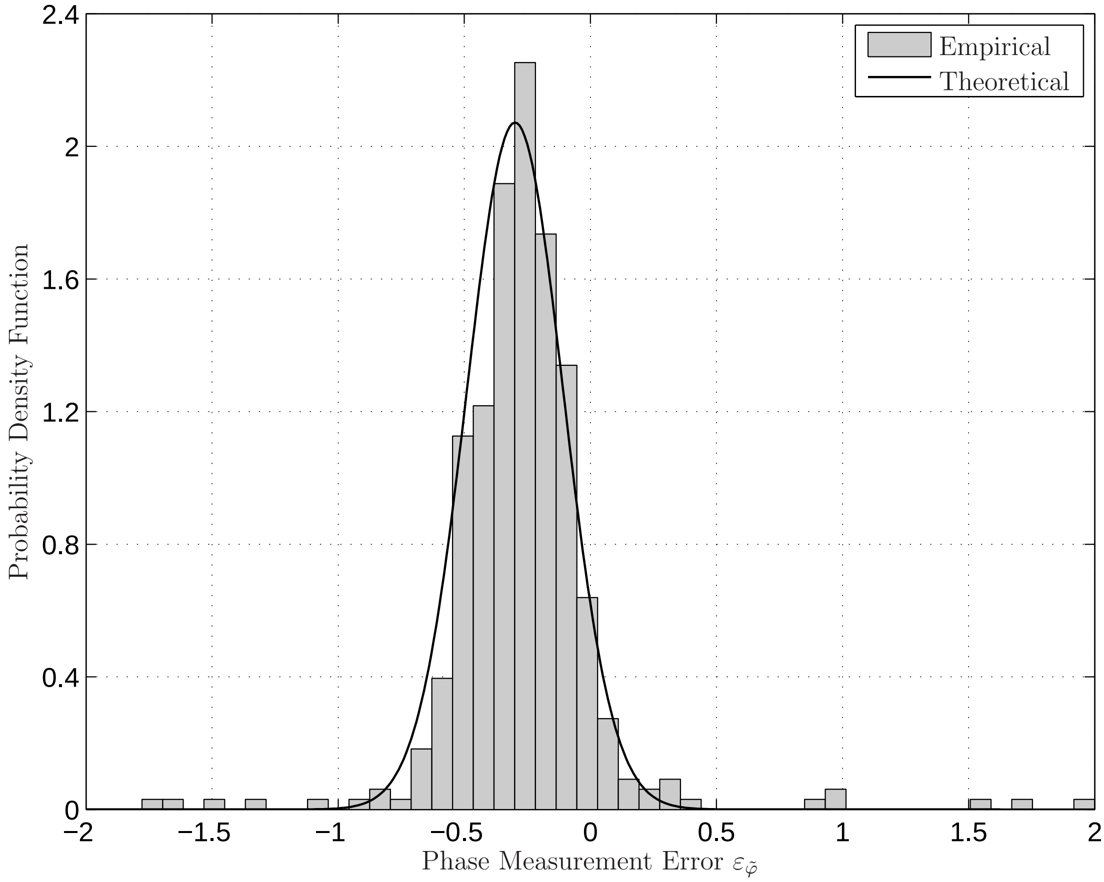

Figure 5.5: The Probability Density Function of the phase measurement errors $\boldsymbol{\varepsilon}_{\tilde{\varphi}}$.

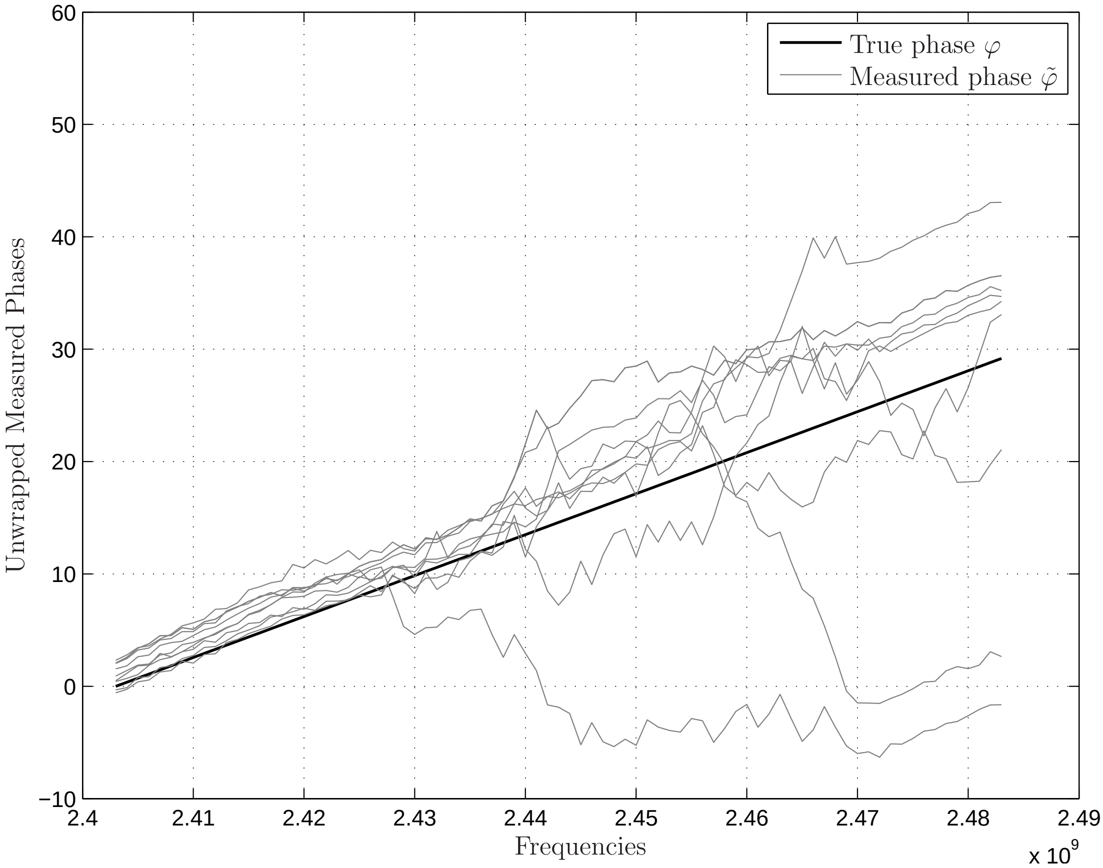

Figure 5.6: The unwrapped true $\boldsymbol{\varphi}$ and measured phases $\tilde{\boldsymbol{\varphi}}$ as a function of their corresponding frequencies in NLOS conditons.

5.3.3.2 Superresolution Algorithm with Outliers Removal Technique

From the studies of superresolution algorithms in [61, 64], it is necessary to note that the performance of superresolution algorithms for DoA estimation showed that for large values of snapshots S and covariance matrix size $M \times M$ (dependent on K) and for uncorrelated signals, the algorithms can almost reach the deterministic CRLB. Obviously, to improve the accuracy of these algorithms in NLOS conditions, increasing the number of snapshots S per frequency f_{n_k} and the number of carrier frequencies K for evaluating phase measurements $\tilde{\boldsymbol{\Phi}}$ lead to an accurate estimate of the sample covariance matrix $\hat{\mathbf{R}}_{\mathrm{x}}$, therein accurate measured distances $\tilde{\mathbf{d}}$. Inadvertently, it is not of much importance the number of snapshots S and carrier frequencies K, if the wireless channel encounters large interferences at specific carrier frequencies from other sources as shown in Figure 5.6 which is very common in indoor environments.

As the wireless channel is unpredictable and unstable with interferences hoping from one frequency to another, a frequency allocated for ranging will one way or another experience interruptions at some point. Therefore, the challenge of improving accuracy and optimizing resources while circumventing interferences and interruptions in the wireless channel can be solved through the use of a large K-mark Golomb ruler designed using the evolutionary genetic algorithm in Subsection 4.3.2 as it enables the specific use of uninterrupted carrier frequencies $\mathbb{F}$ (admissible marks $\mathcal{W}$) for evaluating phase measurements $\tilde{\boldsymbol{\Phi}}$. Therefore, by measuring a large number of snapshots S per frequency while utilizing a large number of carrier frequencies K selected through specific allocation, the accuracy of distance estimates in NLOS conditions can be improved greatly.

As the goal here is to compute multiple measured distances, in addition to increasing S for the measured phases $\tilde{\boldsymbol{\Phi}} = [\tilde{\boldsymbol{\varphi}}_{\mathcal{N}:1}, \cdots, \tilde{\boldsymbol{\varphi}}_{\mathcal{N}:S^2}]$ across all frequencies $\mathbb{F}$ to improve the performance, the measured phases $\tilde{\boldsymbol{\varphi}} = \tilde{\boldsymbol{\varphi}}_{\mathcal{N}:s} \forall\ s = \{1, 2, \cdots, S^2\}$ with a positive ∇ and the smallest norm residual phase error $\|\tilde{\boldsymbol{\varphi}}_{\mathcal{N}:s} - \hat{\boldsymbol{\varphi}}_{\mathcal{N}:s}\|$ using equation (5.9) (the snapshot of measured phases with the minimum phase error) is selected for ranging. Hence, we present a ranging technique which computes multiple measured distances $\tilde{\mathbf{d}}$ by applying a superresolution algorithm separately on the permutation of the phase measurements $\tilde{\boldsymbol{\varphi}} = \{\tilde{\varphi}_{n_1}, \cdots, \tilde{\varphi}_{n_{K-1}}, \tilde{\varphi}_{n_K}\}$ evaluated using K carrier frequencies $\mathbb{F} = \{f_{n_1}, \cdots, f_{n_K}\}$ (using a K-mark Golomb ruler $\mathcal{N} = \{n_1, \cdots, n_{K-1}, n_K\}$). This permutation leads to different Golomb subsets[3] of equal length phase measurements.

[3] A subset of a K-mark Golomb ruler is also a Golomb ruler of length lesser than K.

For illustration, phase measurements $\tilde{\boldsymbol{\varphi}} = \{\tilde{\varphi}_{n_1}, \tilde{\varphi}_{n_2}, \cdots, \tilde{\varphi}_{n_{14}}, \tilde{\varphi}_{n_{15}}\}$ are evaluated using carrier frequencies $\mathbb{F} = \{f_{n_1}, f_{n_2}, \cdots, f_{n_{15}}\}$ allocated through a 15-mark Golomb ruler $\mathcal{N} = \{1, 16, 27, 36, 39, 55, 60, 82, 111, 113, 143, 147, 153, 160, 161\}$ and the permutation of the Golomb ruler leading to different Golomb subsets of phase measurements are

$$\tilde{\boldsymbol{\varphi}} \Longrightarrow \begin{bmatrix} \tilde{\varphi}_{n_1}, & \tilde{\varphi}_{n_1}, & \tilde{\varphi}_{n_1}, & \tilde{\varphi}_{n_1}, & \tilde{\varphi}_{n_1} & \cdots \\ \tilde{\varphi}_{n_3}, & \tilde{\varphi}_{n_2}, & \tilde{\varphi}_{n_3}, & \tilde{\varphi}_{n_4}, & \tilde{\varphi}_{n_3} & \cdots \\ \vdots & \vdots & \vdots & \vdots & \vdots & \vdots \\ \tilde{\varphi}_{n_{K-3}}, & \tilde{\varphi}_{n_{K-4}}, & \tilde{\varphi}_{n_{K-4}}, & \tilde{\varphi}_{n_{K-2}}, & \tilde{\varphi}_{n_{K-2}} & \cdots \\ \tilde{\varphi}_{n_K}, & \tilde{\varphi}_{n_{K-1}}, & \tilde{\varphi}_{n_{K-2}}, & \tilde{\varphi}_{n_{K-1}}, & \tilde{\varphi}_{n_K} & \cdots \end{bmatrix}. \tag{5.11}$$

Therein, a large number of Golomb rulers e.g., 13-mark can be created from the 15-mark Golomb ruler along with their corresponding phase measurements.

Each of the Golomb subsets of phase measurements are then expanded into their set of M phase differences (measure sets) $\mathbb{\Delta}_{\mathcal{V}} = \{\Delta\tilde{\varphi}_1, \cdots, \Delta\tilde{\varphi}_M\}$ along with their corresponding set of M frequency differences $\mathbb{\Delta}_{\mathcal{F}} = \{\Delta f_1, \cdots, \Delta f_M\}$ as in Subsection 4.2.3. Following this, a superresolution algorithm is then applied separately on each subsets to obtain multiple measured distances $\tilde{\mathbf{d}}$ as in Subsection 4.2.4.

A simple and efficient outliers detection technique – a modified z-score [116] centred on the median of the measured distances $\tilde{\mathbf{d}}$ is used to computes residue r as

$$r_i = \left| \frac{0.6745 \cdot (\tilde{\mathbf{d}}_i - \tilde{\mathbf{d}}_{\text{median}})}{\text{median}|\tilde{\mathbf{d}} - \tilde{\mathbf{d}}_{\text{median}}|} \right|, \quad i = \{1, 2, \cdots\}, \tag{5.12}$$

where a measured distance $\tilde{\mathbf{d}}_i$ with residue $r_i \geq 0.5$ is removed from the set of measured distances $\tilde{\mathbf{d}}$. This is done in order to remove measured distances which appear to deviate or are inconsistent with the remainder of the measured distances i.e., to remove distances which are affected by large noise and interference. This technique is shown to be very robust and stable in obtaining accurate measured distance $\tilde{\mathbf{d}}$ in NLOS conditions as seen in Figure 5.7, where the mean of the distance estimates $\tilde{\mathbf{d}}$ (after applying the outliers removal technique on the computed measured distances $\tilde{\mathbf{d}}$) is compared against applying a superresolution algorithm on all the measured phases $\tilde{\boldsymbol{\varphi}}$ without permutation.

The measured distances $\tilde{\mathbf{d}}$ computed with this technique can be used along with the trilateration techniques which requires multiple distances for each target-to-anchor links for target localization to be proposed in Subsection 5.3.4.

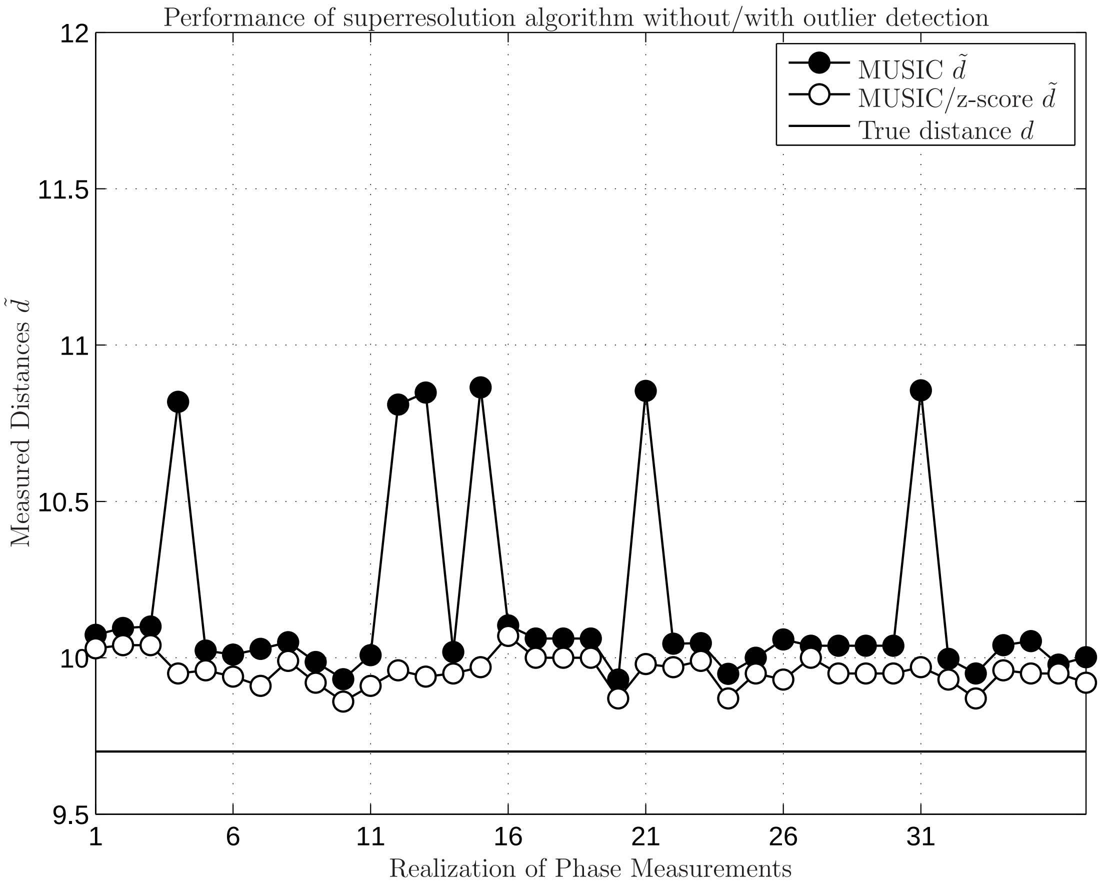

Figure 5.7: The comparison of the superresolution algorithm with/without outliers removal.

One possible way to prevent the multiple parallel computations of superresolution techniques required to improve accuracy while circumventing interferences and interruptions in the wireless channel is by optimizing the choice of the large K-mark Golomb ruler. This can be done by generating multiple sets of K-mark Golomb ruler via the evolutionary genetic algorithm and evaluating the corresponding phase measurements from the PMUs obtained between each anchor-to-anchor links (locations of anchors are known, therein their true distances can be calculated) using each ruler.

The measured distances between all anchors are computed using the superresolution or the simple averaging algorithm on measured phases corresponding to different Golomb rulers. The K-mark Golomb ruler with the minimum residual error between all anchor-to-anchor measured distances and their true distance is opted for in subsequent ranging procedure between targets and anchors. This technique can be done at periodic intervals so as to determine the optimum choice of the K-mark Golomb ruler from multiple sets, thereby selecting the ruler with the least ranging errors due to the high inconsistencies in the wireless environment. Regrettably, this technique could not be implemented and evaluated in the thesis as anchors in the positioning kit currently lack the ability to range with one another.

5.3.3.3 Slope Sampling Algorithm

Despite the accuracy achieved by the superresolution algorithm with outliers removal technique, a drawback to the technique is the extensive computational power and time required to estimate in parallel multiple distances due to the eigendecomposition of the large sample covariance matrix. To this end, we propose a new accurate ranging technique with less computational complexity for obtaining multiple distance estimates $\tilde{\mathbf{d}}$ from a single estimation on the measured phases $\tilde{\boldsymbol{\varphi}}$ using a slope sampling algorithm (an algebraic sampling-based algorithm similar to a search-based maximum likelihood). This algorithm is based on computing residual values from the differences between an expanded set of measured slopes (from the measured phase differences and their corresponding frequency differences) and an expanded set of sample slopes (from a predefined set of sample distances), wherein the distances corresponding to the peaks of the inverse residues using a resolution tolerance and confidence threshold peak search on the obtained spectrum are selected for ranging.

Firstly, vectors of repeated/expanded measured slopes $\boldsymbol{\nabla}_i$ are created using each measured phase difference $\Delta\tilde{\varphi}_i$ and its corresponding frequency difference Δf_i as

$$\boldsymbol{\nabla}_i = \frac{[0, 2\pi, \cdots, \nabla_{\max}\cdot\Delta f_i] + \Delta\tilde{\varphi}_i}{\Delta f_i} \quad \forall \quad i = \{1, 2, \cdots, M\}, \tag{5.13}$$

where the maximum possible slope $\nabla_{\max}$ is obtained as

$$\nabla_{\max} = \frac{\Delta\varphi_{\max}}{\Delta f_{\min}} = \frac{4\pi}{c}\cdot d_{\max} = \frac{4\pi}{c}\cdot\frac{c}{2f_{\min}} = \frac{2\pi}{f_{\min}}, \tag{5.14}$$

and the last value in each $\boldsymbol{\nabla}_i$ is repeated multiple times such that all $\boldsymbol{\nabla}_i$ are of the same length as $\boldsymbol{\nabla}_M$.

Next, a vector of sample slopes $\boldsymbol{\nabla}_{\mathrm{s}}$ is computed from a predefined set of sample distances $\mathbf{d}_{\mathrm{s}}$ (similar to the fine grid in the MUSIC algorithm of Subsection 3.3.1) as

$$\boldsymbol{\nabla}_{\mathrm{s}} = \frac{4\pi\mathbf{d}_{\mathrm{s}}}{c}. \tag{5.15}$$

To compute the residues $\mathbf{r}$, the measured slopes $\boldsymbol{\nabla}$ (of size $M \times N_{\boldsymbol{\nabla}_M}$) and the sample slopes $\boldsymbol{\nabla}_{\mathrm{s}}$ (of size $N_{\mathrm{s}} \times 1$) are both expanded by creating all the possible combinations between the rows of $\boldsymbol{\nabla}$ and $\boldsymbol{\nabla}_{\mathrm{s}}$ such that they both have equal lengths (equal number of rows $M\cdot N_{\mathrm{s}}$). This can be achieved using the index $\mathbf{I}$

$$\mathbf{I} = \begin{bmatrix} 1\cdot\mathbf{1}_M, & 2\cdot\mathbf{1}_M, & \ldots, & N_{\mathrm{s}}\cdot\mathbf{1}_M \\ 1,\cdots,M_1, & 1,\cdots,M_2, & \ldots & ,1,\cdots,M_{N_{\mathrm{s}}} \end{bmatrix}, \tag{5.16}$$

where $\mathbf{1}_M$ is a row vector of 1's with length M. Therefore, a minimum of the differences of slopes $\mathbf{r}_{\min}$ is computed across all rows from the difference between the expanded measured slope $\boldsymbol{\nabla}$ and expanded sample slope $\boldsymbol{\nabla}_{\mathrm{s}}$ given as

$$\mathbf{r}_{\min} = \min\Big[\mathrm{abs}\big[\boldsymbol{\nabla}(\mathbf{I}(2,:),:) - \boldsymbol{\nabla}_{\mathrm{s}}(\mathbf{I}(1,:),:)\big]\Big], \tag{5.17}$$

where $\boldsymbol{\nabla}_{\mathrm{s}}$ is repeated $N_{\boldsymbol{\nabla}_M}$ times to have the same number of columns as $\boldsymbol{\nabla}$.

From the index $\mathbf{I}$ above, the minimum of the differences of slopes $\mathbf{r}_{\min}$ (vector of length $M\cdot N_{\mathrm{s}}$) is such that every $\mathbf{r}_{min}\Big((i-1)\cdot M+1 : i\cdot M\Big)$ are residual values corresponding to each sample distance $\mathbf{d}_{\mathrm{s}}(i)$, for all $i = \{1, 2, \cdots, N_{\mathrm{s}}\}$. Therefore, the minimum of the differences of slopes $\mathbf{r}_{min}$ can be reshaped to a matrix $\mathbf{R}_{\min}$ (of size $M \times N_{\mathrm{s}}$), therein the residues $\mathbf{r}$ for all sample distances $\mathbf{d}_{\mathrm{s}}$ is given as

$$\mathbf{r} = \mathrm{median}\Big[\mathbf{R}_{\min}\Big], \tag{5.18}$$

where $\mathbf{r}$ is the median value in each columns of length N_s and in LOS conditions, the measured distance $\tilde{d}$ is the sample distance with the minimum residue $\min(\mathbf{r})$.

In NLOS conditions, situations occur where there exist no distinct minimum value in the residue $\mathbf{r}$ (no distinct sample distance) due to mulitpath propagations. In this regards, a peak search is performed on the spectrum of the inverse residue $\mathbf{r} = \frac{1}{\mathbf{r}}$ as different peaks corresponds to different measured distances $\tilde{\mathbf{d}}$ as seen in Figure 5.8(a). A local maxima search is then performed on the spectrum of the residues $\mathbf{r}$, such that measured distances corresponding to a peak residue with $\mathbf{r}(i) \geq 0.3 \cdot \max(\mathbf{r})$ are selected and measured distances corresponding to peaks that are within a resolution tolerance t_r in metres using all large peaks as references i.e., if a large peak occurs at index N, then all smaller peaks in the range $[\mathrm{N} - \mathrm{N}_{t_r}, \mathrm{N} + \mathrm{N}_{t_r}]$ are ignored, where $\mathrm{N}_{t_r} = 2t_r \cdot \mathrm{ceil}\big(\frac{N_\mathrm{s}-1}{\mathbf{d}_s(N_\mathrm{s})}\big)$.

From above, the resulting selected measured distances $\tilde{\mathbf{d}}$ are sorted according to their respective residues $\mathbf{r}$. Within these distances, there are distances of low peaks with respect to other peaks to be removed, which is achieved by converting the residues of all distances into confidence values, therein distances with a lower confidence value than the confidence threshold are eliminated. Therefore, the set of measured distances $\tilde{\mathbf{d}} = \{\tilde{d}\}_1^i$ such that the confidence value $\mathbf{c}(i)$ is greater than the confidence threshold c_{th} are selected for ranging, where the corresponding confidence values $\mathbf{c}$ for each set of distances are computed as

$$\begin{aligned}\mathbf{c} =& \frac{\{r\}_1^i}{\min\{r\}_1^i} \\ \mathbf{c} =& \frac{\mathbf{c}}{\sum \mathbf{c}} \quad \forall \quad \{i = 1, \cdots, N_\mathbf{r}\}.\end{aligned} \tag{5.19}$$

In these NLOS channel conditions, this technique computes multiple distance estimates due to the spectrum having multiple large peaks and in most cases the distance corresponding to the global peak (this is likely an accurate measured distance in LOS and soft NLOS conditions) is not an accurate estimate as seen in Figure 5.8(b), where the spectrum of the residue from the slope sampling algorithm and the obtained measured distances $\tilde{\mathbf{d}}$ are shown with a confidence threshold $c_{th} = 0.3$ and resolution tolerance $t_r = 1$m.

In the next subsection, the measured distances computed with this technique will be used with a set of proposed trilateration techniques which require multiple measured distances in each target-to-anchor links for target localization.

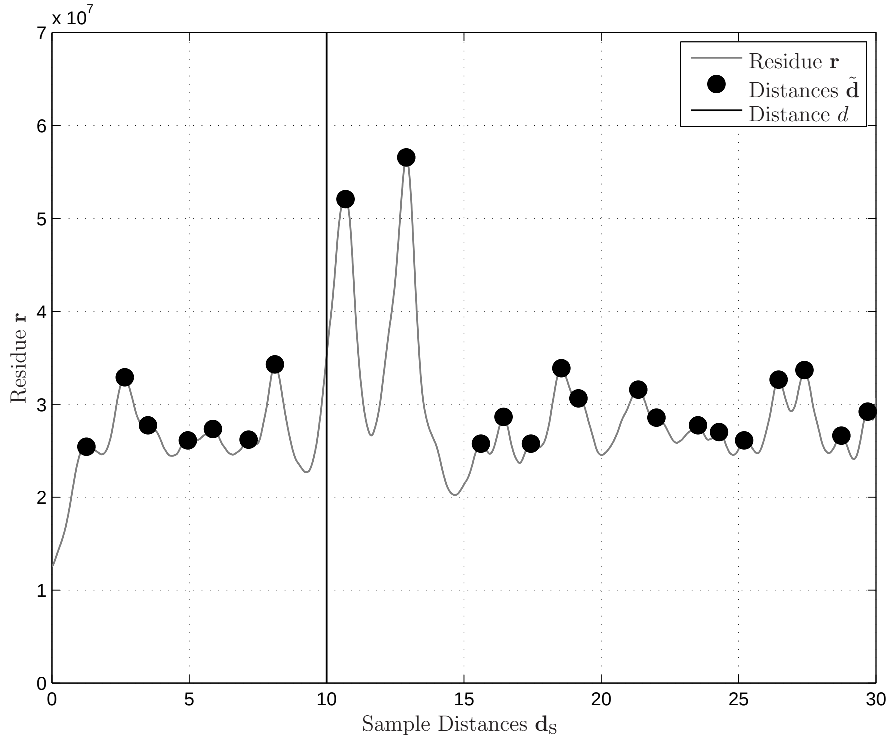

(a) All local maxima.

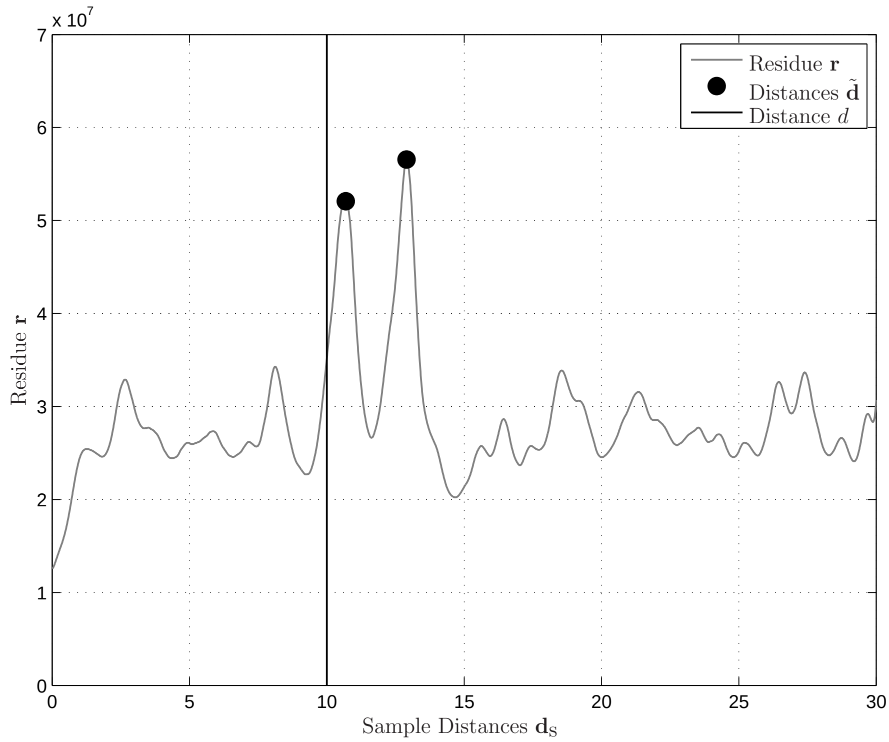

(b) The local maxima using the confidence threshold and resolution tolerance.

Figure 5.8: The spectrum of the residue $\mathbf{r}$ showing the obtained measured distances.

5.3.4 Trilateration Techniques

Trilateration as one of the major problem in wireless localization is the process of estimating the absolute location of unknown targets $\mathbf{\Theta}$ given their distances to a set of known references - the anchors $\mathbf{\Phi}$. In this part of the thesis, we clearly present trilateration techniques which estimates the location of an unknown target $\boldsymbol{\theta}_i$ utilizing the multiple measured distances $\tilde{\mathbf{d}}_{ij}$ between target i and anchor $\boldsymbol{\phi}_j$ which is obtained from the slope sampling algorithm with their respective confidence values $\mathbf{c}_{ij}$.

As it is known, one of the many ways of improving accuracy, precision and robustness in target localization is by providing positioning algorithms with an initial target guess a process called initialization. Therefore, initial location estimates for the targets are computed using a trilateration technique (the intersection of multiple circles) which positioning algorithms (non-iterative and low computation algorithms) requiring an initial guess can improve upon.

Let us consider the case of a target i and two given anchors j and k, all the possible intersections between the measured distances $\tilde{\mathbf{d}}_{ij}$ and $\tilde{\mathbf{d}}_{ik}$ are computed as $\mathbf{\Psi}_{i:jk}$ with their corresponding confidence values $\mathbf{c}_{i:jk} = \mathbf{c}_{ij} \cdot \mathbf{c}_{ik}$ as the product of the confidence values $\mathbf{c}_{ij}$ and $\mathbf{c}_{ik}$ as seen in Figure 5.9(a).

Amongst the intersections $\mathbf{\Psi}$, only one is required as an initial guess to initialize the positioning algorithm. In order to select the initial target estimate $\hat{\boldsymbol{\theta}}_i^0$ from the intersections $\mathbf{\Psi}$, first, intersections which are not inside a convex region to be created around the location of the likely target i are eliminated. This convex region for selecting the initial target estimate $\hat{\boldsymbol{\theta}}_i^0$ is created as follows. First, an upper and lower anchor coordinates $\mathbf{\Phi}_U$ and $\mathbf{\Phi}_L$ are created by

$$\begin{aligned} \mathbf{\Phi}_U &= \left[\mathbf{\Phi} + \tilde{\mathbf{d}}_{\mathrm{m}}\right], \\ \mathbf{\Phi}_L &= \left[\mathbf{\Phi} - \tilde{\mathbf{d}}_{\mathrm{m}}\right], \end{aligned} \tag{5.20}$$

where $\tilde{\mathbf{d}}_{\mathrm{m}} = \{\tilde{d}_{\mathrm{m}(\mathbf{c}_{ij})}\}_{j=1}^{N_a}$ are the measured distances required to create the convex region around the target i. The selection or computation of the measured distance $\tilde{d}_{\mathrm{m}(\mathbf{c}_{ij})}$ between the target i and anchor j involves the following steps:

a) If the distance with the largest confidence value in $\tilde{\mathbf{d}}_{ij}$ corresponds to the largest distance in $\tilde{\mathbf{d}}_{ij}$, this distance is selected;

b) If the above is not the case, the measured distance $\tilde{d}_{\mathrm{m}(\mathbf{c}_{ij})}$ is computed as

$$\tilde{d}_{\mathrm{m}(\mathbf{c}_{ij})} = \tilde{\mathbf{d}}_{ij} \cdot \mathbf{c}_{ij}^{\mathrm{T}}. \tag{5.21}$$

Therefore, the coordinates of the created convex region $\mathbf{\Phi}_r$ are computed as

$$\mathbf{\Phi}_r = \Big[\min\{\mathbf{\Phi}_U\}; \max\{\mathbf{\Phi}_L\} \Big], \tag{5.22}$$

and therefore across all η dimensions, only intersections such that $\mathbf{\Psi}_r = \max\{\mathbf{\Phi}_r\} \geq \mathbf{\Psi} > \min\{\mathbf{\Phi}_r\}$ are selected i.e., intersections inside the created convex region of target i as in Figure 5.9(b), out of which only one intersection is also selected as the initial target estimate $\hat{\boldsymbol{\theta}}_i^0$.

From the first realization of target-to-anchors phase measurements, to select an initial estimate for target i from the intersections $\mathbf{\Psi}_r$ in the convex region, the following two methods are proposed:

a) the intersection $\boldsymbol{\psi}_{r_{\max(\mathbf{c}_{i:jk})}}$ with the maximum confidence value $\max(\mathbf{c}_{i:jk})$ is chosen as the initial target estimate $\hat{\boldsymbol{\theta}}_i^0$;

b) the intersection $\boldsymbol{\psi}_{r_{\min(\mathbf{H})}}$ with the minimum Hessian $\mathbf{H}_{i:l}$ of a cost function $S_{i:l}$ on each intersection $\boldsymbol{\psi}_{r_l}$, with

$$S_{i:l} \triangleq \arg\min_{\mathbf{\Psi}_r} \sum_{j=1}^{N_a} \frac{(\tilde{\mathbf{d}}_{ij} - \hat{d}_{ij:l})^2}{\mathbf{c}_{ij}} \tag{5.23}$$

is chosen as the initial target estimate $\hat{\boldsymbol{\theta}}_i^0$; where $\tilde{\mathbf{d}}_{ij}$ are the measured distances, $\hat{d}_{ij:l}$ is the distance estimate between each intersection $\boldsymbol{\psi}_{r_l}$ and anchor $\boldsymbol{\phi}_j$, and $\mathbf{c}_{ij}$ are the corresponding confidence values of the measured distances $\tilde{\mathbf{d}}_{ij}$.

The Hessian $\mathbf{H}_{i:l}$ of the cost function $S_{j:l}$ is therein computed as

$$\mathbf{H}_{j:l} = \det \begin{bmatrix} \dfrac{\partial^2 S_{i:l}}{\partial x_{r_l}^2} & \dfrac{\partial^2 S_{i:l}}{\partial x_{r_l} \partial y_{r_l}} \\ \dfrac{\partial^2 S_{i:l}}{\partial x_{r_l} \partial y_{r_l}} & \dfrac{\partial^2 S_{i:l}}{\partial y_{r_l}^2} \end{bmatrix} \quad \forall \quad \{l = 1, \cdots, L = N_{\mathbf{\Psi}_r}\}, \tag{5.24}$$

where (x_{r_l}, y_{r_l}) are the coordinates of each intersections $\mathbf{\Psi}_{r_l}$.

For the estimation of the target's coordinates, the measured distances with the minimum residue $\Big[\tilde{\mathbf{d}}_{ij} - \|\boldsymbol{\phi}_j - \hat{\boldsymbol{\theta}}_i^0\|\Big]$ for all target i to anchor $j = \{1, 2, \cdots, N_a\}$ links are passed as inputs to the positioning algorithms along with the initial estimate $\hat{\boldsymbol{\theta}}_i^0$ for computation.

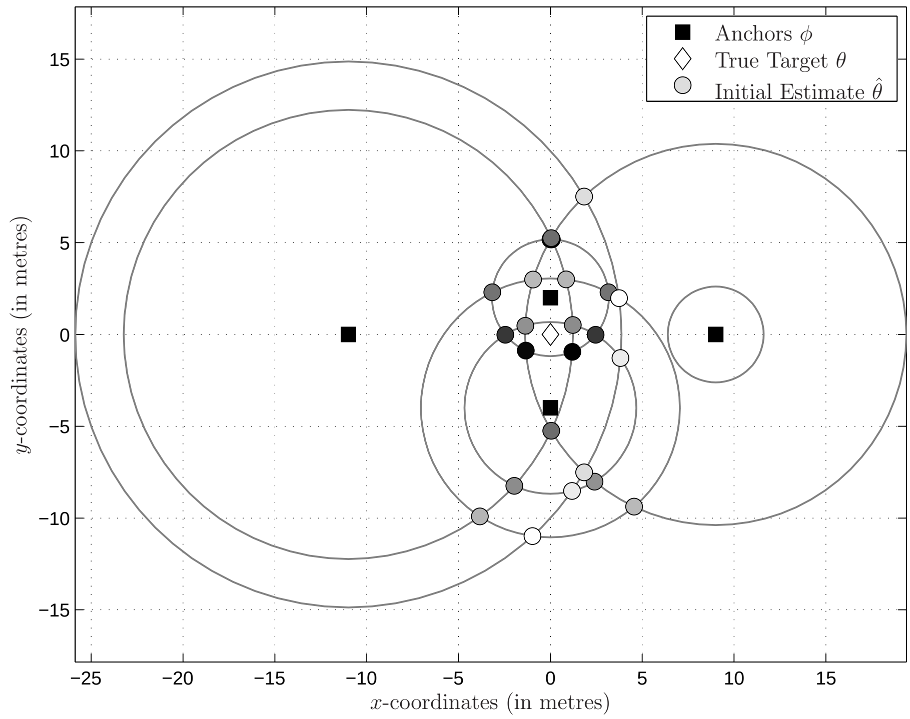

(a) The Intersections $\mathbf{\Psi}$ of all distance estimates, where the darkness of $\hat{\boldsymbol{\theta}}$ corresponds to its confidence value $\mathbf{c}_{i:jk}$.

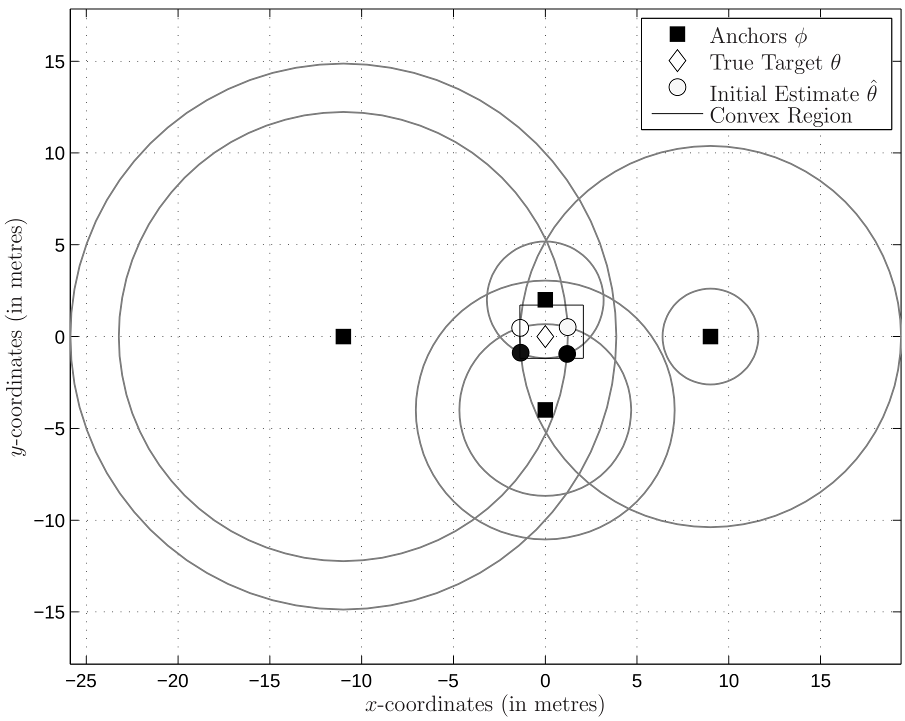

(b) The intersections $\mathbf{\Psi}_r$ inside the created convex region hull.

Figure 5.9: Illustration of the trilateration technique to obtain an initial target estimate.

Subsequently from the second realization of phase measurements, the selection of the initial target estimate $\hat{\boldsymbol{\theta}}_i^0$ achieved by through the intersection $\boldsymbol{\psi}_{r_{\max(\mathbf{c}_{i:jk})}}$ with the maximum confidence value is replaced by selecting the intersection $\boldsymbol{\psi}_r$ with the minimum distance to the target position $\hat{\boldsymbol{\theta}}_i$ computed from the first (previous) realization of phase measurements – a form of tracking and similarly for other subsequent realizations, while the selection of the intersection $\boldsymbol{\psi}_{r_{\min(\mathbf{H})}}$ with the minimum Hessian $\mathbf{H}_{i:l}$ of the cost function $S_{i:l}$ remains the same. Therein, the measured distance for each target i to anchor j links remains the measured distances with the minimum residue $\left[\tilde{\mathbf{d}}_{ij} - \|\boldsymbol{\phi}_j - \hat{\boldsymbol{\theta}}_i^0\|\right]$ for all target i to anchor $j = \{1, 2, \cdots, N_a\}$ links, which are then passed as inputs to the positioning algorithms along with the initial estimate $\hat{\boldsymbol{\theta}}_i^0$ for the estimation of the target's current location $\hat{\boldsymbol{\theta}}_i$.

In the next section, we provide a detailed description of simulation and real-time analyses performed in this thesis for the evaluation of the proposed ranging and trilateration techniques.

5.4 Performance Evaluation

For the necessary performance measures such as accuracy, precision and robustness to be satisfied for indoor wireless localization, the proposed ranging and trilateration techniques in this thesis must be analyzed under different and difficult network localization scenarios using simulated and real-time phase measurements evaluated in both LOS and NLOS conditions.

Firstly, let us consider a network of $N = 8$ devices with $N_a = 5$ anchors forming an irregular localization scenario as shown in Figure 5.10 and $N_t = 3$ targets in which two targets are inside the convex hull of the anchors and one target is outside the convex hull. Here, the targets and anchors form a non-cooperative network[4], where the targets only communicate with the anchors to evaluate phase measurements. For simulation analysis, in the case of LOS conditions, the phase measurements which are modeled as

$$\tilde{\varphi} \sim f(\tilde{\varphi}; \varphi, \kappa), \tag{5.25}$$

with $f_(\tilde{\varphi}; \varphi, \kappa)$ the PDF of the Tikhonov distribution

$$f(\tilde{\varphi}; \varphi, \kappa) \triangleq \frac{1}{2\pi I_0(\kappa)} \cdot \exp(\kappa \cos(\tilde{\varphi} - \varphi)), \quad -\pi \leq x \leq \pi, \tag{5.26}$$

[4]Non-cooperative positioning is used for consistency in both the simulated and real-time positioning as targets can not communicate with one another in the ZIGPOS positioning kit.

where $I_n(\kappa)$ is the n-th order modified Bessel function of the first kind and κ is a shape parameter which in the case of phase estimates is in fact given by the signal-to-noise-ratio (SNR) of input signals [108, Eq. (37)], and that relates to the error variance by $\sigma^2_{\tilde{\varphi}} \approx \frac{1}{2\kappa}$. In NLOS conditions, phase measurements are modeled as the sum

$$\tilde{\varphi} \sim f(\tilde{\varphi}; \varphi, \kappa) + \mathcal{U}(\tilde{\varphi}; b_{\max}), \tag{5.27}$$

where $\mathcal{U}(\tilde{\varphi}; b_{\max})$ generates uniform random variables between $[0, b_{\max}]$.

For the ranging between the targets and anchors, the true phases $\boldsymbol{\varphi}$ are evaluated using equation (5.7), where the carrier frequencies $\mathbb{F} = \{2403.0, 2408.5, 2410.0, 2410.5, 2415.0, 2425.5, 2433.5, 2445.5, 2454.5, 2463.0, 2465.5, 2469.0, 2479.0, 2482.0, 2483.0\}$MHz are allocated through the 15-mark Golomb ruler $\mathcal{N} = \{1, 12, 15, 16, 25, 46, 62, 85, 104, 121, 126, 133, 153, 159, 161\}$ were selected for efficiency and simulating the measured phases $\tilde{\boldsymbol{\varphi}}$ with a step frequency of 0.5MHz similar to those in Figure 5.3. The multiple measured distances $\tilde{\mathbf{d}}$ and their corresponding confidence values $\mathbf{c}$ are obtained using the slope sampling ranging algorithm with a confidence threshold $c_{th} = 0.3$ and resolution tolerance $t_r = 1$m.

For target localization, the trilateration techniques (using either the intersections with the maximum confidence value (**1**) or the intersections with the minimum Hessian (**2**)) were used to compute an initial target estimate for the SMDS algorithm[5], which was then used to estimate the location of the different targets. In Figure 5.10, the location estimates of the targets using the SMDS algorithm with the intersection techniques (**SMDS 1** and **SMDS 2**) under soft NLOS conditions – phase measurement errors $\sigma^2_{\tilde{\varphi}} = 0.3$ and maximum possible bias $b_{\max} = 0.5$ were shown. Results of the target estimates depict a strong accuracy, precision and robustness of the presented ranging and trilateration techniques for target localization, where 95% of the target estimates have a RMSE of less than 0.2m. Thereafter, the presented ranging and trilateration techniques were analyzed in strong NLOS conditions – phase measurement errors $\sigma^2_{\tilde{\varphi}} = 0.3$ and maximum possible bias $b_{\max} = 2$. The target location estimates from the resulting techniques were shown in Figure 5.11, where it is seen again the techniques depict a strong robustness with good accuracy and precision for target localization under such difficult conditions with 80% of estimates having a RMSE of ≤ 0.5m.

Finally, a plot of the RMSE of the target estimates against the maximum possible bias $b_{\max}$ with a constant phase measurement error $\sigma^2_{\tilde{\varphi}} = 0.3$ utilizing multiple realizations

[5]SMDS was chosen as it is the most accurate algorithm in both LOS and NLOS conditions among the compared state of the art algorithms.

for smoothing is shown in Figure 5.12. The results emphasize the accuracy and robustness achieved by the presented ranging and trilateration techniques for wireless localization under LOS and NLOS conditions. It is quite clear that the trilateration technique of selecting the intersection with the maximum confidence value for the first realization and replacing this from the subsequent realization by the intersection with the minimum distance to the target estimate from the previous realization performs best with much more stability that the other intersection scheme in all channel conditions.

Next, the presented ranging and trilateration techniques were also analyzed utilizing evaluated real-time Phase Measurement Units from the ZIGPOS positioning kit. To this end, the localization devices – targets and anchors were deployed in an indoor environment – the foyer of the Information Resource Center (IRC) of Jacobs University Bremen (JUB) as seen in Figures 5.13, 5.14 and 5.15 with possible LOS and NLOS conditions depicting strong multi-paths, reflections and absorption while utilizing similar localization scenarios as in simulations. For the evaluation of the PMUs, similar ranging configurations parameters (carrier frequencies $\mathbb{F}$ and step frequency 0.5MHz) and the other parameters include a transmit power of 4mW, antenna diversity and a distance offset of 0.5m. The full results are shown in Figure 5.16 which illustrate the efficiency, accuracy, precision and robustness achieved by the presented ranging and trilateration techniques for wireless localization in indoor environments.

5.5 Conclusions

In this chapter, we presented accurate ranging techniques to obtain multiple distance estimates from a single realization of phase measurements by applying superresolution techniques to different permuted set of phase measurements with an outliers detection technique, and a new slope sampling algorithm utilizing a resolution tolerance and confidence threshold peak search on the obtained spectrum of the residues. These multiple distance estimates were then used to estimate the target position using the SMDS which requires an initial target estimate obtained using the intersections of measured distances and the target position from previous realization. Finally, we then performed experiments and analysis for target localization in indoor environments utilizing simulated and real time phase measurements under difficult Line-of-Sight and Non-Line-of-Sight conditions. These techniques satisfied important performance measures for indoor positioning system using different localization scenarios where results depicted the accuracy, robustness and stability achievable with the proposed techniques.

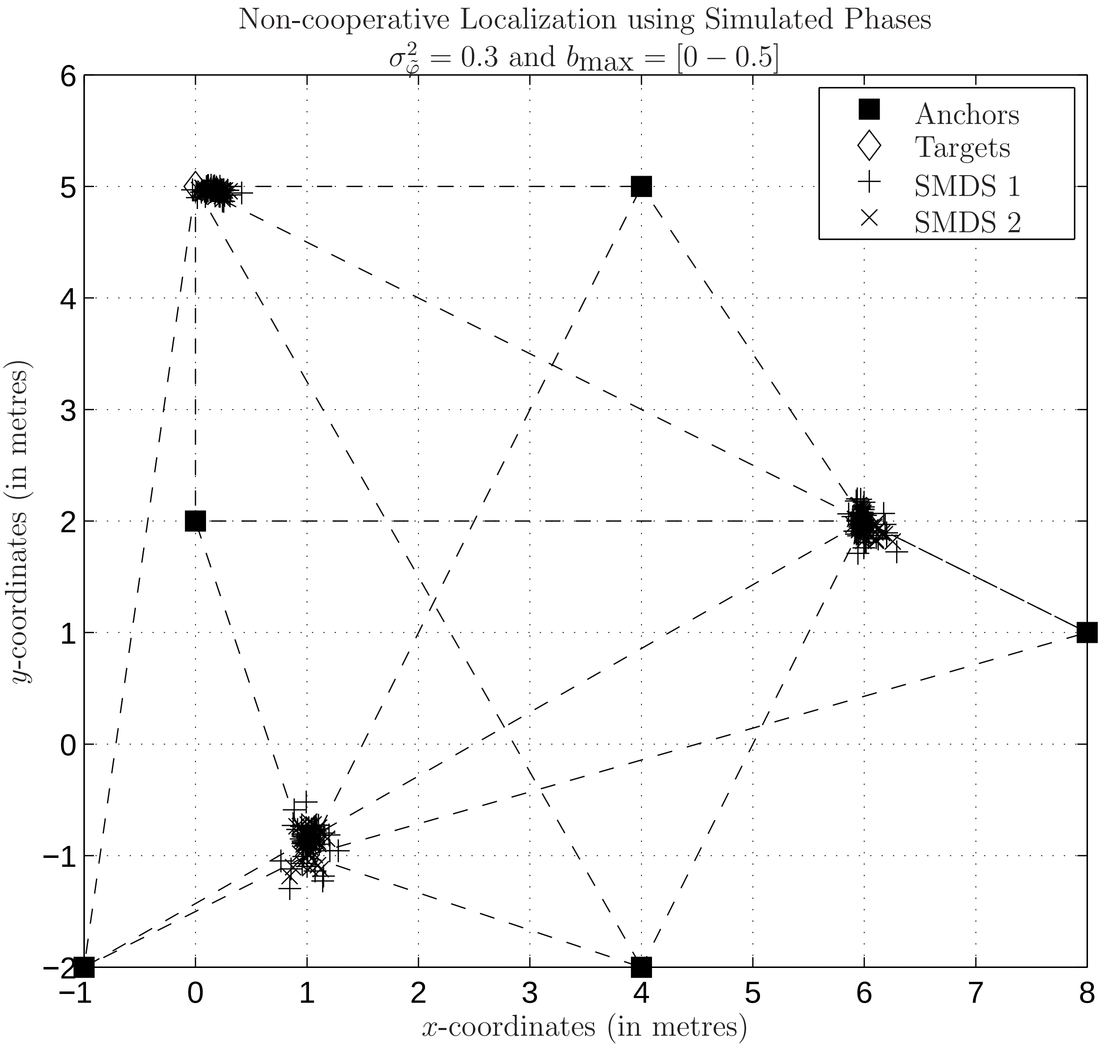

Figure 5.10: Soft NLOS conditions with phase errors and phase bias.

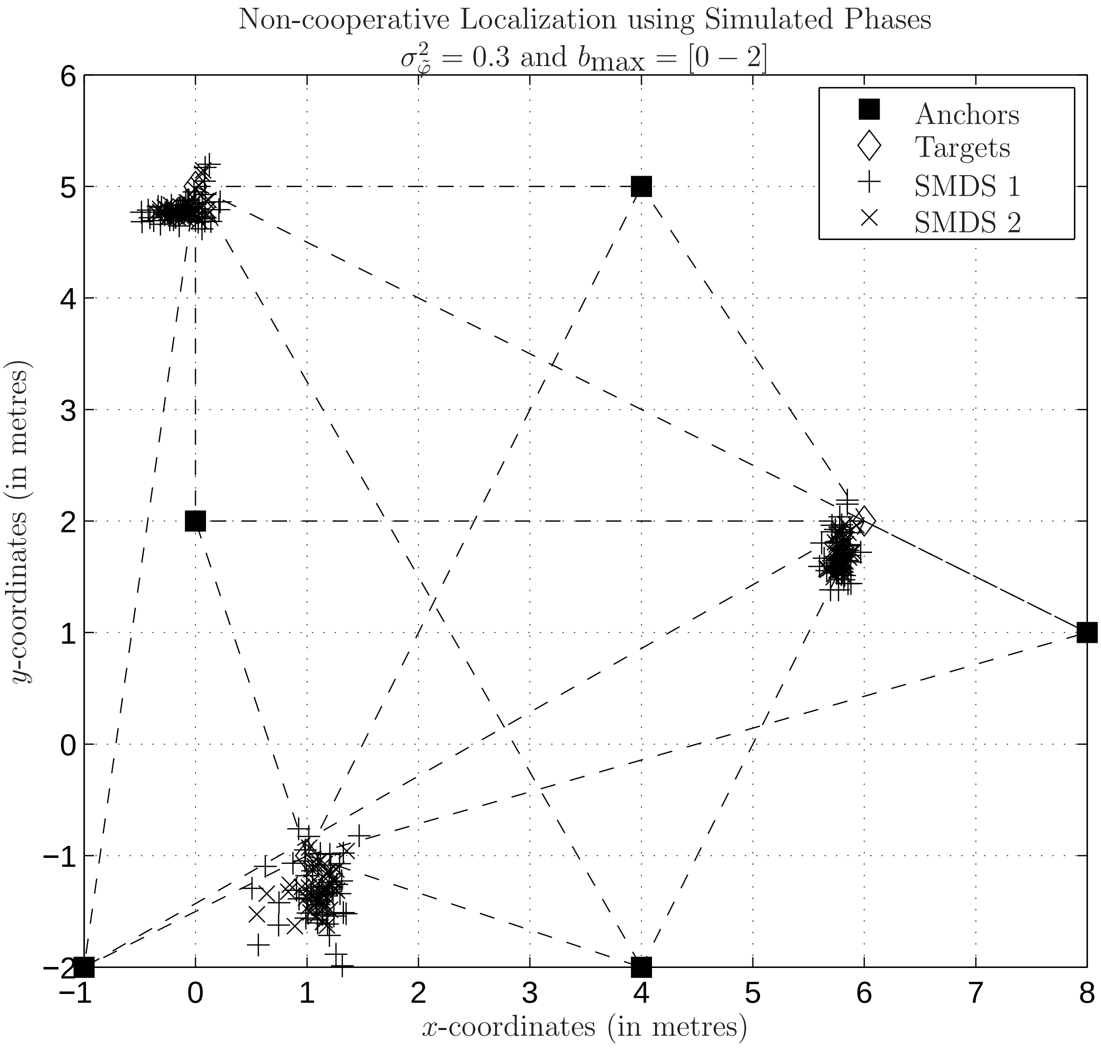

Figure 5.11: Strong NLOS conditions with phase errors and phase bias.

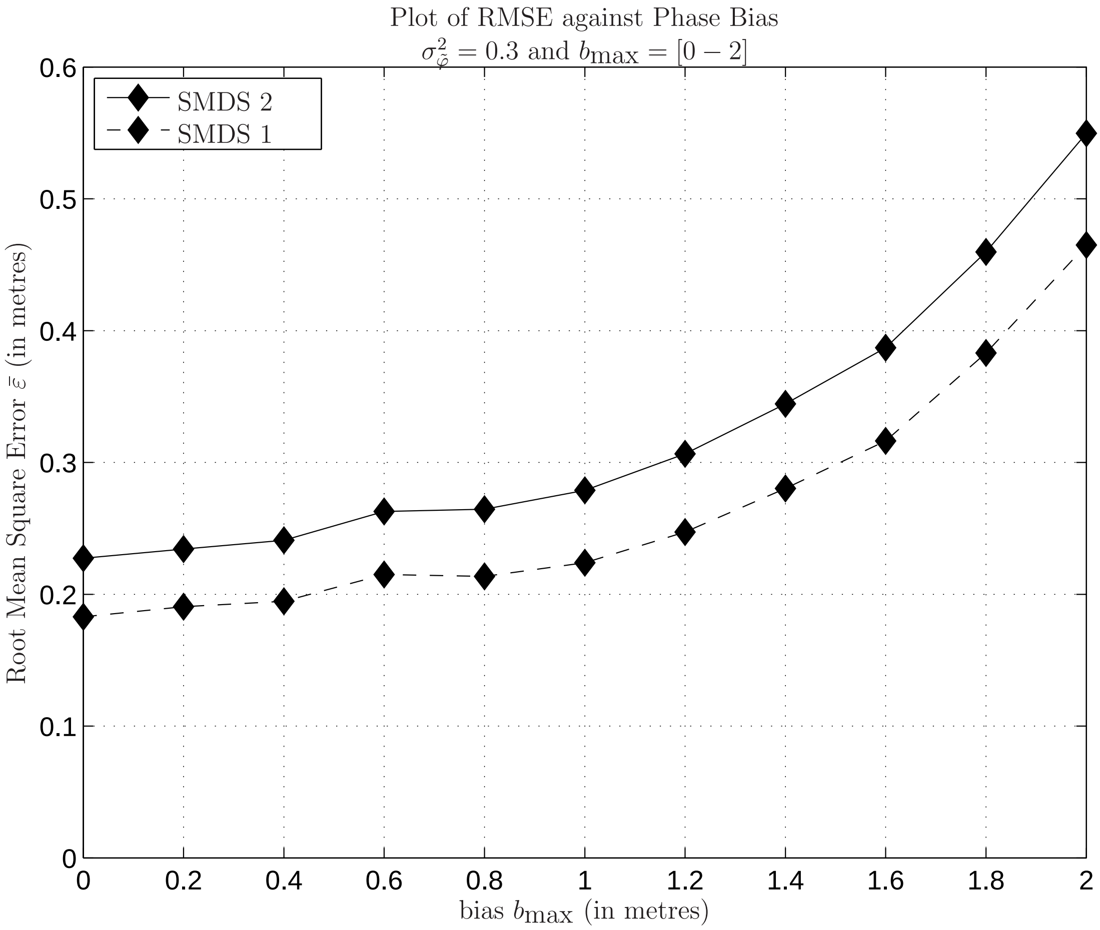

Figure 5.12: Plot of the RMSE against phase bias $b_{\max}$ for Target Localization in both LOS and NLOS conditions.

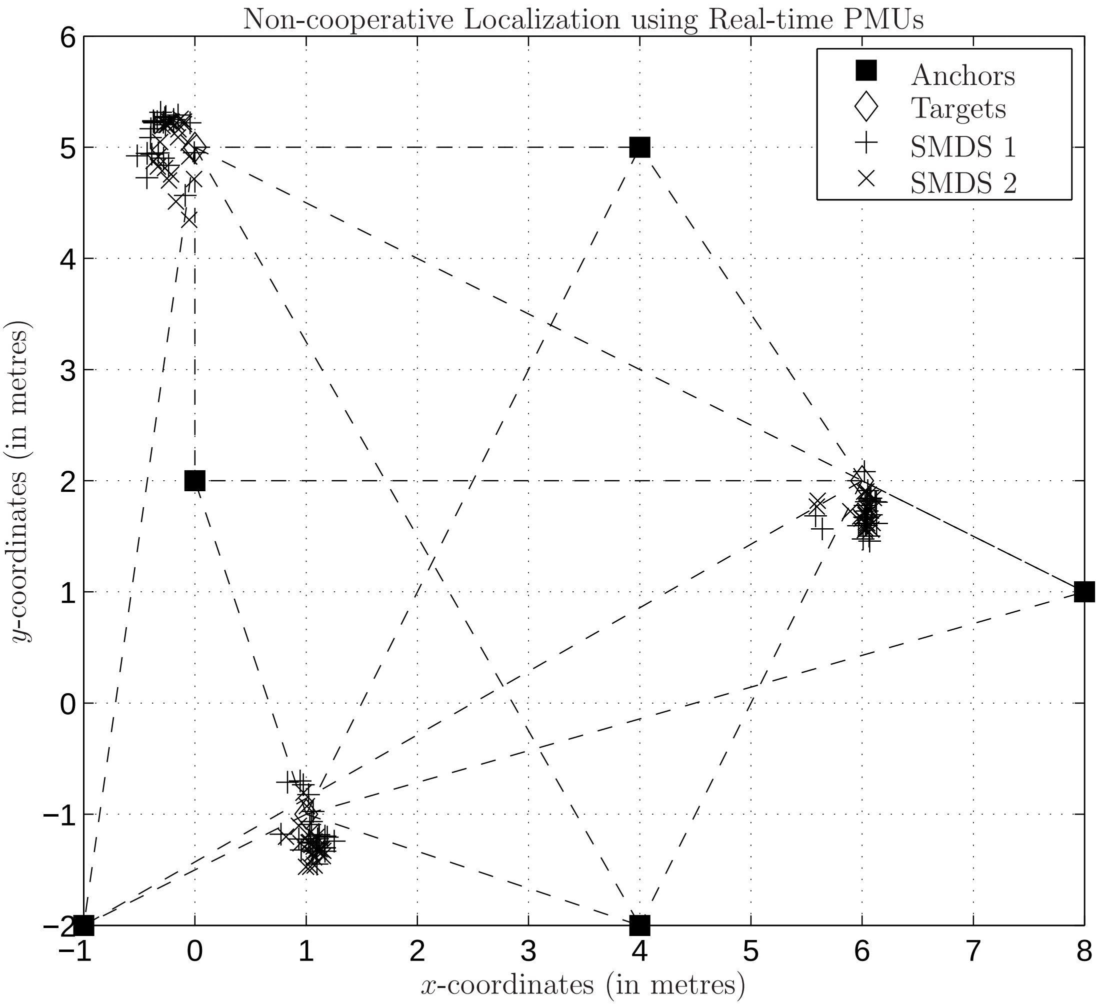

Figure 5.16: Target Localization in NLOS conditions using Real-time PMUs.

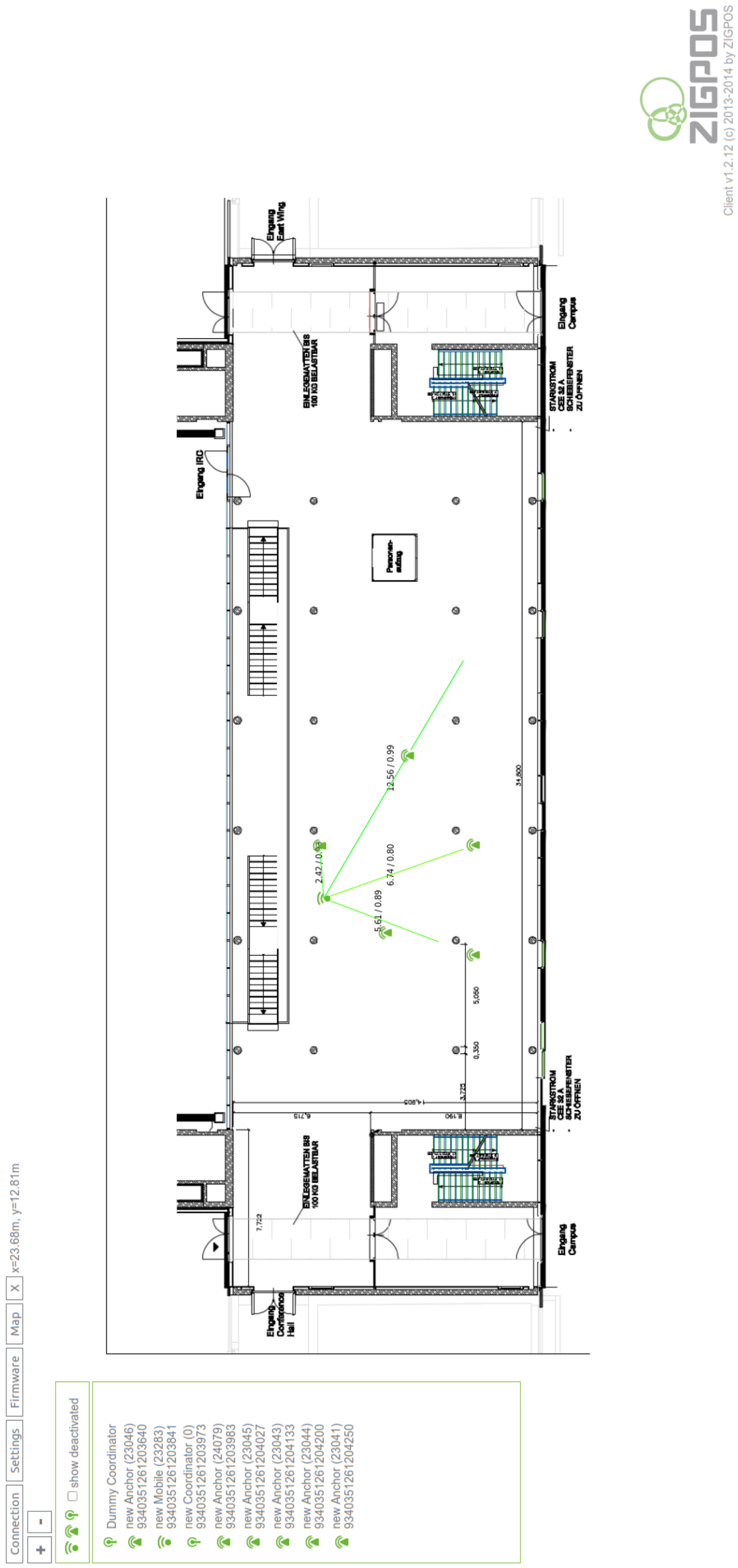

Figure 5.13: Target Localization using an Indoor Positioning System [32].

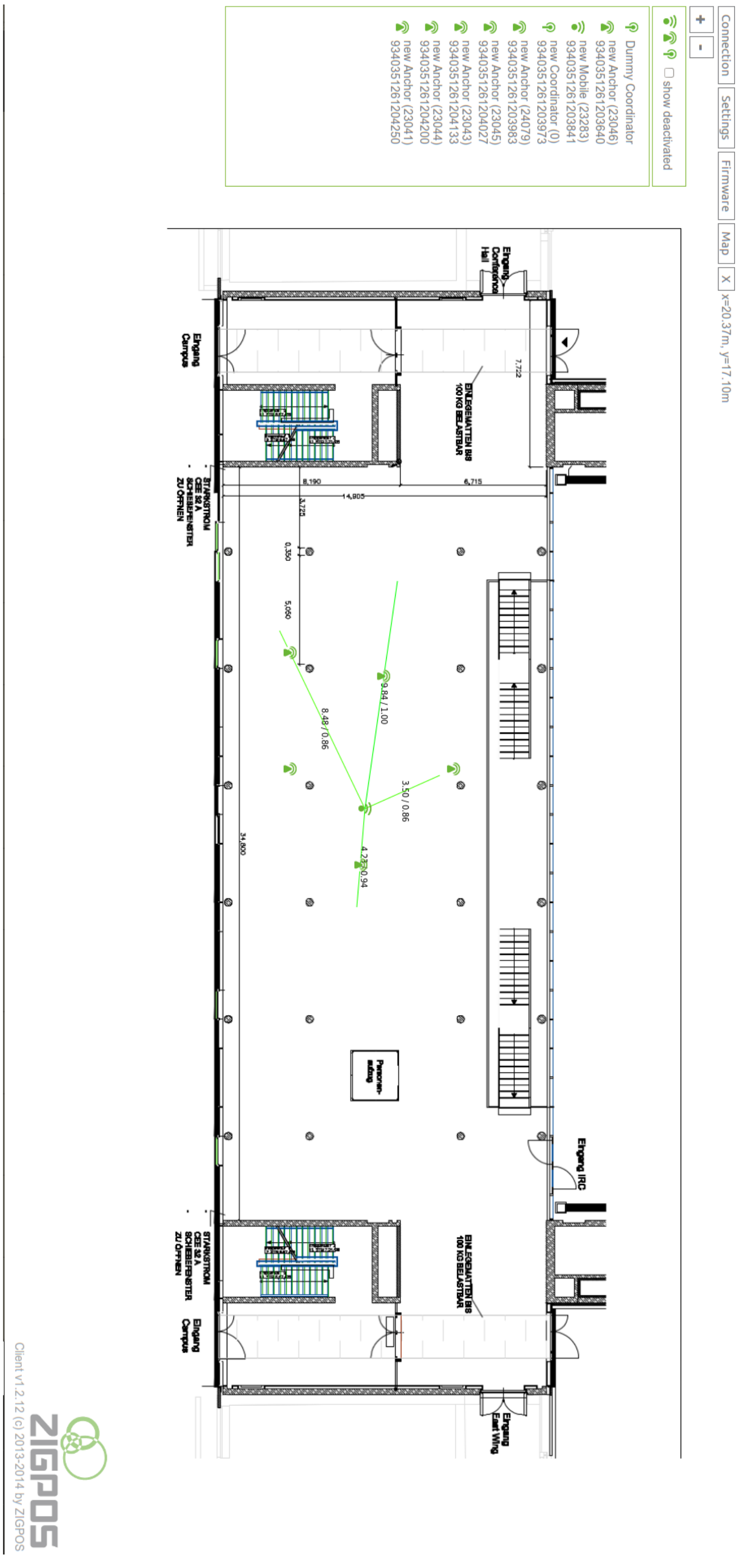

Figure 5.14: Target Localization using an Indoor Positioning System [32].

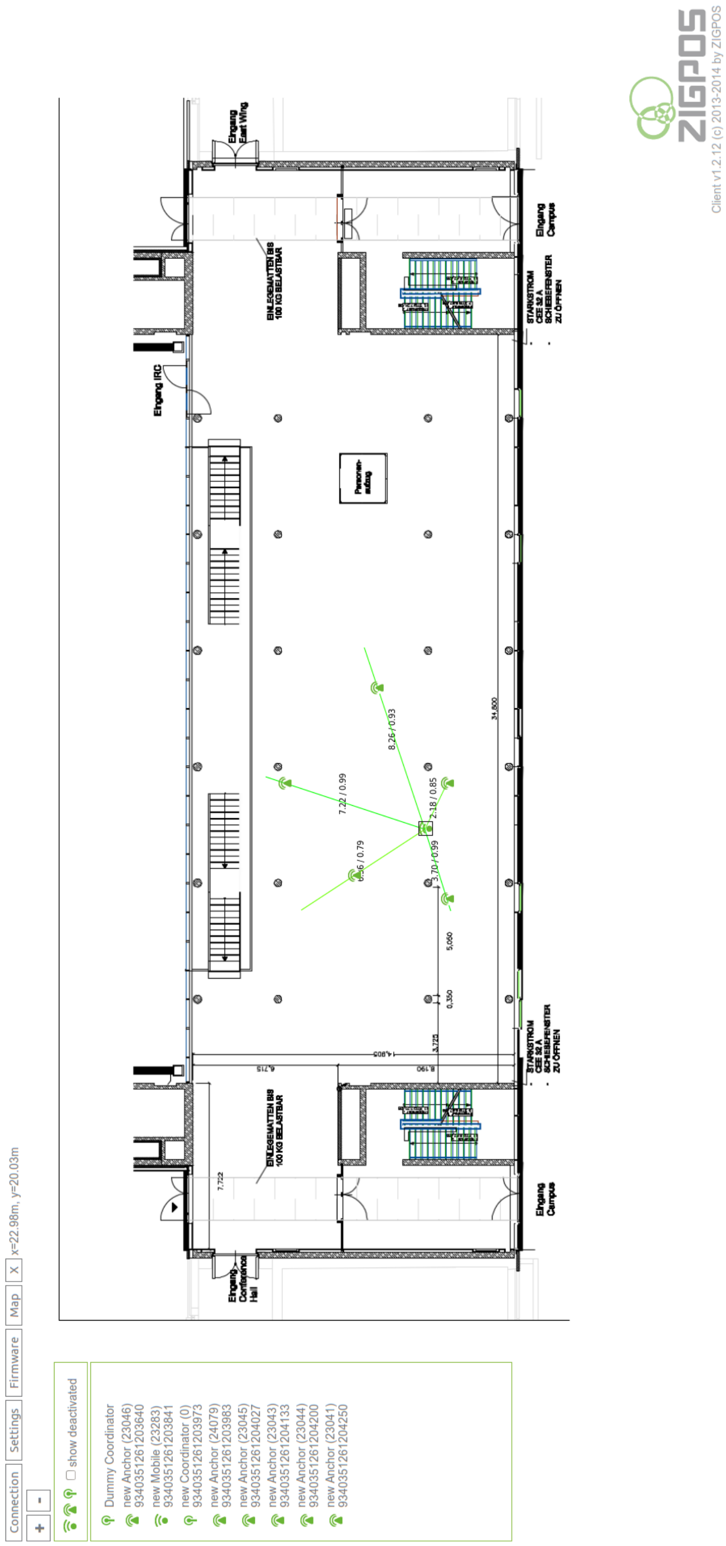

Figure 5.15: Target Localization using an Indoor Positioning System [32].

Chapter 6

Conclusions And Future Works

6.1 Summary and Conclusions

In this thesis, we attempt to solve the problem of a mutually conditional ranging and trilateration for wireless localization, mostly in indoor environments We attempt a unification of the two problems – ranging and positioning, with the aim at improving the accuracy, reliability, flexibility, and scalability of wireless localization systems, thereby presenting high resolution ranging techniques as well as robust and accurate positioning techniques. The results of the thesis can be summarized as follows.

In Chapter 2, we provided an error analysis by estimating and reconstructing the statistics of the ranging error without a priori knowledge of the wireless channel using the Gaussian kernel and Edgeworth Expansion methods. Results showed that the Edgeworth technique is a more efficient technique than the Gaussian Kernel method.

In Chapter 3, we proposed a ranging algorithm, which combines superresolution algorithms such as MUSIC and Root MUSIC with the powerful notion of a sparse ruler, to perform efficient and accurate Time of Arrival-based ranging. The optimized sparse solution depicted a superior performance when compared against the naive uniform solution while reaching the fundamental limits depicted by the CRLB.

In Chapter 4, an efficient and accurate solution to the multipoint ranging problem was presented, based on an adaptation of superresolution techniques, with optimized sampling. Under a unified framework, we constructed a variation of the superresolution algorithms to perform distance estimation over sparse sample sets determined by Golomb rulers. The design of the mutually orthogonal sets of Golomb rulers required for multipoint ranging method was achieved via the proposed evolutionary genetic algorithm which also generates optimal Golomb rulers. A CRLB analysis of the optimized multipoint ranging solution was performed to quantify the gains achievable.

In Chapter 5, performance evaluation for applications in wireless localization utilizing simulated and real time measurements were performed. First, a new accurate ranging techniques to obtain multiple distance estimates by applying superresolution techniques to different set of measurements with an outliers detection technique and a new slope sampling algorithm utilizing a peak search on a computed spectrum of residues were presented. The SMDS algorithm which requires an initial target estimate obtained using proposed trilateration techniques (intersection of measured distances) were used for target localization in different localization scenarios.

6.2 Future Works

From the results shown in this thesis, various and different directions can be further for future works, implementations and advancements, From example, the proposed reconstruction methods in Chapter 2 would be used to estimate the statistics of the ranging errors of phase measurements from a single realization in assist the construction of positioning algorithms in taking advantage of this a priori statistics in the form of weighting strategies for the therein computed measured distances. This therefore will provide more variability in the analysis of the localization problem for the purpose of wireless localization. In terms of a new direction, a new positioning algorithm utilizing the minimization of a weighted least square objective function will be investigated as well. Also, the solution of the multipoint ranging problem provided in 4 will be furthered in real time application scenarios to investigate its visibility for for optimization of resources while maintaining efficiency and accuracy in wireless localization.

Ranging and Positioning techniques will be analyzed, investigated and proposed for new technologies, mainly UWB and WiFi to take advantage of the enormous potential in terms of the accuracy of UWB devices and the already available large deployment and scalability of WiFi devices without requiring any special hardwares or modification.

Finally as a final wrap up, we would take a closer look into positioning in the form of semantic localization, e:g: “I am at the corridor”, “I am the printer room” rather than just geographic coordinates. Therein, the goal would be not only to determine the coordinates of the target but rather the semantics associated with coordinates in the pre-defined location profiles of an environment - office, malls, streets etc.

Appendix A

Pseudo-codes

Algorithm 1 - Unwrap Algorithm

$\tilde{\boldsymbol{\varphi}}_{\mathcal{N}:s} \longleftarrow$ Measured phases for a single snapshot (given)
$\mathbb{F} \longleftarrow$ Carrier frequencies of the corresponding phases (given)
$K \longleftarrow$ Number of carrier frequencies used (given)
$\mathbb{F} = \mathbb{F} - f_{n_1}$
while flag $= 1$ **do**

$$\nabla = \frac{\sum_{k=1}^{K} f_{n_k} \cdot \tilde{\boldsymbol{\varphi}}_{n_k:s} - \frac{1}{K}\sum_{k=1}^{K} f_{n_k} \cdot \sum_{k=1}^{K} \tilde{\boldsymbol{\varphi}}_{n_k:s}}{\sum_{k=1}^{K} f_{n_k}^2 - \frac{1}{K}\Big(\sum_{k=1}^{K} f_{n_k}\Big)^2}$$

$$\mathrm{I} = \frac{1}{K}\sum_{k=1}^{K} \tilde{\boldsymbol{\varphi}}_{n_k:s} - \nabla \cdot \frac{1}{K}\sum_{k=1}^{K} f_{n_k}$$

$\tilde{\boldsymbol{\varphi}}_{\mathcal{N}:s} = \mathrm{sign}(\nabla) \cdot \tilde{\boldsymbol{\varphi}}_{\mathcal{N}:s}$
$\tilde{\boldsymbol{\varphi}}_{\mathcal{N}:s} = \big[\tilde{\boldsymbol{\varphi}}_{\mathcal{N}:s} + 2\pi; \tilde{\boldsymbol{\varphi}}_{\mathcal{N}:s}; \tilde{\boldsymbol{\varphi}}_{\mathcal{N}:s} - 2\pi\big]$
$\hat{\boldsymbol{\varphi}}_{\mathcal{N}:s} = \nabla \cdot \mathbb{F} + \mathrm{I}$
$\mathbf{I}_{\text{index}} = \min |(\tilde{\boldsymbol{\varphi}}_{\mathcal{N}:s} - \hat{\boldsymbol{\varphi}}_{\mathcal{N}:s}|$
$\tilde{\boldsymbol{\varphi}}_{\mathcal{N}:s} = \tilde{\boldsymbol{\varphi}}_{\mathcal{N}:s}(\mathbf{I}_{\text{index}} + (0:3:3K-1)$
if $\|\tilde{\boldsymbol{\varphi}}_{\mathcal{N}:s} - \tilde{\boldsymbol{\varphi}}_{\mathcal{N}:s}(2)\|$ **then** flag $= 0$
end if
end while

Algorithm 2 - Sparse Ruler Generation Algorithm

$K \longleftarrow$ Desired order of the ruler (given)
$C \longleftarrow$ Maximum number of mutations (given)
$s_{\max} := K - 1$
while $\nexists\, \mathcal{S}_p | f(\mathcal{S}_p) = K\frac{(K-1)}{2}$ **do**
  $\mathcal{S}^* := \{1, 2, \cdots, s_{\max}\}$
  for $p := 1 \rightarrow P$ **do**
    count $\leftarrow 0$
    $\mathcal{S}_p \leftarrow$ randomly select $K - 1$ elements of $\mathcal{S}^*$
    $\mathcal{S}_p \leftarrow$ randomly permute the elements of $\mathcal{S}_p$
    while count $<= C$ **do**
      $\mathcal{S}_p^\dagger = \mathcal{M}(\mathcal{S}_p)$.
      if $f(\mathcal{S}_p^\dagger) < f(\mathcal{S}_p)$ **then**
        $S_p \leftarrow \mathcal{S}_p^\dagger$
      end if
      count $\leftarrow$ count + 1
    end while
  end for
  $\mathbb{P}^\dagger = \{\mathcal{S}_p\}_{p=1}^P$
  if $\nexists\, \mathcal{S}_p | R_p = 0$ **then**
    $s_{\max} \leftarrow s_{\max} + 1$
    restart
  else
    $\mathbb{P}^\dagger_{♂} \leftarrow \{\mathcal{S}_p | R_p = 0\}$
    $\mathcal{S}_{♂} = \{\mathcal{S}_p \in \mathbb{P}^\dagger_{♂} | f(\mathcal{S}_p) < f(\mathcal{S}_q)\ \forall\, q \neq p\}$
    $\mathbb{P}^\dagger_{♀} \leftarrow \mathbb{P}^\dagger \setminus \mathcal{S}_{♂}$
  end if
  for $p := 1 \rightarrow P - 1$ **do**
    $\mathcal{S}_p^\dagger \leftarrow \mathcal{C}(\mathcal{S}_p, \mathcal{S}_{♂})$
    if $f(\mathcal{S}_p^\dagger) < f(\mathcal{S}_p)$ **then**
      $\mathcal{S}_p \leftarrow \mathcal{S}_p^\dagger$
    else if $f(\mathcal{S}_p^\dagger) < f(\mathcal{S}_{♂})$ **then**
      $\mathcal{S}_{♂} \leftarrow \mathcal{S}_p^\dagger$
    end if
  end for
end while
function Fitness Function
  $N_p \leftarrow$ length of $\mathcal{N}_p$ associated to $\mathcal{S}_p$ (input)
  $R_p \leftarrow$ number of repeated elements in $\mathcal{S}_p$ (input)
  $f(\mathcal{S}_p) \leftarrow N_p \times (R_p + 1)$.
  return $f(\mathcal{S}_p)$
end function

Algorithm 3 - Mutually-orthogonal Golomb Rulers Generation Algorithm

```
W ⟵ Set of admissible marks (given)
K ⟵ Desired order of the ruler (given)
C ⟵ Maximum number of mutations (given)
G ⟵ Maximum number of generations (given)
s_max := 3K
while ∄ S_p | f(S_p) = K (K−1)/2 do
    S* := {1, 2, ···, s_max}
    for p := 1 → P do
        count ← 0
        S_p ← randomly select K − 1 elements of S*
        S_p ← randomly permute the elements of S_p
        while count <= C do
            S_p† = M(S_p).
            if f(S_p†) < f(S_p) then
                S_p ← S_p†
            end if
            count ← count + 1
        end while
    end for
    ℙ† = {S_p}_{p=1}^P
    if ∄ S_p | R_p = 0 then
        s_max ← s_max + 1
        restart
    else
        ℙ†_♂ ← {S_p | R_p = 0}
        S_♂ = {S_p ∈ ℙ†_♂ | f(S_p) < f(S_q) ∀ q ≠ p}
        ℙ†_♀ ← ℙ† \ S_♂
    end if
    count ← 0
    while count < G or ∃ S_p | f(S_p) = K (K−1)/2 do
        for p := 1 → P − 1 do
            S_p† ← C(S_p, S_♂)
            if f(S_p†) < f(S_p) then
                S_p ← S_p†
            else if f(S_p†) < f(S_♂) then
                S_♂ ← S_p†
            end if
        end for
    end while
end while
function Fitness Function
    N_p ← length of N_p associated to S_p (input)
    R_p ← number of repeated elements in S_p (input)
    F_p ← number of forbidden marks in N_p (input)
    f(S_p) ← N_p × (R_p + F_p + 1).
    return f(S_p)
end function
```

Own Publications

Journals

- Omotayo Oshiga, Stefano Severi and Giuseppe Abreu: "Superresolution Multipoint Ranging with Optimized Sampling via Orthogonally Designed Golomb Rulers,", IEEE Transactions on Wireless Communications, 2014. (Submitted – under final review)

Conferences

- Omotayo Oshiga, Stefano Severi and Giuseppe Thadeu Freitas de Abreu: "Non-parametric Estimation of Error Bounds in LOS and NLOS Environments," 10th Workshop on Positioning, Navigation and Communication, (WPNC 2013), March 20-21, 2013.

- Omotayo Oshiga, Stefano Severi and Giuseppe Thadeu Freitas de Abreu: "Optimized Super-Resolution Ranging over ToA Measurements," Proc. IEEE Wireless Communications and Networking Conference, (WCNC, 2014), April 6-9, 2014.

- Omotayo Oshiga and Giuseppe Thadeu Freitas de Abreu: "Analysis of Wireless Localization with Golomb-optimized Multipoint Ranging," The IEEE Eleventh International Symposium on Wireless Communication Systems , (ISWCS, 2014), August 26-29, 2014.

- Omotayo Oshiga and Giuseppe Thadeu Freitas de Abreu: "Design of Orthogonal Golomb Rulers with Applications in Wireless Localization," Proc. IEEE Fourty-Eighth Asilomar Conference on Signals, Systems and Computers, (Asilomar 2014), November 2-5, 2014.

- Omotayo Oshiga and Giuseppe Thadeu Freitas de Abreu: "Efficient Slope Sampling Ranging and Trilateration Techniques for Wireless Localization," 12th Workshop on Positioning, Navigation and Communication, (WPNC 2013), March 11-12, 2015.

Bibliography

[1] Federal Communication Commission, "Notice of Proposed Rulemaking Docket no. 94-102," 1996.

[2] International Telecommunication Union, "The World in 2014: ICT Facts and Figures," April 2014. [Online]. Available: http://www.itu.int/en/ITU-D/Statistics/Pages/facts/default.aspx

[3] M. Rohan, "Location Based Services (LBS) Market worth $39.87 Billion by 2019," 2014. [Online]. Available: http://www.marketsandmarkets.com/PressReleases/location-based-service.asp

[4] FP7 EU BUTLER Project, "287901 Integrated Project - uBiquitous, secUre inTernet-of-things with Location and contEx-awaReness," Oct 2011 - Oct 2014. [Online]. Available: http://www.iot-butler.eu/about-butler

[5] FP7 EU IoT-A Project, "257521 Integrated Project - Internet of Things Architecture," Sept 2010 - Sept 2013. [Online]. Available: http://www.iot-a.eu/public

[6] FP7 EU OpenIoT Project, "287305 Integrated Project - Open Source cloud solution for the Internet of Things," Sept 2007 - Sept 2013. [Online]. Available: http://www.iot-a.eu/public

[7] ABI Research, "Internet of Everything Research Service," June 2013. [Online]. Available: https://www.abiresearch.com/market-research/service/internet-of-everything

[8] P. Harrop and R. Das, "Wireless sensor networks (WSN) 2012-2022: Forecasts, technologies, players - the new market for ubiquitous sensor networks (USN)," December 2012. [Online]. Available: www.IDTechEx.com/ips

[9] L. Wirola, T. Laine, and J. Syrjrinne, "Mass-market requirements for indoor positioning and indoor navigation," in *Indoor Positioning and Indoor Navigation (IPIN), 2010 International Conference on*, 2010, pp. 1–7.

[10] R. Verdone and D. Dardari and G. Mazzini and A. Conti, "Wireless sensor and actuator networks: technologies, analysis and design," Academic Press, 2010.

[11] P. Harrop and R. Das, "Mobile phone indoor positioning systems (IPS) and real time locating systems (RTLS) 2014-2024 - forecasts, players, opportunities," July, 2013. [Online]. Available: www.IDTechEx.com/ips

[12] J. Xu, W. Liu, F. Lang, Y. Zhang, and C. Wang, “Distance Measurement Model Based on RSSI in WSN,” *Wireless Sensor Network*, vol. 2, no. 8, pp. 606–611, 2010.

[13] G. Chandrasekaran, M. A. Ergin, J. Yang, S. Liu, Y. Chen, M. Gruteser, and R. P. Martin, “Empirical evaluation of the limits on localization using signal strength,” in *IEEE 6th Communications Society Conference on Sensor and Ad Hoc Communications and Networks (SECON’09)*, 2009.

[14] E. Elnahrawy, L. Xiaoyan, and R. P. Martin, “The limits of localization using signal strength: a comparative study,” in *IEEE 1st Communications Society Conference on Sensor and Ad Hoc Communications and Networks (SECON’04)*, 2004, pp. 406–414.

[15] A. I. Baba and M. M. Atia, “Burst mode symmetric double sided two way ranging,” in *IFIP Wireless Days (WD’11)*, 2011, pp. 1–3.

[16] K. Myungkyun and J. Chong, “A new double two-way ranging algorithm for ranging system,” in *2nd IEEE International Conference on Network Infrastructure and Digital Content (NIDC’10)*, 2010, pp. 470–473.

[17] M. Scherhaufl, M. Pichler, E. Schimback, D. J. Muller, A. Ziroff, and A. Stelzer, “Indoor localization of passive UHF RFID tags based on phase-of-arrival evaluation,” *IEEE Trans. on Microwave Theory and Techniques*, vol. 61, no. 12, pp. 4724–4729, 2013.

[18] A. Povalac and J. Sebesta, “Phase difference of arrival distance estimation for RFID tags in frequency domain,” in *IEEE International Conference on RFID-Technologies and Applications (RFID-TA’11)*, 2011, pp. 188–193.

[19] F. Ahmad, M. G. Amin, and P. Setlur, “Through-the-wall target localization using dual- frequency CW radars,” *Proc. SPIE Sensors, and Command, Control, Communications, and Intelligence (C3I) Technologies for Homeland Security and Homeland Defense*, vol. 62010H, 2006. [Online]. Available: http://dx.doi.org/10.1117/12.666019

[20] L. Hui, H. Darabi, P. Banerjee, and L. Jing, “Survey of wireless indoor positioning techniques and systems,” *IEEE Trans. on Systems, Man, and Cybernetics, Part C: Applications and Reviews*, vol. 37, no. 6, pp. 1067–1080, 2007.

[21] G. Yanying, A. Lo, and I. Niemegeers, “A survey of indoor positioning systems for wireless personal networks,” *IEEE Communications Surveys Tutorials*, vol. 11, no. 1, pp. 13–32, 2009.

[22] R. Peng and M. L. Sichitiu, “AoA localization for wireless sensor networks,” in *IEEE 3rd Communications Society Conference on Sensor and Ad Hoc Communications and Networks (SECON’06)*, vol. 1, 2006, pp. 374–382.

[23] A. Zamora, J. Vidal, and D. H. Brooks, “Closed-form solution for positioning based on angle of arrival measurements,” in *IEEE 13th International Symposium on Personal, Indoor and Mobile Radio Communications*, vol. 4, Sept 2002, pp. 1522–1526.

[24] S. Gangcan, X. Xuefei, and K. Yang, “AoA-based constrained total least-squares location algorithm,” in *Proc. on the National Conference on Information Technology and Computer Science*, 2012.

[25] D. Niculescu and B. Nath, "Ad hoc positioning system (APS) using AOA," in *Proc. 22rd Annual Joint Conference of the IEEE Computer and Communications Societies (INFOCOM'03)*, vol. 3, 2003, pp. 1734–1743 vol.3.

[26] S. Wright and J. Nocedal, *Numerical optimization.* Springer New York, 1999, vol. 2.

[27] D. Macagnano, G. Destino, and G. Abreu, "A comprehensive tutorial on localization: algorithms and performance analysis tools," *International Journal of Wireless Information Networks*, vol. 19, no. 4, pp. 290–314, 2012.

[28] G. Abreu and G. Destino, "Super MDS: Source location from distance and angle information," in *IEEE Wireless Communications and Networking Conference (WCNC'07)*, 2007, pp. 4430–4434.

[29] M. A. Cox and T. F. Cox, *Multidimensional scaling.* Springer, 2008.

[30] J. Dattorro, *Convex Optimization and Euclidean Distance Geometry*, 61st ed. Meboo Publishing, 2005. [Online]. Available: http://www.stanford.edu/dattorro/mybook.html

[31] A. Beck, P. Stoica, and L. Jian, "Exact and approximate solutions of source localization problems," *Signal Processing, IEEE Transactions on*, vol. 56, no. 5, pp. 1770–1778, May 2008.

[32] ZIGPOS Gmbh, "ZIGPOS real-time locating system evaluation kit," March, 2013. [Online]. Available: zigpos.net/zigpos/index.php?c=2&a=37&s=positioning

[33] K. Feng, C. L. Chen, and C. H. Chen, "GALE: An enhanced geometry-assisted location estimation algorithm for NLOS environments," *Mobile Computing, IEEE Transactions on*, vol. 7, no. 2, pp. 199 –213, Febuary 2008.

[34] X. Wang, Z. Wang, and B. O'Dea, "A TOA-based location algorithm reducing the errors due to non-line-of-sight (NLOS) propagation," *Vehicular Technology, IEEE Transactions on*, vol. 52, no. 1, pp. 112–116, Jan 2003.

[35] S. Boyd and L. Vandenberghe, *Convex Optimization.* New York, NY, USA: Cambridge University Press, 2004.

[36] G. Destino and G. Abreu, "Weighing strategy for network localization under scarce ranging information," *IEEE Transactions on Wireless Communications*, vol. 8, no. 7, pp. 3668–3678, 2009.

[37] I. Borg and P. J. Groenen, *Modern Multidimensional Scaling: Theory and Applications*, ser. Springer Series in Statistics. Springer, 2007. [Online]. Available: http://books.google.de/books?id=nRal-OSpknUC

[38] P. J. Groenen, W. Heiser, and J. J. Meulman, "Global optimization in least-squares multidimensional scaling by distance smoothing," *Journal of classification*, vol. 16, no. 2, pp. 225–254, 1999.

[39] J. Saloranta, D. Macagnano, and G. Abreu, "Interval-scaling for multitarget localization," in *Positioning Navigation and Communication (WPNC), 2012 9th Workshop on*, March 2012, pp. 59–64.

[40] J. Saloranta, D. Macagnano, S. Severi, and G. Abreu, "Sensor localization with algebraic confidence," in *Signals, Systems and Computers (ASILOMAR), 2012 Conference Record of the Forty Sixth Asilomar Conference on*, Nov 2012, pp. 227–231.

[41] H. V. Poor, *An introduction to signal detection and estimation (2nd ed.)*. New York, NY, USA: Springer-Verlag New York, Inc., 1994.

[42] H. V. Trees, *Detection, Estimation, and Modulation Theory*. Wiley, 2004, no. V. 1.

[43] S. Kay, *Fundamentals Statistical Processing Volume 1 and 2*. Prentice Hall, 2001.

[44] W. Shi-Xun, L. Ji-Ping, and L. Shou-Yin, "Improved positioning algorithm based on two step least square in nlos environments," *The Journal of China Universities of Posts and Telecommunications*, vol. 18, no. 5, pp. 58–63, 2011.

[45] J. Saloranta, S. Severi, D. Macagnano, and G. Abreu, "Algebraic confidence for sensor localization," in *Proc. Asilomar Conf. Signals, Systems, and Computers*, 2012.

[46] J. Y. Huang and Q. Wan, "The CRLB for wsns location estimation in NLOS environments," in *Communications, Circuits and Systems (ICCCAS), 2010 International Conference on*, July 2010, pp. 83 –86.

[47] N. Patwari, A. Hero, M. Perkins, N. Correal, and R. O'Dea, "Relative location estimation in wireless sensor networks," *IEEE Transactions on Signal Processing*, vol. 51, no. 8, pp. 2137–2148, 2003.

[48] S. Blinnikov and R. Moessner, "Expansions for nearly gaussian distributions," *Astronomy and Astrophysics Supplement Series*, vol. 130, pp. 193–205, 1998.

[49] J. D. Parson, *The Mobile Radio Propagation Channel, 2nd Edition*, 2nd ed. Wiley, November 2000.

[50] G. Abreu, "CTH16-4: Accurate simulation of piecewise continuous arbitrary nakagami-m phasor processes," in *IEEE Global Telecommunications Conference, (GLOBECOM '06)*, December 2006, pp. 1–6.

[51] I. S. Gradshteĭn, I. M. Ruizhik, Y. V. Geronimus, Y. Tseytlin, and A. Jeffrey, *Table of Integrals, Series, and Products.*, 1965. [Online]. Available: http://books.google.de/books?id=gxoXcgAACAAJ

[52] E. Weisstein, "Double factorial," Dec. 2012. [Online]. Available: http://mathworld.wolfram.com/DoubleFactorial.html

[53] E. W. Weisstein, "Nakagami distribution," October 2012. [Online]. Available: http://reference.wolfram.com/mathematica/ref/NakagamiDistribution.html

[54] E. Weisstein, "Gamma function," October 2012. [Online]. Available: http://mathworld.wolfram.com/GammaFunction.html

[55] C. Bourin and P. Bondon, "Efficiency of high-order moment estimates," *Signal Processing, IEEE Transactions on*, vol. 46, no. 1, pp. 255 –258, January 1998.

[56] D. Torrieri, “Statistical theory of passive location systems,” *Aerospace and Electronic Systems, IEEE Transactions on*, vol. AES-20, no. 2, pp. 183–198, March 1984.

[57] R. Hach, “Symetric double sided - two way ranging,” in *Contribution 802.15-05-0334-00-004a to the IEEE 802.15.4a Ranging Subcommittee*, June 2005.

[58] Z. Shouhong and D. Zhiguo, “A simple approach of range-based positioning with low computational complexity,” *IEEE Trans. on Wireless Communications*, vol. 8, no. 12, pp. 5832–5836, 2009.

[59] T. E. Tuncer and B. Friedlander, *Classical and Modern Direction of Arrival Estimation*. Elsevier Science, 2009. [Online]. Available: http://books.google.de/books?id=1aQbxKJI2CsC

[60] R. O. Schmidt, “Multiple emitter location and signal parameter estimation,” *IEEE Trans. on Antennas and Propagation*, vol. 34, no. 3, pp. 276–280, 1986.

[61] P. Stoica and K. Sharman, “Maximum likelihood methods for DoA estimation,” *IEEE Trans. on Acoustics, Speech and Signal Processing*, vol. 38, no. 7, pp. 1132–1143, 1990.

[62] A. B. Gershman and P. Stoica, “Mode with extra-roots (MODEX): a new DoA estimation algorithm with an improved threshold performance,” in *Proc. IEEE International Conference on Acoustics, Speech, and Signal Processing (ICASSP ’99)*, vol. 5, 1999, pp. 2833–2836 vol.5.

[63] F. Li, H. Liu, and R. J. Vaccaro, “Performance analysis for DOA estimation algorithms: unification, simplification, and observations,” *IEEE Trans. on Aerospace and Electronic Systems*, vol. 29, no. 4, pp. 1170–1184, 1993.

[64] A. Barabell, “Improving the resolution performance of eigenstructure- based direction-finding algorithms,” in *Proc. IEEE International Conference on Acoustics, Speech, and Signal Processing (ICASSP ’83)*, vol. 8, 1983, pp. 336–339.

[65] V. F. Pisarenko, “The retrieval of harmonics from a covariance function,” *Geophysical Journal International*, vol. 33, no. 3, pp. 347–366, 1973. [Online]. Available: http://gji.oxfordjournals.org/content/33/3/347.full.pdf+html

[66] W. T. Rankin, “Optimal golomb rulers: An exhaustive parallel search implementation,” Ph.D. dissertation, Duke University, 1993.

[67] A. H. Dewdney, “Computer recreations,” pp. 16–26, December 1985.

[68] K. D. Boese, A. B. Kahng, and S. Muddu, “A new adaptive multi-start technique for combinatorial global optimizations,” *Oper. Res. Lett.*, vol. 16, no. 2, pp. 101–113, 1994.

[69] B. Feeney, “Determining optimum and near-optimum golomb rulers using genetic algorithms. master thesis, computer science, university college cork,” October 2003.

[70] C. Cotta, I. Dotú, A. F. Fernández, and P. van Hentenryck, “Local search-based hybrid algorithms for finding colomg rulers,” *Constraints*, vol. 12, no. 3, pp. 263–291, September 2007.

[71] S. W. Soliday, A. Homaifar, and G. Lebby, "Genetic algorithm approach to the search for golomb rulers," in *Proceedings of the 6th International Conference on Genetic Algorithms*. San Francisco, CA, USA: Morgan Kaufmann Publishers Inc., 1995, pp. 528–535.

[72] T. Jia and R. M. Buehrer, "A new cramer-rao lower bound for TOA-based localization," in *IEEE Military Communications Conference (MILCOM'08)*, November 2008, pp. 1–5.

[73] R. Kaune, "Accuracy studies for TDoA and ToA localization," in 15^{th} *International Conference on Information Fusion (FUSION'12)*, July 2012, pp. 408–415.

[74] C. S. Limited, "CS5000 real time location system," May 2012. [Online]. Available: http://www.convergence.com.hk/wp-content/uploads/2013/03/RTLS-UserManual-v3-PR3b.pdf

[75] Dresden Elektronik ingeniuertechnik Gmbh, "Dresden elektronik and ZIGPOS announce real-time locating system kit with new atmel ranging technology," March, 2013. [Online]. Available: www.prlog.org/12092596

[76] A. V. Medina, J. A. Gómez, J. A. Ribeiro, and E. Dorronzoro, "Indoor position system based on a zigbee network," *Communications in Computer and Information Science*, vol. 362, pp. 6–16, 2013.

[77] S. Azzouzi, M. Cremer, U. Dettmar, T. Knie, and R. Kronberger, "Improved AoA based localization of UHF RFID tags using spatial diversity," in *IEEE International Conference on RFID-Technologies and Applications (RFID-TA'11)*, 2011, pp. 174–180.

[78] A. Moragrega and C. Ibars, "Performance analysis of cooperative and range based localization algorithms for ZigBee and 802.15.4a wireless sensor networks," in *IEEE 21st International Symposium on Personal Indoor and Mobile Radio Communications (PIMRC'10)*, 2010, pp. 1996–2001.

[79] L. J. Xing, L. Zhiwei, and F. C. Shin, "Symmetric double side two way ranging with unequal reply time," in *IEEE 66th Vehicular Technology Conference (VTC'07)*, 2007, pp. 1980–1983.

[80] L. Qianqian, M. Lin, M. Peng, C. Zhiming, and Y. Shi, "A cmos low power, wide dynamic range RSSI with integrated AGC loop," in *IEEE International Conference on Anti-Counterfeiting, Security and Identification (ASID)*, June 2011, pp. 173–176.

[81] K. Wang, L. Xuemei, M. Kaixue, K. S. Yeo, C. Xiang, and W. Zhigong, "A CMOS low-power temperature-robust RSSI using weak-inversion limiting amplifiers," *Journal of Circuits, Systems and Computers*, vol. 22, no. 10, p. 1340034, 2013.

[82] "IEEE standard for local and metropolitan area networks–part 15.4: Low-rate wireless personal area networks LR-WPANs amendment 3: Physical layer PHY specifications for low-data-rate, wireless, smart metering utility networks," pp. 1–252, 2011.

[83] P. Szulakiewicz, R. Kotrys, M. Krasicki, P. Remlein, and A. Stelter, "OFDM interfering signal rejection from 802.11ac channel," in *IEEE 23rd International Symposium on Personal Indoor and Mobile Radio Communications (PIMRC'12)*, 2012, pp. 2015–2018.

[84] M. Rubsamen and A. B. Gershman, "DoA estimation for nonuniform sensor arrays: From manifold separation to fourier domain MUSIC methods," *IEEE Trans. on Signal Processing*, vol. 57, no. 2, pp. 588–599, 2009.

[85] X. Jing and Z. C. Du, "An improved fast Root MUSIC algorithm for DOA estimation," in *IEEE International Conference on Image Analysis and Signal Processing (IASP'12)*, 2012, pp. 1–3.

[86] M. M. Abdalla, M. B. Abuitbel, and M. A. Hassan, "Performance evaluation of direction of arrival estimation using MUSIC and ESPRIT algorithms for mobile communication systems," in *6th Joint IFIP Wireless and Mobile Networking Conference (WMNC'13)*, 2013, pp. 1–7.

[87] A. Faye, A. B. Youm, and J. D. Ndaw, "LVQ based DOA estimation," in *5th International Conference on Computational Intelligence, Communication Systems and Networks (CICSyN'13)*, 2013, pp. 245–250.

[88] C. E. Kassis, J. Picheral, and C. Mokbel, "Advantages of nonuniform arrays using Root MUSIC," *Journal of Signal Processing*, vol. 90, no. 2, pp. 689 – 695, 2010. [Online]. Available: http://www.sciencedirect.com/science/article/pii/S0165168409003272

[89] H. C. Song and B. woo Yoon, "Direction finding of wideband sources in sparse arrays," in *Proc. Sensor Array and Multichannel Signal Processing Workshop*, 2002, pp. 518–522.

[90] B. woo Yoon, H. C. Song, K. R. Baek, and J. S. Park, "Direction finding of wideband sources in aliasing conditions," in *Proc. on The 8th Russian-Korean International Symposium on Science and Technology (KORUS'04)*, vol. 1, 2004, pp. 18–22.

[91] D. R. Keller, T. K. Moon, and J. H. Gunther, "Narrowband source localization from a moving array of sensors," in *Proc. IEEE The* 40^{th} *Asilomar Conference on Signal, Systems and Computers (ASILOMAR'06)*, 2006, pp. 2285–2289.

[92] N. Tayem, "2-D DOA estimation of multiple coherent sources using a new antenna array configuration," in *Proc. IEEE The* 46^{th} *Asilomar Conference on Signal, Systems and Computers (ASILOMAR'12)*, 2012, pp. 212–216.

[93] Q. Chongying, C. Zhijie, W. Yongliang, and Z. Yongshun, "DOA estimation for coherent sources in unknown nonuniform noise fields," *IEEE Trans. on Aerospace and Electronic Systems*, vol. 43, no. 3, pp. 1195–1204, 2007.

[94] D. D. Ariananda and G. Leus, "DoA estimation of correlated signals using a dynamic linear array," in *Proc. IEEE The* 46^{th} *Asilomar Conference on Signal, Systems and Computers (ASILOMAR'12)*, 2012, pp. 2028–2035.

[95] D. Weiziu and R. L. Kirlin, "Improved spatial smoothing techniques for DOA estimation of coherent signals," *IEEE Trans. on Signal Processing*, vol. 39, no. 5, pp. 1208–1210, 1991.

[96] W. Bu-hong, W. Yong-liang, and C. Hui, "Weighted spatial smoothing for direction-of-arrival estimation of coherent signals," in *IEEE Antennas and Propagation Society International Symposium*, vol. 2, 2002, pp. 668–671.

[97] S. Sidon, "Ein satz über trigonometrische polynome und seine anwendung in der theorie der fourier-reihen," *Mathematische Annalen*, vol. 106, no. 1, pp. 536–539, 1932. [Online]. Available: http://dx.doi.org/10.1007/BF01455900

[98] W. C. Babcock, "Intermodulation interference in radio systems/frequency of occurrence and control by channel selection," *Bell System Technical Journal*, vol. 31, pp. 63 – 73, 1953.

[99] G. S. Bloom and S. W. Golomb, "Applications of numbered undirected graphs," *Proceedings of the IEEE*, vol. 65, no. 4, pp. 562–570, 1977.

[100] A. Dimitromanolakis, "Analysis of the golomb ruler and the sidon set problems and determination of large near-optimal golomb rulers," Master's thesis, Technical University of Crete, June 2002.

[101] C. Meyer and P. A. Papakonstantinou, "On the complexity of constructing golomb rulers," *Discrete Applied Mathematics*, vol. 157, no. 4, pp. 738 – 748, 2009. [Online]. Available: http://www.sciencedirect.com/science/article/pii/S0166218X08003053

[102] Distributed.net. (2013) Optimal golomb rulers. [Online]. Available: http://www.distributed.net/Projects

[103] K. Drakakis, "A review of the available construction methods for golomb rulers," *Advances in Mathematics of Communications AMC*, vol. 3, no. 3, pp. 235 – 250, Aug. 2009.

[104] C. Cotta and A. J. Fernandez, *A Hybrid GRASP Evolutionary Algorithm Approach to Golomb Ruler Search*, ser. Lecture Notes in Computer Science. Springer Berlin Heidelberg, 2004, vol. 3242, pp. 481–490.

[105] N. Ayari, T. V. Luong, and A. Jemai, "A hybrid genetic algorithm for golomb ruler problem," in *IEEE/ACS International Conference on Computer Systems and Applications (AICCSA'10)*, 2010, pp. 1–4.

[106] J. Horton, "How octopuses work," 2013, [Online; accessed 4-Dec-2012]. [Online]. Available: http://animals.howstuffworks.com/marine-life/octopus5.htm

[107] G. Abreu, "On the generation of tikhonov variates," *IEEE Trans. on Communications*, vol. 56, no. 7, pp. 1157–1168, July 2008.

[108] A. J. Viterbi, "Phase-locked loop dynamics in the presence of noise by fokker-planck techniques," *Proc. IEEE*, pp. 1737 – 1753, 1963.

[109] W. C. . Lindsey, "Nonlinear analysis of generalized tracking systems," *Proc. IEEE*, vol. 57, no. 10, pp. 1705 – 1722, Oct. 1969.

[110] H. Leib and S. Pasupathy, "The phase of a vector perturbed by gaussian noise and differentially coherent receivers," *IEEE Trans. Inform. Theory*, vol. 34, no. 6, Nov. 1988.

[111] M. Abramowitz and I. A. Stegun, *Handbook of Mathematical Functions with Formulas, Graphs, and Mathematical Tables*, 10th ed. Dover Publications, 1965.

[112] C. C. Sheng, C. Yi-Jen, J. M. Lin, and L. C. Hsien, "Geometrical positioning schemes for MS location estimation," in *IEEE International Symposium on Computer, Consumer and Control (IS3C'12)*, June 2012, pp. 487–490.

[113] S. Junyang, A. Molisch, and J. Salmi, “Accurate passive location estimation using ToA measurements,” *IEEE Trans. on Wireless Communications*, vol. 11, no. 6, pp. 2182–2192, June 2012.

[114] Atmel Corporation, “Atmel AVR2150: RTB evaluation application - quick start guide; application note; atmel corporation,” May, 2012. [Online]. Available: http://url.ie/vh8f

[115] ——, “The Atmel REB233SMAD-EK hardware platform,” March, 2013. [Online]. Available: http://www.atmel.com/tools/REB233SMAD-EK.aspx

[116] V. J. Hodge and J. Austin, “A survey of outlier detection methodologies,” *Artificial Intelligence Review*, vol. 22, no. 2, pp. 85–126, 2004.

[117] A. Mhamdi and A. Samet, “Direction of arrival estimation for nonuniform linear antenna,” in *Communications, Computing and Control Applications (CCCA), 2011 International Conference on*, 2011, pp. 1–5.

[118] B. Tay, W. Liu, H. Chai, and P. Chong, “Distributed RSSI-sharing for two-way ranging base station selection,” in *Control Automation Robotics Vision (ICARCV), 2010 11th International Conference on*, 2010, pp. 90–95.

[119] H. Ahn, H. Hur, and W. Choi, “One-way ranging technique for CSS-based indoor localization,” in *Industrial Informatics, 2008. INDIN 2008. 6th IEEE International Conference on*, 2008, pp. 1513–1518.

[120] F. Akgul and K. Pahlavan, “AoA-assisted NLOS error mitigation for ToA-based indoor positioning systems,” in *Military Communications Conference, 2007. MILCOM 2007. IEEE*, 2007, pp. 1–5.

[121] J. B. Shearer, “Near optimal golomb rulers.” September 2003. [Online]. Available: http://www.feiri.de/ogr/nearopt.html

[122] S. Severi, G. Abreu, G. Destino, and D. Dardari, “Efficient and accurate localization in multihop networks,” in *Proc. Asilomar Conf. Signals, Systems, and Computers*, November 2009.

[123] N. Patwari, J. N. Ash, S. Kyperountas, A. O. Hero, R. L. Moses, and N. S. Correal, “Locating the nodes: cooperative localization in wireless sensor networks,” *Signal Processing Magazine, IEEE*, vol. 22, no. 4, pp. 54 – 69, July 2005.

[124] T. Wang, “Cramer-rao bound for localization with a priori knowledge on biased range measurements,” *Aerospace and Electronic Systems, IEEE Transactions on*, vol. 48, no. 1, pp. 468 –476, January 2012.

[125] Q. Yihong and H. Kobayashi, “On geolocation accuracy with prior information in non-line-of-sight environment,” in *Proc. on the 56th IEEE Vehicular Technology Conference, 2002*, vol. 1, 2002, pp. 285 – 288.

[126] D. Jourdan, J. Deyst, M. Z. Win, and N. Roy, “Monte carlo localization in dense multipath environments using UWB ranging,” in *Proc. on the 56th IEEE Ultra-Wideband International Conference, 2005*, September 2005, pp. 314 – 319.

[127] V. Cevher, “Elec 633 graphical models class,” University Lecture, 2008.

[128] O. Oshiga, S. Severi, and G. Abreu, "Optimized superresolution ranging over ToA measurements," in *IEEE Wireless Communications and Networking Conference (WCNC'14)*, 2014.

[129] B. Dil, S. Dulman, and P. Havinga, "Range-based localization in mobile sensor networks," vol. 3868, pp. 164–179, 2006.

[130] Y. Junlin, C. Tiberius, G. Janssen, P. Teunissen, and G. Bellusci, "Review of range-based positioning algorithms," *IEEE Aerospace and Electronic Systems Magazine*, vol. 28, no. 8, pp. 2–27, 2013.

[131] Y. Kegen, "3-D localization error analysis in wireless networks," *IEEE Trans. on Wireless Communications*, vol. 6, no. 10, pp. 3472–3481, 2007.

[132] B. Ristic, M. Morelande, A. Farina, and S. Dulman, "On proximity-based range-free node localisation in wireless sensor networks," in *9th International Conference on Information Fusion*, 2006, pp. 1–8.

[133] S. Zhang, J. Cao, C. Li-Jun, and D. Chen, "Accurate and energy-efficient range-free localization for mobile sensor networks," *IEEE Trans. on Mobile Computing*, vol. 9, no. 6, pp. 897–910, 2010.

[134] Y. Zhang, W. Wenwu, and Y. Chen, "A range-based localization algorithm for wireless sensor networks," *Journal of Communications and Networks*, vol. 7, no. 4, pp. 429–437, 2005.

[135] X. Yuan, "Coherent source direction-finding using a sparsely-distributed acoustic vector-sensor array," *IEEE Trans. on Aerospace and Electronic Systems*, vol. 48, no. 3, pp. 2710–2715, 2012.

[136] P. Pal and P. Vaidyanathan, "Nested arrays: A novel approach to array processing with enhanced degrees of freedom," *IEEE Trans. on Signal Processing*, vol. 58, no. 8, pp. 4167–4181, 2010.

[137] Wikipedia, "Golomb ruler – Wikipedia, the free encyclopedia," 2013, [Online; accessed 11-Dec-2013]. [Online]. Available: http://en.wikipedia.org/wiki/Golomb_ruler

[138] M. Ishiguro, "Minimum redundancy linear arrays for a large number of antennas," *Journal of Radio Science*, vol. 15, no. 6, pp. 1163–1170, 1980. [Online]. Available: http://dx.doi.org/10.1029/RS015i006p01163

[139] A. Moffet, "Minimum-redundancy linear arrays," *IEEE Trans on Antennas and Propagation*, vol. 16, no. 2, pp. 172–175, 1968.

[140] S. D. Bedrosian, "Nonuniform linear arrays: Graph-theoretic approach to minimum redundancy," *Proceedings of the IEEE*, vol. 74, no. 7, pp. 1040–1043, 1986.

[141] H. Mehrpouyan and M. R. Khanzadi, *On the statistical models for slow varying phase noise in communication systems.* unpublished, 2011, vol. 27.